POLYMER ADSORPTION ON SILICA AND WETTABILITY OF GRAPHENE OXIDE SURFACES, EXPERIMENTS AND SIMULATIONS

By

HAMID MORTAZAVIAN

Bachelor of Science in Polymer Engineering
Amirkabir University of Technology
Tehran, Iran
2007

Master of Science in Composite Engineering
MalekAshtar University of Technology
Tehran, Iran
2010

Submitted to the Faculty of the
Graduate College of the
Oklahoma State University
in partial fulfillment of
the requirements for
the Degree of
DOCTOR OF PHILOSOPHY
May, 2016

POLYMER ADSORPTION ON SILICA AND

WETTABILITY OF GRAPHENE OXIDE SURFACES,

EXPERIMENTS AND SIMULATIONS

Dissertation Approved:

Dr. Frank D. Blum

Dissertation Adviser

Dr. Jeffery L. White

Dr. Toby L. Nelson

Dr. Sadagopan Krishnan

Dr. Heather Fahlenkamp

ACKNOWLEDGEMENTS

My deepest gratitude is to my advisor, Dr. Frank D. Blum for his constant guidance, support, and encouragements, without which this work would have not been possible. I have been fortunate to have an advisor who gave me the freedom to research and explore on my own, and at the same time mentor me whenever I needed his advice.

I would like to express my deepest appreciation to Dr. Christopher J. Fennell for all his support. He educated me on molecular modeling and encouraged me to write in a consistent manner. I would like to thank my advisory committee members, Dr. Jeffery L. White, Dr. Toby L. Nelson, Dr. Sadagopan Krishnan, and Dr. Heather Fahlenkamp for their support and valuable comments.

I owe a deep sense of gratitude to my fellow lab mates, Dr. Bal Khatiwada, Dr. Charmaine Munro, Dr. Tan Zhang, Dr. Madhubhashini Madduma Arachchilage, Helanka Perera, Bhishma Sedai, and Ugo Arua for their support, valuable suggestions, and for creating a friendly environment in the lab.

I also would like to thank all the faculty and staff members of the Department of Chemistry, Oklahoma State University for being very helpful and friendly. I am thankful to the National Science Foundation (US) under Grant 1005606 for the financial support.

Last, but not the least, I would like to thank my family and friends who were always willing to help. I am thankful to my parents that without their support and love I would have not come this far. Special thanks to my brothers Vahid and Mohammad Mehdi, my dear sister, Fatemeh, and my dear siblings-in-law Niloufar and Meysam. The final deep appreciation is for Diba.

Name: HAMID MORTAZAVIAN

Date of Degree: MAY, 2016

Title of Study: POLYMER ADSORPTION ON SILICA AND WETTABILITY OF GRAPHENE OXIDE SURFACES, EXPERIMENTS AND SIMULATIONS

Major Field: CHEMISTRY

Abstract:

Among the various classifications of polymer composites, studying polymers adsorbed to a surface such as silica is important due to their numerous applications. Adsorbed polymers usually show different properties than their bulk counterparts due to their interactions with the surface. In this study, we observed tightly- and loosely-bound polymer and mobile components in poly(vinyl acetate) (PVAc) on silica both with temperature-modulated differential scanning calorimetry (TMDSC) experiments and computer simulations. The more-mobile component which correlated to the region of low density at the air interface is reported for the first time using TMDSC thermograms. Pore size distribution and pore volume development of adsorbed PMMA samples showed different behavior below and above the tightly-bound amount of the polymer. The amount of tightly-bound polymer was obtained by a linear regression analysis of the ratio of the area under the two glass transitions. The values obtained vary from 0.52 to 0.86 mg PVAc/m^2 silica depending upon the molecular mass for the amounts of PVAc and the specific surface area of fumed silica.

Direct comparisons of the thermal properties and intermolecular interactions were performed between PVAc and poly(methyl methacrylate) (PMMA) with similar molecular masses and adsorbed amounts on silica. A larger amount of tightly-bound polymer and a greater change in glass transition were observed for adsorbed PMMA compared to adsorbed PVAc. These observations suggested that the interactions between PMMA and silica were stronger than those between PVAc and silica. Molecular modeling of these surface polymers showed that PMMA associates more strongly with silica than does PVAc through additional hydrogen-bonding interactions.

Graphene oxide (GO) material surface characteristics make it easy to functionalize, making it a water repellant surface. To test the effect of chemical makeup and size of attached groups on the surface wettability of GO, we performed experimental water contact angle measurements and molecular modeling investigations on functionalized GO surfaces. Experimental and molecular simulation water contact angle measurements showed quantitative agreement for functionalizing groups with the same chain length at a variety of surface coverages.

TABLE OF CONTENTS

Chapter Page

LIST OF TABLES

LIST OF FIGURES

Figure Page

Figure Page

CHAPTER I

INTRODUCTION

1.1. POLYMERS AT INTERFACES

The conformations, interfacial structures and intermolecular interactions of polymers in proximity to an interface have been studied extensively.[1,2] The properties of polymers near the interface are usually different from their counterpart bulk polymers.[3-11] The adsorption of polymers on surfaces is affected by a variety of parameters such as the effect of the solvent,[1,12,13] the polarity of the polymer and polarity and porosity of the interface,[14,15] nature of the surface and the intermolecular interactions between polymer and surface,[16-21] molecular mass and polydispersity of polymer,[22-27] temperature,[28,29] and solution concentration.[23,30]

In the case when a polymer is adsorbed from solution, as the concentration of polymer increases, the adsorbed amount of polymer per surface area increases until it reaches a constant value that is independent of the polymer concentration. This is the behavior modeled by the Langmuir adsorption isotherm, first developed by Langmuir in 1915.[31] This adsorption isotherm is based on monolayer coverage of a gas on a

nonporous surface where a dynamic equilibrium exists between adsorbed gaseous molecules and free molecules. A number of different approaches have been proposed in the literature for deriving the Langmuir adsorption isotherm such as the statistical thermodynamic derivation by Adamson.[32] In this model, the total number of adsorption sites, S_0, can be shown to be:

$$S_0 = S_1 + S_2 \tag{1.1}$$

where S_1 is the number of unoccupied sites and S_2 is the number of sites already occupied by the adsorbate molecules. Assuming that the adsorption rate is proportional to S_1 and the gas pressure (p) and desorption rate is proportional to S_2, one can derive the following equation at equilibrium where the adsorption and desorption rates are equal:

$$k_1 S_1 p = k_1 p(S_0 - S_2) = k_2 S_2 \tag{1.2}$$

the conventional Langmuir equation can then be derived by dividing Equation 1.2 by S_0:

$$\theta = \frac{pb}{1 + pb} \tag{1.3}$$

where $b = K_1/K_2$ and is called the Langmuir constant and θ is the fraction of surface covered and is equal to S_2/S_0.

The Langmuir adsorption isotherm can also be applied to the adsorption of polymers from solution onto the surface of a substrate. The fraction of the surface covered by the adsorbed polymer can be expressed as mg of polymer adsorbed per m^2 of the surface. The amount of the polymer adsorbed on a substrate such as silica can be determined using thermogravimetric analysis (TGA). The adsorbed amount can be calculated based on the

mass loss due to the polymer and the mass of the residual material, which would contain only silica after heating, and the specific surface area of silica:

$$AA = \frac{\Delta M}{(1 - \Delta M) \times A} \quad (1.4)$$

where *AA* is the adsorbed amount which is mg of polymer adsorbed per m^2 of surface, ΔM is the mass fraction of polymer in the sample, and *A* is the specific surface area (m^2/g) of the substrate.

1.1.1. Structure of polymer chains near the surfaces

The conformations of polymer chains are forced to change near a surface due to the intermolecular interactions between the polymer chains and the interface.[33-35] Jenkel and Rumbach[36] proposed the conformational structure of polymer chains at the interface as being composed of trains, loops, and tails as shown in Figure 1.1. Trains are segments close to the surface and have most of their mers in contact with the substrate. Loops are the unbound segments in between the trains and tails are free non-adsorbed chain ends. The bound fraction, which refers to the trains, is an important parameter in calculations and has been estimated in this work to be around 1 mg/m^2 on most surfaces.[37]

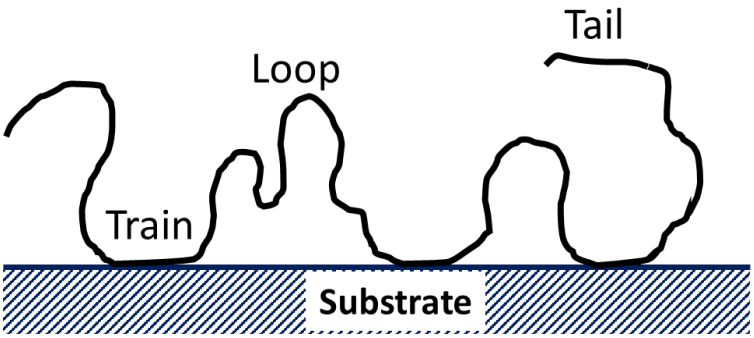

Figure 1.1. Conformation of a polymer chain adsorbed on a surface.

There are two types of adsorption processes; they are characterized by the interaction strength between the polymer chains and the surface. If the process involves strong interactions, such as covalent bonds between the adsorbate and the substrate, it is known as chemisorption. If there are only weaker interactions such as van der Waals and hydrogen bonding between the polymer and the substrate, the process is known as physisorption. Because these interactions are effective over short distances, only the few segments that are directly bonded to the surface and perhaps near neighbors are affected very much. The restriction in segmental motions of the polymer chains directly bonded at the interface, will affect neighboring segments.

1.2. METHODOLOGIES FOR CHARACTERIZATION OF ADSORBED POLYMERS

The demand for novel polymeric materials and consequently new characterization methods are rising due to the wide range of applications of polymers and polymer composites. Most polymer characterization techniques are used to determine molecular mass, molecular structure, morphology, and thermal and mechanical properties. It is important to take advantage of the knowledge gained by using multiple modes of characterization methods. By combining thermal analysis techniques such as thermogravimetric analysis (TGA) and differential scanning calorimetry (DSC) with spectroscopic techniques such as nuclear magnetic resonance (NMR), Fourier transform infrared (FTIR), mass spectroscopy (MS), X-ray diffraction (XRD), and surface and interfacial studies using scanning electron microscopy (SEM), transmission electron microscopy (TEM), Brunauer-Emmett-Teller (BET) surface area measurements and molecular modeling techniques, many of the physical and chemical properties of polymer composites and surface adsorbed polymers can be determined.[38-50] By coupling a few of

the above-mentioned techniques, we were able to investigate the molecular structure, dynamics, and intermolecular interactions of adsorbed polymers at interfaces. For example, the polymer structure and chain dynamics can be probed by techniques such as TMDSC[14,27,45,51] and NMR[42,52,53] and the interactions between polymer chains and the substrate can be probed using FTIR[15,48] and molecular dynamics (MD) simulations.[54-56]

1.2.1. Differential scanning calorimetry (DSC)

Differential scanning calorimetry (DSC) is, perhaps the most popular thermal analysis technique; it provides quantitative calorimetric information during a linear temperature ramp.[57] DSC can measure changes in the heat capacity (C_p) of materials with temperature. The ΔC_p is tracked as the change in the heat flow when the sample is heated or cooled. Using DSC, qualitative and quantitative information about the melting temperature (T_m), crystallization temperature (T_c), cold crystallization temperature (T_{cc}), glass transition temperature (T_g), and heat capacity difference at T_g (ΔC_p) of polymers and related compounds can be obtained.[58] Figure 1.2 shows the most common design of DSC instrumentation, which is the heat flux calorimeter with a disk-type measuring system. In this measuring system, the heat flow is transferred symmetrically through a thermally conductive disk (constantan) to metal pans, which are located on the raised platform of the disk symmetrical to the center. An empty aluminum pan is used as the reference and the sample is packed in the other pan. Temperature sensors are fixed on the surface of the disk. A thermocouple, which connects the temperature sensors beneath the metallic disk, measures the differential heat flow to the sample and to the reference pan. Since there are different heat flow rates for the sample and reference, a differential temperature signal (ΔT) is generated which is proportional to the difference in heat flow

rates. In other words, the thermocouple measures the differential heat flow rate as $\Delta T/R = dQ/dt$, where ΔT is the temperature difference between the pans, R is the thermal resistance of the metallic disk, and dQ/dt is heat flow.[59,60]

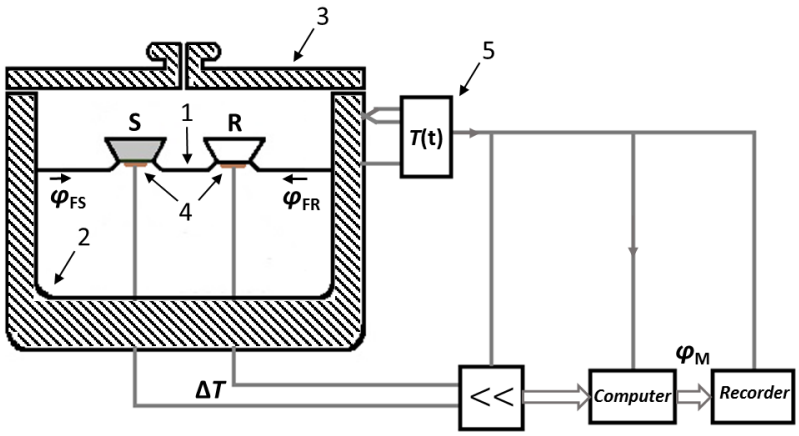

Figure 1.2. Heat flux DSC system. 1 disk, 2 furnace, 3 lid, 4 differential thermocouples, 5 programmer and controller. S and R, are crucible with sample and reference. Φ_{FS}, Φ_{FR}, and Φ_m are heat flow rates from furnace to sample, from furnace to reference, and measured heat flow rate, respectively.

DSC is used to investigate the thermal behavior of bulk polymers and composites by measuring the temperatures and heat flows of materials involved in transitions, as a function of time and temperature.[47,61,62] In the conventional DSC measurement of a polymeric material, the sample is heated to a temperature higher than T_g or T_m at a controlled and constant heating rate in a temperature range in which the material is thermally stable. The sample is then cooled down to a temperature below T_g, and reheated. Heating the sample above the glass or melt transition temperature erases the thermal history of the sample. Because of that, the first cooling cycle or second heating cycle is normally used to study the thermal events of a sample. DSC has some

advantages; these include simple sample preparation, short experiment times and a wide range of temperatures available in heating and cooling cycles. There are some limitations in using conventional DSC. Firstly, since DSC measures the sum of the thermal events, the results may be difficult to interpret when there are overlapping transitions. Secondly, this technique is not sensitive enough to measure weak transitions and lastly, heat flow signals in DSC depend on the sample size and heating rate and they decrease with the decrease in either of these parameters.

1.2.1.1. Temperature modulated differential scanning calorimetry (TMDSC)

It is important to determine if there are multiple events occurring at similar temperatures and also to distinguish weak transitions from noise in complex composite materials. Temperature-modulated DSC (TMDSC) is a variant of DSC which, in addition to offering the same information as conventional DSC, provides additional insight in the thermal behavior of materials by separating the heat flow data into reversing and non-reversing events.[63] TMDSC and its derivatives have been used to resolve both weak and multicomponent transitions that would be difficult to distinguish in a conventional DSC scan.[64-68]

TMDSC uses the same heat flux cell design and measures the difference in heat flow between a sample and a reference as a function of time and temperature. In TMDSC, a different temperature program is applied compared to the heating profile of the conventional DSC. In TMDSC heating and cooling processes, in addition to the conventional linear heating ramp, a sinusoidal modulation (+/- X ºC/min) is superimposed to yield a continuously increasing heating profile which is not linear.[66] The effect of this more complex temperature program can be interpreted such that two

experiments (one at the conventional linear heating rate and one at a sinusoidal heating rate) are run simultaneously on the sample. Heating rate, temperature amplitude of modulation, and period of modulation are the parameters for these simultaneous experiments.

Conventional DSC compares the difference in the amount of energy adsorbed or released by a sample and a reference as a function of temperature and time where no (or at least little) temperature gradient exists. In this case, a combination of heat flow signals results, where one depends on the rate of temperature change and the other depends on the temperature at which the transition occurs.[69] Heat flow rate can be expressed as:

$$\frac{dQ}{dt} = C_P \frac{dT}{dt} + f(t,T) \tag{1.5}$$

where dQ/dt is total heat flow rate (mW), C_P is the reversing heat capacity (J/g), and dT/dt is the heating rate. C_P(dT/dt) represents the thermal component which depends on the heat capacity of the material, and $f(t, T)$ represents the kinetic process, which is often irreversible.

The temperature profile of TMDSC contains a trend that is modulated by small perturbations and can be expressed as:[69]

$$T = T_0 + qt + B\sin(\omega t) \tag{1.6}$$

where T_0 is the initial temperature, q is the heating rate, ω is the frequency, and B is the amplitude of temperature modulation. The TMDSC signal can be described as the following:

$$\frac{dQ}{dt} = C_P q + f'(t,T) + C_P B\omega \cos(\omega t) + C \sin(\omega t). \quad (1.7)$$

The first two terms provide the same information as in conventional DSC for reversing and non-reversing events. The additional terms contain information regarding the heat capacity from the heat flow that responds the rate of change of temperature. Figure 1.3 compares TMDSC thermograms for reversing, non-reversing, and total heat flow of adsorbed PVAc on silica at around glass transition of the sample.

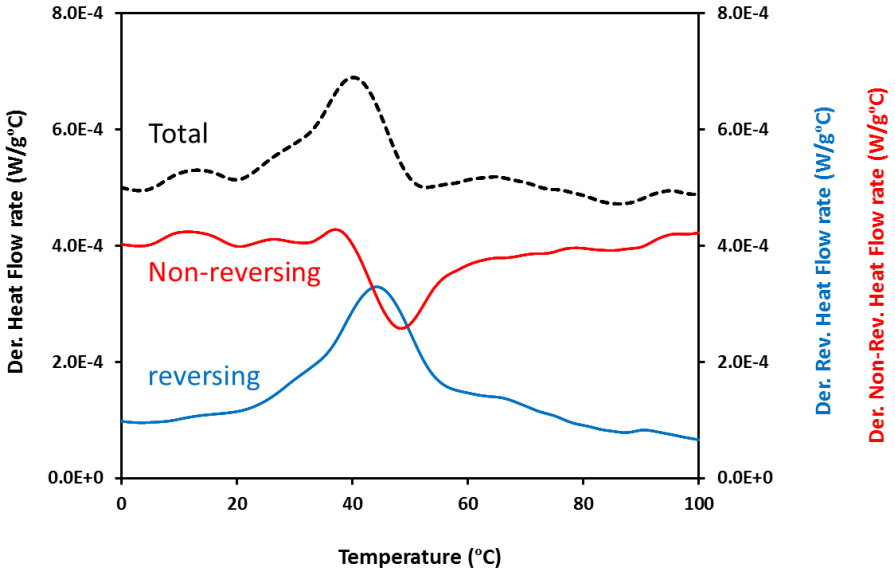

Figure 1.3. TMDSC thermogram of adsorbed PVAc on Cab-O-Sil silica showing derivative of total heat flow (dashed black line), non-reversing (red line), and reversing (blue line) curves.

1.2.2. Glass transition temperature

The glass transition is the reversible transition at which long-range translational motion occurs for amorphous solid polymer chain segments.[70,71] This is a transition from the glassy (without significant molecular mobility) into the rubbery (with more mobility than glassy) state and happens with an increase in ΔC_p.[72,73] In order to compare the thermal behavior of polymers in the glass transition region, a specific temperature called glass transition temperature (T_g) can be defined. T_g is approximately the midpoint of the transition range where, the transition between the glassy and rubbery states occurs. For DSC measurements, T_g is the temperature at half-height of the heating capacity decrease (Figure 1.4) or the temperature at which the first derivative of heat flow rate reaches the maximum (Figure 1.3).

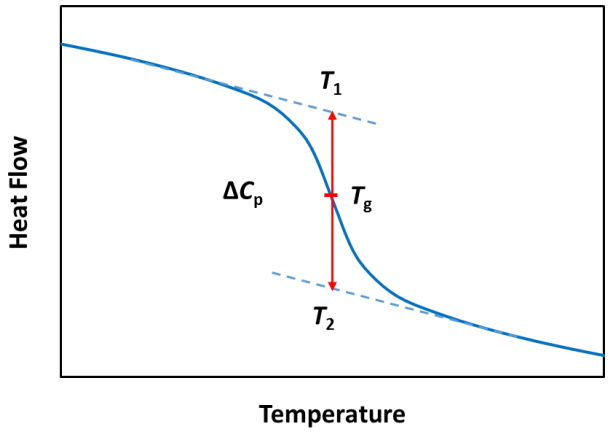

Figure 1.4. Determination of glass transition temperature in a DSC heating scan curve (endotherm down).

The following three contributions are the main effects on the increment of ΔC_p at T_g:

$$\Delta C_P = \Delta C^c + \Delta C^h + \Delta C^v \qquad (1.8)$$

where ΔC^c, ΔC^h and ΔC^v are the conformational, free volume and vibrational frequency contributions to the heat capacity change, respectively.[74,75] Additionally, T_g can be observed by change in the slope of volume, enthalpy and entropy, compressibility and thermal expansion with temperature.[76] There are different theories of glass transition; these include free-volume, kinetic and thermodynamic theories. The free-volume theory will be discussed in this section and other theories might be found elsewhere.[37,57]

1.2.2.1. The free-volume theory

One of the main theories of glass transition temperature is the ″free-volume″ theory first developed by Eyring.[77] In this model, molecular motion depends upon the existence of holes, vacancies or voids; the hole moves when a segment of a polymer molecule moves to the hole. The presence of these holes is critical for molecular motion and they are collectively called free volume. With increasing temperature, the oscillations due to the thermal motions of polymer chains, and therefore the free volume increases. The temperature at which the free volume is sufficient for positional change of polymer segments is the T_g.

Fox and Flory[78,79] studied the relationship of glass transition and free volume with molecular mass and relaxation time. They found that free volume above T_g could be related to the expansion coefficients in rubbery and glassy states (α_R and α_G respectively) as shown below:

$$v_f = K + (\alpha_R - \alpha_G)T \qquad (1.9)$$

where K represents the free volume at 0 K. Observing the same specific volume/temperature relationships for polystyrene with different molecular masses below

T_g showed that the polymer segments' conformational arrangement is independent of temperature and molecular mass below the T_g.[80] The free volume at T_g then was shown to be:

$$v_f = v - \left(v_{0,R} + \alpha_G T\right) \tag{1.10}$$

$$v = v_{0,R} + \alpha_R T \tag{1.11}$$

where v is the specific volume, $v_{0,G}$ and $v_{0,R}$ are the volume extrapolation to 0 K. Figure 1.5 illustrates a practical means of estimating v_f when all the free volume comes from the expansion of free volume.

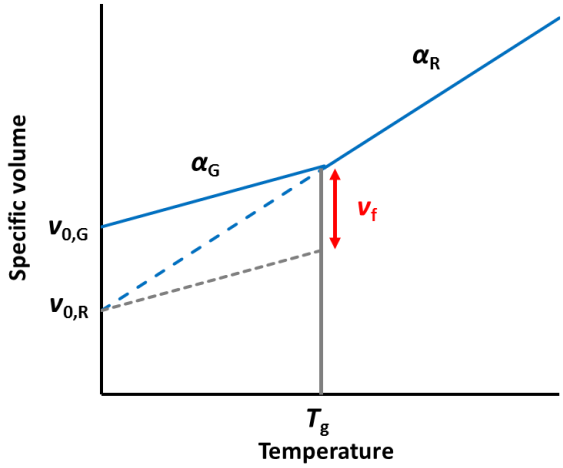

Figure 1.5. The temperature dependence of free volume in an amorphous polymer around T_g.[37]

1.2.2.2. Factors that affect the T_g

The value of T_g depends on the mobility of the polymer chains and decreases with the mobility of the polymer segments. Generally, anything that restricts conformational changes within the polymeric chain should raise the T_g. A polymer chain that moves

easily can change from a glassy to a rubbery state at a low temperature. However, a polymer that does not move as easily, requires a relatively higher temperature for the transition from the glassy to rubbery state. There are several factors such as molecular mass, crosslinking, crystallization, chemical structures, tacticity, and presence of fillers and plasticizers that can affect the T_g.[81-90] In general, T_g increases with the factors that increase the required energy for the onset of molecular motion.

The polymers with low molecular mass have more mobility than similar polymers with higher molecular mass due to the presence of more chain-ends. Usually the chain-end segments have more freedom, and hence more free volume, to move compare to the central segments. The general relationship between T_g and molecular mass M, is related to the T_g at infinite molecular mass ($T_{g\infty}$):[91]

$$T_g = T_{g\infty} - \frac{K}{(\alpha_R - \alpha_G)M} \qquad (1.12)$$

where K is a constant that depends on the polymer. This equation follows the free volume theory where the free volume decreases with an increasing number of connected mers and a decreasing number of chain-ends.

Varying the crosslinking and crystallinity of polymers also affects their thermal behavior. The T_g increases with the increasing crosslink density of the polymer. Since crosslinking decreases the conformational entropy, mobility decreases and T_g increases. Semicrystalline polymers such as polyethylene and polyamide also show glass transitions in their amorphous regimes. T_g usually increases with decreasing molecular motion. Many semicrystalline polymers exhibit two glass transitions: a lower one corresponding

to the fully amorphous sections of the polymer and the higher T_g that occurs in the semicrystalline parts of the polymer.

The chemical structure of polymers also plays an important role in thermal activity. In vinyl homopolymers with flexible side-chains, the T_g decreases due to the internal diluent effect of the flexible side-chains with decreasing the frictional interactions between chains.[89,92] Typically, as the number of -CH_2- groups in a side-chain increases, the T_g decreases due to the increase in the free volume and also because of their effect on chain packing, and the enabling motions about their side chains. However, with longer side-chains there is a chance of the enhancement of crystallinity and increase in T_g. Polymers with bulky groups such as aromatic rings, tend to have relatively elevated T_g's. This is because of the steric hindrance effect of bulky side-chains and the increase in the energy required for molecular motion.

The effect of tacticity on T_g is significant. The energy difference between the two main stereo isomers for syndiotactic polymers is greater than that of isotactic polymers when none of the substituents are hydrogen. For example, the T_gs of syndiotactic and isotactic PMMA are around 120 and 40 ºC, respectively.[93] However, in case of PMA and other polymers where one substituent is hydrogen, there is no significant difference in the glass transitions of the different tacticities.[94]

Plasticization also affects the thermal and mechanical properties; it lowers the T_g by increasing flexibility and reducing stiffness. There are two main categories of plasticizers: internal and external plasticizers. Internal plasticizers are a part of the polymeric system, e.g., the monomer of a polymer with a lower T_g in a copolymer compound. The polymer with the lower T_g would be expected to have decreased packing

efficiency and increased available free volume in the system. External plasticizers, which usually are low vapor pressure materials, are more widely used. The molecular mass and chemical structure of the plasticizers as well as their polarity and size are important because they affect the polymer/plasticizer compatibility.[53,82]

Intermolecular and intramolecular hydrogen bonding between polymer segments can also affect the glass transition of polymers and polymer blends.[95] For example, N-methylated polyamide with less hydrogen bonding shows a lower T_g. Increasing the number of -CH_2- groups between carboxamide groups of a nylon structure causes the structure to become more like polyethylene and the T_g decreases. The hydrogen bonding between polymer chains and a surface has a significant effect on the thermal properties of the polymer chains at the interface.[14,51] The amount of hydrogen bonding on surface has a direct relationship with the glass transition of the chains close to the surface. Once on the surface, it is difficult to remove the chains especially in the case of multiple attachment points. Although breaking one hydrogen bond is easy, breaking two of them is more complicated; this is because they either need to be broken simultaneously or the second bond should be broken before the first one reforms. It is even more difficult in the case of several hydrogen bonds. Therefore, the kinetics of breaking hydrogen bonds is often slower than the kinetics of bonding them.[37]

1.3. SIGNIFICANCE OF ADSORPTION

Adsorption is the enrichment of atoms, ions, or molecules from a gas or liquid on an interfacial layer neighboring to a solid wall.[96] In this process, the adsorbate phase attaches to the adsorbent solid surface in a chemical (chemisorption) or physical (physisorption) process.[97] Chemisorption occurs when the adsorbate adsorbs to the

surface by forming chemical bonds. Chemisorption is limited to monolayer coverage because it requires bond formation.[98,99] Physisorption occurs when the adsorbate adsorbs to the surface without the formation of chemical bonds and only through weaker interactions such as van der Waals. Physisorption, which is studied in this work, is a reversible process due to weak interactions and may not be limited to monolayer coverage because the interactions are not limited to the number of available sites. The possibility of formation of multilayer coverage gives the opportunity to calculate the pore volume.[32] The equilibrium adsorbed amount on a surface depends on the intermolecular (adsorbate/adsorbate and adsorbate/adsorbent) interactions and parameters like temperature and gas pressure. Several methods have been developed for surface characterization by the adsorption process. Here, we explain some basic concepts and methods.

1.3.1. Surface tension

Surface tension, which can also be considered as surface energy, is one of the most important properties of liquid-gas interfaces and causes liquids to reduce specific surface areas.[100,101] Surface tension (γ), which depends on the composition of the liquid and vapor, temperature, and pressure is introduced as the proportionality constant between the work, ΔW, which is needed to increase the surface area of the liquid, and the change in surface area, ΔA:

$$\Delta W = \gamma \times \Delta A \qquad (1.13)$$

The surface tension is also defined as the force that acts on the liquid surface and tends to minimize the surface area. Therefore, in the absence of a force normal to the

surface, the surface remains flat. But, when the pressure on one side of the liquid/gas interface is larger than the pressure on the other side, the surface becomes curved to cancel the force due to pressure. The pressure difference between the two phases, ΔP, and the curvature of the surface are related according the Young-Laplace equation:

$$\Delta P = \gamma(\frac{1}{R_1} + \frac{1}{R_2}) \tag{1.14}$$

where ΔP is the Laplace pressure and R_1 and R_2 are the two principal radii of curvature.[102] For a spherical droplet with a radius R, the equation becomes:

$$\Delta P = \frac{2\gamma}{R} \tag{1.15}$$

Saturated vapor pressure, which refers to the pressure applied by a vapor in thermodynamic equilibrium with a liquid surface, is larger for a planar liquid surface ($R_1 = R_2 = \infty$) than for a curved liquid surface. The Kelvin equation[103] describes the relationship between the capillary radius and the saturated vapor pressure P:

$$RT \ln \frac{P}{P_0} = \gamma V_m(\frac{1}{R_1} + \frac{1}{R_2}) \tag{1.16}$$

where P_0 is vapor pressure above a flat surface and V_m is the molar volume of the liquid. For a spherical surface with radius, r, the equation becomes[104]

$$RT \ln \frac{P}{P_0} = \frac{2\gamma V_m}{r}. \tag{1.17}$$

The Kelvin equation can be applied to describe the capillary condensation process. The capillary condensation is the process of filling pore spaces with condensed liquid from the vapor at vapor pressures below the saturated vapor pressure. However, since the Kelvin equation does not take adsorbate/adsorbent interactions and adsorbed film

thickness into consideration, the modified Kelvin equation[105,106] provides a better description of experimental data by considering the adsorbed layer thickness on the pore wall, t_c, and also the effect of adsorbate/adsorbent interaction strength in terms of the contact angle, θ, of the liquid against the pore wall.

$$RT \ln \frac{P}{P_0} = -\frac{2\gamma \cos\theta}{\Delta\rho(r - t_c)} \qquad (1.18)$$

where $\Delta\rho$ is the difference in the bulk liquid and gas density and r is the mean radius of the curvature of the meniscus of the pore liquid. The modified Kelvin equation is the basis for many methods which are used to analyze the porous properties of mesoporous materials.[99]

1.3.2. Adsorption isotherm

The International Union of Pure and Applied Chemistry (IUPAC) has classified the sorption isotherm of materials with pore sizes ranging from 2 to 50 nm into six kinds of isotherms.[99] The appropriate IUPAC classification for each is shown in Figure 1.6. Type I, which is the Langmuir isotherm occurs usually and when the isotherm approaches a limiting value as p/p_0 goes to 1 and typically occurs for microporous materials. This condition is met mostly in chemisorption, where all the sites are occupied. Because of the narrow pore width and the high adsorption potential, micro pore filling is observed at relatively low pressures. Type II typically occurs for non-porous or macroporous materials with strong adsorbate/adsorbent interactions. In this isotherm, a clear monolayer/multilayer adsorption is observed and one can separate them at the inflection point, which is called point B where monolayer coverage is complete and multilayer coverage begins. The reversible type III isotherm is typical for nonporous materials with

weak interfacial interactions. This isotherm does not show a point B since it is convex for the entire range of the relative pressure. For types IV and V, the adsorption and desorption isotherms do not overlap over a certain external pressure region and they show a hysteresis loop. These isotherms typically occur for mesoporous materials. Type IV is more common for mesoporous adsorbents and show the formation of a monolayer at low pressures followed by multilayer formation at higher pressures as in case of type II isotherm. The initial part of type V sorption isotherm is related to type III isotherm indicating relatively weak attractive interactions. The hysteresis loop shows capillary condensation and the onset of the hysteresis loop shows the beginning of capillary condensation. Type VI isotherm is used to explain materials with strong adsorbent/adsorbate interactions and usually occurs at temperatures near the melting point of the adsorbed gas for a uniform and non-porous surface.[107-111]

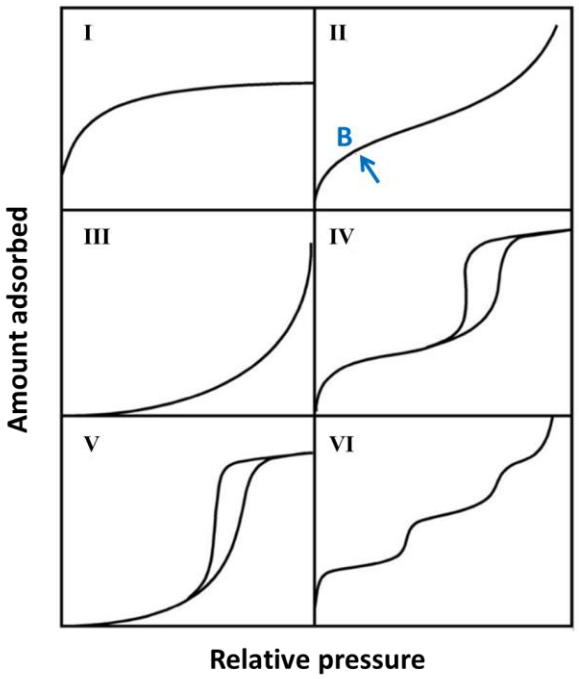

Figure 1.6. IUPAC classification of sorption isotherms.[96]

1.3.3. Pore size classifications

The IUPAC proposed the classification of pores based on their internal pore width.[96] In the case of a cylindrical pore, the pore width is the diameter of the cylinder and in the case of a slit, it is the wall to wall distance. If the internal pore width is less than 2 nm, the pore is known as a *micropore*. Pores with internal pore widths between 2 and 50 nm are *mesopores* and those with internal pore widths greater than 50 nm are classified as *macropores*.[112,113]

1.3.4. BET theory

Brunauer, Emmett, and Teller extended the Langmuir approach to multilayer adsorption and their equation is known as the BET equation.[114] The basic assumption was that the Langmuir equation applied to each layer.[32] The BET equation is used to determine the specific surface area; it uses adsorbing non-corrosive gases like nitrogen, argon, and carbon dioxide and can be put in the form of:

$$\frac{1}{v[(p_0/p)-1]} = \frac{c-1}{v_m c} \times \frac{p}{p_0} + \frac{1}{v_m c} \qquad (1.19)$$

where p and p_0 are the equilibrium and saturated pressure of the adsorbate gas at the temperature of adsorption, v is the volume of gas adsorbed at standard temperature and pressure (STP) and v_m is the volume of gas adsorbed at STP to produce a monolayer on the surface of the sample, c is a dimensionless constant, related to the enthalpy of the adsorbate on the sample and can be calculated using the parameters of a linear regression of the BET plot at the linear region usually between the relative pressures (p/p_0) of 0.05 and 0.30. However, it is sometimes challenging to separate the mono-multilayer adsorption processes, which usually is completed at relative pressure below 0.1. As a

result, the range of linearity of the BET plot over which the calculation is done should be reported. The BET constant, *c*, and the monolayer adsorbed gas quantity, v_m, can be determined using the slope, *S*, and intercept, *I*, of the linear BET fit of $1/v[(p_0/p)-1]$ as a function of p/p_0:

$$c = 1 + \frac{S}{I} \tag{1.20}$$

$$v_m = \frac{1}{S + I} \tag{1.21}$$

There are some problems with using the BET method. The area calculated by BET analysis in the case of very narrow cylindrical pores in the range of ultra-micropores (< 7 Å) is usually smaller than the real geometric area of pores. The reason is the extreme curvature of the pore channels and relatively large size of the adsorbate molecules. In some mesoporous materials with pore widths less than 40 Å the pore condensation is observed at pressures close to the monolayer/multilayer formation pressure and this may lead to an overestimation of monolayer capacity and consequently the BET surface area of the sample. A formal procedure has been suggested for reducing the bias in finding the linear range of BET plots. The BET constant, *c*, must be a positive and any negative number indicates that we work out of the valid range of BET theory.[99]

The BET equation has become the standard for determining the specific surface area usually with nitrogen at 77 K as the adsorbate. It is a relatively easy approach and the results are reasonably consistent. This equation covers isotherm types II to IV. A schematic diagram of the BET surface area measurement instrument is shown in Figure 1.7. In this method, the sample holder is first outgassed under vacuum and high

temperature and then the nitrogen gas is purged to the evacuated space above the sample. The sample holder goes down until the level of liquid nitrogen is above the sample. A sufficient volume of nitrogen gas is adsorbed on the sample to reach the first desired relative pressure. The volume of nitrogen at this pressure is measured and the pressure is increased to reach higher targeted relative pressures. The multipoint volume results then can be fitted to the BET theory to get the specific surface area. By increasing the relative pressure to around $p/p_0 = 1$ and subsequently decreasing it to around zero. In the case where there is hysteresis between the adsorption and desorption results, one can measure the pore size distribution applying one of the following models or one of many other available models.

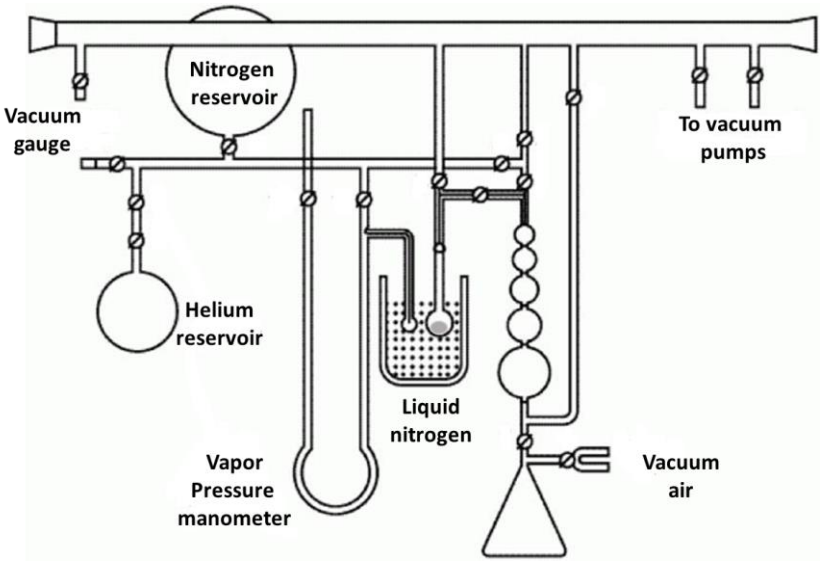

Figure 1.7. A schematic diagram of the BET instrument.

1.3.5. BJH method

The Barrett-Joyner-Halenda (BJH)[115] method was originally proposed to determine the pore size distribution of relatively wide-pore adsorbents based on the Kelvin equation.

However, it was repeatedly shown that it could be successfully applied to almost all types of porous materials. The model is based on the assumption that when the relative initial pressure is close to unity, all pores are filled with liquid. The desorption part of the isotherm is generally used as the initial data in BJH calculations (although applying of the adsorption part of the sorption is also possible). BJH can be formulated as:

$$V_{pn} = \left(\frac{r_{pn}}{r_{Kn} + \Delta t_n/2}\right)^2 \left(\Delta V_n - \Delta t_n \sum_{j=1}^{n-1} A c_j\right) \qquad (1.22)$$

where r_p is pore radius, v_p is pore volume, r_K is the inner capillary radius, Δt is thickness of adsorbed layer of nitrogen and A_c is the area exposed by the pore from which the physically adsorbed gas is desorbed.

1.3.6. Density functional theory (DFT)

Most classical macroscopic theories such as the BJH method do not give detailed and realistic descriptions of micropores and narrow mesopores. These models usually underestimate the pore sizes. To fill the gap between the molecular level and macroscopic approaches and have a more realistic description for the sorption and phase behavior of fluid in narrow pores in molecular level, microscopic theories seem to be necessary. Density Functional Theory (DFT) or molecular modeling methods such as Monte Carlo simulation (MC) and Molecular Dynamics (MD) offer a more accurate approach to calculate the pore size and pore volume distributions.[116-119] These methods have been extensively used to characterize micro- and mesoporous carbon, silica and zeolites.[117,120-122]

Non-Local Density Functional Theory (NLDFT) and Monte Carlo simulation (grand canonical ensemble) methods describe the local fluid structure near curved solid walls in

a more accurate way and the adsorption isotherm is determined based on the intermolecular potentials of the adsorbate/adsorbate and adsorbate/adsorbent interactions. The microscopic approaches are based on the assumption that the total isotherm consists of individual single-pore isotherms multiplied by their relative distribution $f(W)$:

$$N\left(\frac{P}{P_0}\right) = \int_{W_{min}}^{W_{max}} N\left(\frac{P}{P_0}, W\right) f(W) dW \qquad (1.23)$$

where $N(P/P_0)$ is the experimental adsorption isotherm, W is pore width and $N(P/P_0,W)$ is the isotherm of a single pore of width W.

1.4. COMPUTER MODELING INSIGHT

Together with experimental studies, computer modeling can be employed to provide more insight to intermolecular interactions, dynamics and structures of molecules in complicated systems. Molecular modeling is a theoretical system that is used to describe properties of molecular systems by means of an appropriate computational approach. Computational methods should be selected based on the experimental properties of interest and computer models should appropriately represent the system. Simulations are often used as a counterpart to experiments, not only to validate the experiments, but also to quantify the properties and provide information that is beyond the limits of experimental observation. Molecular simulations have the potential to characterize new materials without synthesizing them and are often used when experiments are not possible, time consuming or tedious.[123]

To simulate the behavior of systems for different purposes across scales in length and time, a variety of different methods have been developed. These computational

approaches include: ab initio and semi-empirical quantum mechanics (QM), molecular dynamics (MD) and Monte Carlo (MC), mesoscale simulations (coarse graining), and finite-element methods (FEM). Each of these methods is suitable for specific studies at certain time and length scales as schematically shown in Figure 1.8.

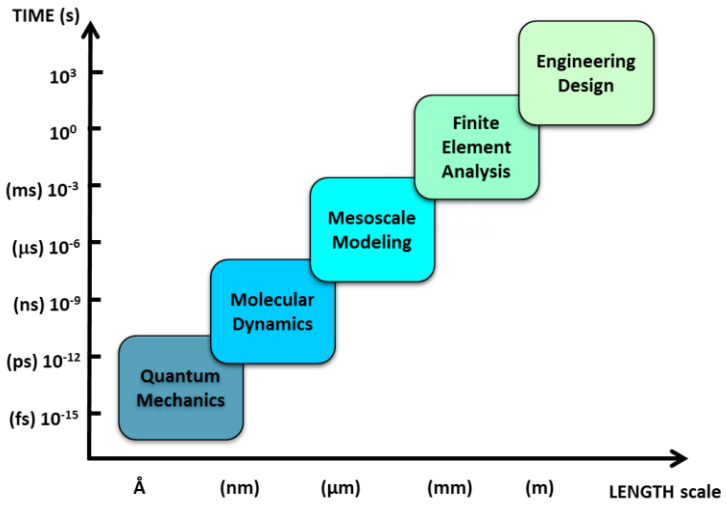

Figure 1.8. A hierarchical multiscale scheme of different modeling techniques across scales in length and time.[124]

The most common model for a molecular system contains atoms as point masses with positions in space that interact with each other. These interactions, which are functions of the positions and properties of the atoms, are fundamental quantities in molecular modeling and are defined as interaction energy. One of the critical issues in molecular modeling is the construction of appropriate functions for interaction energies. There are many parameter sets used to calculate the interaction energy, known as force fields. Force fields can be as simple as functions of interatomic distances to the solution of the Schrödinger equation for all the electrons of all atoms in the system.

The interest of the current work is to use computer simulation of molecules applying the fundamental equations to describe the intermolecular interactions between different systems. A brief introduction of the molecular dynamics will be given here. Chapters II, III, and V will then describe techniques and tools that are used to study and compare the dynamics and structures of different systems. It is important to notice that classical MD has been used. That means the quantum effects and laws of quantum physics, e. g., the motion of electrons have not been considered. Therefore, we need to consider the inaccuracies that arise from neglecting the quantum effects.

1.4.1. Molecular dynamics simulation

Molecular dynamics (MD) is a computer simulation technique used to estimate the equilibrium and dynamic properties of a system. MD simulation is used to determine interactions between bonded and non-bonded atoms which are defined as spheres with vector positions, *r*. The potential energy of the system only depends on the position of atoms and can be calculated as:

$$U(r) = U_{bonded}(r) + U_{non-bonded}(r). \tag{1.24}$$

The first term considers intramolecular interactions and the second term considers intermolecular interactions. The bonded potential energy can be formulated as:

$$E_{bonded} = \sum_{bonds} K_{r,ij}\left(r_{ij} - r_{ij,e}\right)^2 + \sum_{\substack{bond \\ angles}} K_{\theta,ijk}\left(\theta_{ijk} - \theta_{ijk,e}\right)^2 + \sum_{\substack{dihedral \\ angles}} \frac{1}{2} V_{\varphi,ijkl}\left[1 + \cos(n\varphi_{ijkl} - \varphi_{ijkl,e})\right] \tag{1.25}$$

where r, θ, and φ are bond length, bond angle, and torsional dihedral angle and K is a force constant. The terms including e in each potential term represent the equilibrium values and are force field parameters. Bonds and bond angles have harmonic functions and the dihedral term has a trigonometric form.

The non-bonded interactions are a mixture of Coulomb and Lennard-Jones terms.[125] The Coulombic term calculates the electrostatic interactions of partial charges between atoms and Lennard-Jones calculates van der Waals interactions, describing atomic repulsion because of overlaps of atoms and atomic attraction due to London dispersion.[126]

$$E_{non-bonded} = \frac{1}{4\pi\varepsilon_0} \sum_{ij\ nonbonded} \frac{q_i q_j}{r_{ij}} + \sum_{ij\ nonbonded} 4\varepsilon_{ij} \left(\left(\frac{\sigma_{ij}}{r_{ij}} \right)^{12} - \left(\frac{\sigma_{ij}}{r_{ij}} \right)^{6} \right) \qquad (1.26)$$

where q_i, q_j, and σ_{ij} are force-field parameters and r is the distance between two atoms.

MD simulations are not only used to describe energies of different states, but also used to simulate the time dependent behavior of molecular systems. In this method, the time evolution of the system is followed using the numerical integration of the equations of motion:

$$-\frac{\partial E}{\partial x} = m\,\frac{\partial^2 x}{\partial t^2} \quad \text{or} \quad F(t) = m \cdot a \qquad (1.27)$$

where, F is the force vector at time t, m is the mass, and a is the acceleration of the atom. The force applied on the particle is evaluated from the derivative of the energy function, E, which includes potential and kinetic energies. To calculate this equation analytically,

tracking the position x changes with respect to time is necessary. By substituting the numerical second derivative in Equation 1.27:

$$\frac{\partial^2 x}{\partial t^2} = \frac{x(t+\Delta t) + x(t-\Delta t) - 2x(t)}{\Delta t^2} = \frac{F(t)}{m} \qquad (1.28)$$

solving for $x(t + \Delta t)$, which describes the position at the next time step,[127] Equation 1.29 is derived.

$$x(t+\Delta \mathrm{t}) = 2x(\mathrm{t}) - x(\mathrm{t}-\Delta \mathrm{t}) + \frac{\Delta t^2 F(t)}{m} \qquad (1.29)$$

An energy-minimized structure is used as the initial guess structure. At this point, $t = 0$ and there is no $x(t\text{-}\Delta t)$. $F(t)$ is also zero since the structure is energy minimized. Therefore, the first displacement ($x(0+\Delta t)$) is chosen based on the temperature in a random direction.

$$k_B T = m\langle v_x^2 \rangle \qquad (1.30)$$

$$\text{where} \quad v_x = \frac{x(0+\Delta t) - x(0)}{\Delta t}.$$

Here we set a time step Δt and determine the force at the new geometry and take a new step using Equation 1.29. At the end of the simulation, we will obtain a trajectory that is a collection of coordinates as a function of time with a fixed number of particles.

1.5. WETTING THEORY

Wetting phenomena describe the intermolecular interactions between a liquid and a solid surface in the presence of a gas (usually air). Wettability is defined as the balance between the adhesive forces between liquid and surface and cohesive forces within the liquid and the surface. If the adhesion between the liquid and the surface is greater than

the cohesion within the liquid, the liquid will wet the surface and if the cohesion is greater than the adhesion, a droplet will be formed.

1.5.1. Superhydrophobicity

Superhydrophobicity is a phenomenon in which liquid water cannot wet the surface it rests on. A solid surface is considered superhydrophobic if it exhibits a water contact angle (CA) greater than 150° and a roll-off angle (contact angle hysteresis) less than 10°.[128] This non-wetting phenomenon (Lotus effect)[129] has been observed in nature on the surface of the lotus leaf, where water droplets on the surface form spherical balls (θ_{CA} around 160°) and minimize the contact surface. The very high water repellency and very low sliding angle result in self-cleaning properties, where dust particles are collected by water droplets as they roll off the surface.[130] Water repellent surfaces are very important in terms of technological applications as frictionless, self-cleaning, and anti-icing surfaces. Superhydrophobicity is achieved by a combination of surface roughness and a low-surface energy coating.[131] The roughness is usually as a result of micro or nano-size structures that enhance the hydrophobic properties of the surface.[132] Nanoscale roughness decreases the transition state energy between metastable states and microscale roughness could increase the Laplace pressure.[133]

1.5.2. Wetting of smooth solid surfaces

The wetting of a surface can be described by the tangent of the sessile water droplet at the connection point of the three phases of liquid, air and solid. The tangent is the contact angle (CA) and the connection border line between the surface and the sessile droplet is known as the contact line (CL). Figure 1.9 shows the contact angle of a droplet at the

triple phase (water, solid surface and air) contact point. The estimation of interfacial tension between the solid surface and the liquid is done by measuring the CA of the droplet at the CL. Water droplets on surfaces with relatively low surface energy maintain a semi-spherical shape and exhibit a more than 90º CA. The reason for this is that the cohesive forces within the water droplet overcomes the adhesion forces at the interface. Surfaces with CAs greater than 90º are known as hydrophobic surfaces.

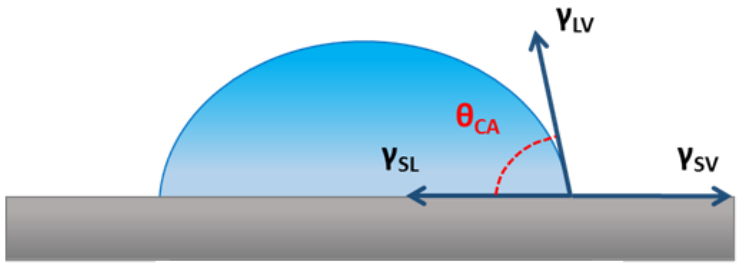

Figure 1.9. The contact angle of a droplet at the triple phase contact.

The wettability of a flat surface, described by the CA of a liquid droplet on a solid surface, is given by Young's equation.[134] By the projection of the three interfacial tensions in Figure 1.9 the contact angle can be derived as:

$$\cos\theta = \frac{\gamma_{SV} - \gamma_{SL}}{\gamma_{LV}} \qquad (1.31)$$

where γ_{SL}, γ_{SV}, and γ_{LV} are the interfacial surface tensions of the solid-liquid, solid-gas, and liquid-gas interfaces, respectively. Young's equation results from the thermodynamic equilibrium of the free energy at the solid-liquid-vapor interphase and shows that the CA of liquid on surface is a function of both liquid and solid surface tension. Surfaces with lower surface tensions maintain relatively higher CAs and liquids with lower surface energies tend to exhibit lower CAs.

1.5.3. Heterogeneous surface

The Young-Laplace equation suggests a single contact angle for a homogenous ideal surface. However, in reality, there is a degree of heterogeneity for any clean and smooth surface due to small variations in the inherent roughness of the surface as well as possible contaminations. Heterogeneous surfaces exhibit a series of CAs. The minimum and maximum of these CAs are named the receding and advancing, respectively (Figure 1.10). The receding CA is measured before the triple contact point recedes and the advancing CA is measured before this point of the droplet advances.[135,136] The difference between the advancing and receding CAs is referred to as hysteresis and shown as:

$$\theta_{Hysteresis} = \theta_{Advancing} - \theta_{Receding} \qquad (1.32)$$

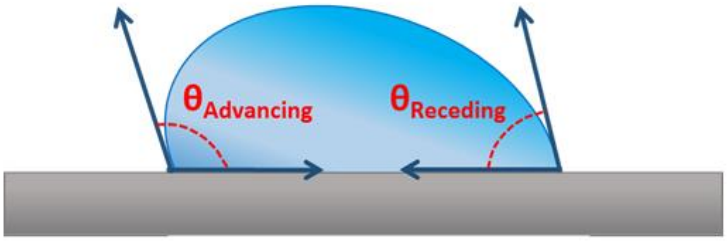

Figure 1.10. The advancing and receding contact angles of a droplet on a surface.

1.5.4. Wetting of rough surfaces

The absence of an ideal smooth surface requires the modification of the Young model and consideration of the effect of surface roughness on wettability. Several models such as those of Wenzel[137] and Cassie-Baxter[138] have been proposed to describe the contact angle at a rough solid surface. The contact angle of a surface in a Wenzel state is predicted by Wenzel's equation, which describes a homogeneous wetting regime:[132]

$$\cos\theta' = \frac{r(\gamma_{SV} - \gamma_{SL})}{\gamma_{LV}} = r\ \cos\theta \qquad (1.33)$$

where θ' is the Wenzel apparent contact angle on a rough surface, θ is the Young's CA on the corresponding smooth surface, and r is the surface roughness factor. This factor, r, which always has a value greater than 1, represents the ratio of real area to apparent contact area. In this model, the roughening process makes a hydrophobic surface more hydrophobic and a hydrophilic surface more hydrophilic.

With an increase in the roughness of the surface, the hydrophobicity of the surface will be increased due to the trapping of air between the grooves of the interface and the presence of a layer between the surface and the liquid droplet. Cassie and Baxter modified the Wenzel model to consider the air as a fraction of surface that enhances the wettability properties of the surface:

$$\cos\theta' = r_f\ f\cos\theta\ + f - 1 \qquad (1.34)$$

where r_f is the roughness ratio of the wet surface area and f is the fraction of solid surface area wet by the liquid. One might notice that the reduction in the solid fraction and increase in the air fraction can enhance the water repellency. Figure 1.11 shows the behavior of water droplets on rough surfaces according to the Wenzel and Cassie-Baxter models.

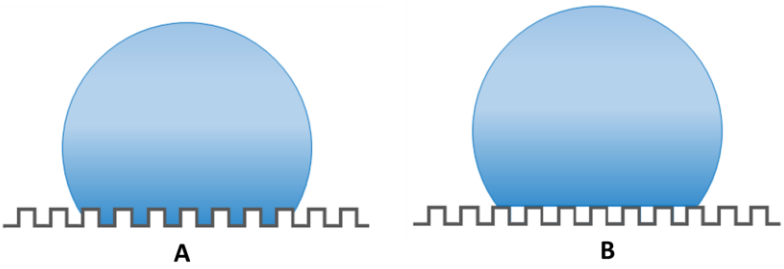

Figure 1.11. The wetting states on surfaces A) Wenzel and B) Cassie-Baxter.

Several experimental and modeling studies have focused on developing surface roughness to improve superhydrophobicity through the investigation of both microscale and nanoscale features.[139,140] Many other studies have been done to enhance the superhydrophobicity by lowering the surface energy.[141-143] There are two approaches, top-to-bottom (e.g., physical and chemical etching and lithography) and bottom-to-top (e.g., physical and chemical depositions), in order to prepare a micro/nano textured solid surfaces. A wide range of techniques such as electrodeposition,[144-146] chemical bath deposition,[147,148] chemical etching,[149] spin coating,[150,151] photolithography,[152] chemical vapor deposition,[153] spraying,[154,155] Bosch processes,[156] and sandblasting[157] have been applied to create a micro- and/or nanostructured surface following one of the mentioned approaches. Decreasing the surface energy of materials is the second requirement for preparing a superhydrophobic surface and is usually done by functionalizing the surface with -(CF_x) and -(CH_x) groups using silanization and acetone treatments.[154,156]

1.5.5. Characterization techniques

Usually there is a difference between the physical characterization of a real surface and the simplified theoretical understanding of wetting. This is even more evident in the case of more structurally complicated and hierarchical superhydrophobic surfaces. It seems critical to be familiar with assumptions of characterization techniques and understand the limitations and nature of each measurement technique. The contact angle has always been a primary property used to quantify the hydrophobicity of surfaces. However, the static contact angle measurement alone is not enough for the

characterization of heterogeneous surfaces. Therefore, a number of studies use dynamic methods and hysteresis to get a more complete characterization of surface structures. Knowing all of this, it still seems that a more detailed technique with a focus on nanoscale wetting is needed. There are some methods such as goniometry and Wilhelmy that are used to characterize the wettability properties of a surface. The most popular technique that we also use in this work is the contact angle goniometry.

1.5.5.1. Contact angle goniometry

The contact angle is a wettability measurement at the triple phase contact line that ignores the effect of any surface chemical heterogeneity away from the contact line. Therefore the theoretical models suggested for non-ideal surfaces such as Wenzel and Cassie-Baxter are not valid unless the properties of the entire surface are represented well by the triple point line.[158] However, inconsistency between the wettability at the triple point and within the water droplet should not be an issue if the chemistry and roughness is uniform through the surface.

Water contact measurements are usually done by taking images of 2 to 5 μl deionized water droplets placed in different spots of the surface. The tangent to the connection point of the three phases can be drawn by different methods such as snake-based[159] and LB-ADSA[160] techniques. In this work, the water droplet images were digitally captured via a high resolution Proscope camera capable of recording 15 fps at a 640x480 resolution. Figure 1.12 shows a handmade instrument that was used to take images and the fitting of the droplet image using the LB-ADSA approach.

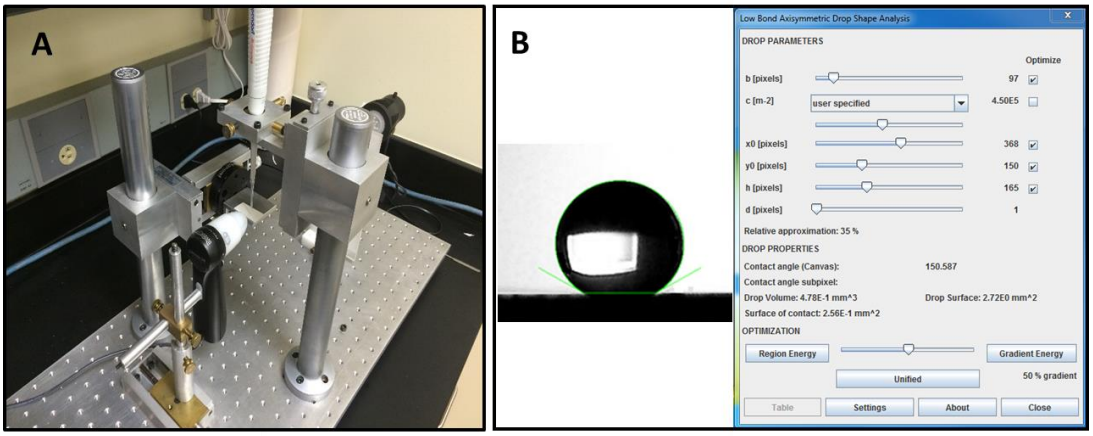

Figure 1.12. A) Homemade contact angle measurement instrument, B) a droplet of water on treated graphene oxide surface and the LB-ADSA interface with appropriate parameters to fit a circle to the droplet.

1.5.6. Microscopic contact angle

The macroscopic contact angle, θ_∞, is related to the microscopic contact angle θ through the modified Young's equation; it considers the contact line tension τ and the contact area radius r_B of a microscopic droplet.[161]

$$\gamma_{SV} = \gamma_{SL} + \gamma_{LV}\cos\theta + \frac{\tau}{r_B}. \qquad (1.35)$$

The Young's equation is recovered as $1/r_B \to 0$. The relationship between the macroscopic and microscopic contact angles can be written as:

$$\cos\theta = \cos\theta_\infty - \frac{\tau}{\gamma_{LV}}\frac{1}{r_B} \qquad (1.36)$$

1.5.7. Hydrophobicity of graphene surfaces

Among the substrates developed for superhydrophobic materials, carbon-based nanomaterials such as carbon nanotubes (CNT) and graphene have attracted extensive attention due to their low densities and high surface roughnesses.[139] Graphene is a two-dimensional form of carbon with a planar hexagonal arrangement of sp^2 bonded carbon atoms. Novoselov and co-workers demonstrated, for the first time, that single two-dimensional sheets could be isolated from graphite using a straightforward micromechanical cleavage technique.[162] This flat monolayer, honeycomb lattice form of carbon atoms is the starting point of calculations on graphite, carbon nanotubes and fullerenes.[163] Single-layer graphene which might be the thinnest and strongest material ever measured,[164,165] has gained a lot of interest due to its novel mechanical, thermal, and electrical properties.[166-174] Graphene sheets, also exhibit a very large specific surface area (up to 2630 $m^2 g^{-1}$).[175]

Graphene can be obtained by various methods such as micromechanical cleavage of graphite,[162] chemical exfoliation,[176] chemical vapor deposition,[177] and epitaxial growth.[178] Aggregation is one of the biggest hindrances to the exploitation of the properties of graphene sheets. Obtaining the high specific surface area associated with individual graphene layers is unfeasible due to the natural tendency of graphene sheets to re-aggregate to form graphite as a result of weak van der Waals interactions.

In general, surface roughness and the removal of the epoxide, hydroxyl, carbonyl, and carboxylic acid functional groups from the surface increase the contact angle of graphene sheets. To further enhance the hydrophobicity of the structure and thus prepare a superhydrophobic surface, low surface energy coatings can be useful. Wang et al.[179]

showed that graphene layers are more water repellant than graphite. They measured a contact angle of 127° for water on graphene. Shin and coworkers[180] studied the surface energy of epitaxial growth graphene sheets on a SiC surface. They observed a significant increase in the contact angle after adding one layer of graphene to the surface (from 69° to 92°). Although they claimed that there is no thickness dependence of the contact angle, Taherian and coworkers[181] observed that the contact angle of a water droplet changes with the number of layers. They reported a contact angle of 95-100° for a single layer and around 90° for 2 to 6 layers of graphene sheets. Rafiee and coworkers[182] also showed that the contact angle depends on the number of layers of graphene. Shih et al.[183] stated that previously the contact angle (around 125°) that has been known for a long time was not accurate and that the highest contact angle is reported to be 96°. Zhang and coworkers[184] recently found that in asymmetrically functionalized monolayer graphene, grafted functional groups on one side of graphene can change the contact angle of water on the other side significantly. Lin et al.[141] applied silane treatment to a graphene aerogel (three dimensional structure with conductive interconnections between the individual sheets)[185] and the resulting contact angle was as high as 160°. It seems that due to the huge effect of the substrate on which the graphene has been coated, unreliable and differing conclusions on the contact angle and wettability of these coated surfaces have been reported.

1.6. REFERENCES

(1) Fleer, G.; Cohen Stuart, M. A.; Scheutjens, J. M. H. M.; Cosgrove, T.; Vincent, B. *Polymers at interfaces*; Springer Science & Business Media: London, UK, **1993**.

(2) Fukao, K.; Miyamoto, Y. *Phys. Rev. E* **2001**, *64*, 011803.

(3) Zou, H.; Wu, S.; Shen, J. *Chem. Rev* **2008**, *108*, 3893.

(4) Parida, S. K.; Dash, S.; Patel, S.; Mishra, B. *Adv. Colloid Interface Sci.* **2006**, *121*, 77.

(5) Shin, Y.; Lee, D.; Lee, K.; Ahn, K. H.; Kim, B. *J. Ind. Eng. Chem.* **2008**, *14*, 515.

(6) Metin, B.; Blum, F. D. *Langmuir* **2009**, *26*, 5226.

(7) Madathingal, R. R.; Wunder, S. L. *Thermochim. Acta* **2011**, *526*, 83.

(8) Lin, Y.; Liu, L.; Xu, G.; Zhang, D.; Guan, A.; Wu, G. *J. Phys. Chem. C* **2015**, *119*, 12956.

(9) Kim, S.; Mundra, M. K.; Roth, C. B.; Torkelson, J. M. *Macromolecules* **2010**, *43*, 5158.

(10) Mundra, M.; Ellison, C.; Rittigstein, P.; Torkelson, J. *Eur. Phys. J. Spec. Top.* **2007**, *141*, 143.

(11) Füllbrandt, M.; Purohit, P. J.; Schönhals, A. *Macromolecules* **2013**, *46*, 4626.

(12) Ober, R.; Paz, L.; Taupin, C.; Pincus, P.; Boileau, S. *Macromolecules* **1983**, *16*, 50.

(13) Linse, P. *Soft Matter* **2012**, *8*, 5140.

(14) Blum, F. D.; Young, E. N.; Smith, G.; Sitton, O. C. *Langmuir* **2006**, *22*, 4741.

(15) Kulkeratiyut, S.; Kulkeratiyut, S.; Blum, F. D. *J. Polym. Sci., Part B: Polym. Phys.* **2006**, *44*, 2071.

(16) Lee, L.-T.; Somasundaran, P. *Langmuir* **1989**, *5*, 854.

(17) Chakraborty, A. K.; Golumbfskie, A. J. *Annu. Rev. Phys. Chem.* **2001**, *52*, 537.

(18) Zeng, Q.; Yu, A.; Lu, G. *Prog. Polym. Sci.* **2008**, *33*, 191.

(19) Ghanbari, A.; Ndoro, T. V.; Leroy, F.; Rahimi, M.; Böhm, M. C.; Müller-Plathe, F. *Macromolecules* **2011**, *45*, 572.

(20) Yang, M.; Koutsos, V.; Zaiser, M. *J. Phys. Chem. B* **2005**, *109*, 10009.

(21) Tallury, S. S.; Pasquinelli, M. A. *J. Phys. Chem. B* **2010**, *114*, 4122.

(22) Van der Beek, G.; Cohen Stuart, M.; Fleer, G.; Hofman, J. *Langmuir* **1989**, *5*, 1180.

(23) Silberberg, A. *J. Chem. Phys.* **1968**, *48*, 2835.

(24) Felter, R.; Ray, L. *J. Colloid Interface Sci* **1970**, *32*, 349.

(25) Stuart, M.; Scheutjens, J. M. H.; Fleer, G. *J. Polym. Sci. Polym. Phys.* **1980**, *18*, 559.

(26) Vander Linden, C.; Van Leemput, R. *J. Colloid Interface Sci* **1978**, *67*, 48.

(27) Kabomo, M. T.; Blum, F. D.; Kulkeratiyut, S.; Kulkeratiyut, S.; Krisanangkura, P. *J. Polym. Sci., Part B: Polym. Phys.* **2008**, *46*, 649.

(28) Wiśniewska, M. *Appl. Surf. Sci.* **2012**, *258*, 3094.

(29) Kozlov, M.; McCarthy, T. J. *Langmuir* **2004**, *20*, 9170.

(30) Bouchaud, E.; Daoud, M. *J. Phys.* **1987**, *48*, 1991.

(31) Langmuir, I. *J. Am. Chem. Soc.* **1918**, *40*, 1361.

(32) Adamson, A. W.; Gast, A. P. *Physical chemistry of surfaces*; John Wiley & Sons, Inc.: Los Angeles, Californi, **1967**.

(33) Klein, J.; Pincus, P. *Macromolecules* **1982**, *15*, 1129.

(34) Eisenriegler, E.; Kremer, K.; Binder, K. *J. Chem. Phys.* **1982**, *77*, 6296.

(35) Jones, R. A.; Richards, R. W. *Polymers at surfaces and interfaces*; Cambridge University Press, **1999**.

(36) Enkel, E., Rumbach, B. Z. *Electrochem.* **1951**, *55*, 612.

(37) Sperling, L. H. *Introduction to physical polymer science*; John Wiley & Sons, 2015.

(38) Balazs, A. C.; Emrick, T.; Russell, T. P. *Science* **2006**, *314*, 1107.

(39) Hudec, I.; Sain, M. M.; Kozankova, J. *Polym. Test.* **1991**, *10*, 387.

(40) Wallace, W.; Van Zanten, J.; Wu, W. *Phys. Rev. E* **1995**, *52*, R3329.

(41) Washiyama, J.; Creton, C.; Kramer, E. J. *Macromolecules* **1992**, *25*, 4751.

(42) Okuom, M. O.; Metin, B.; Blum, F. D. *Langmuir* **2008**, *24*, 2539.

(43) Blum, F. D.; Xu, G.; Liang, M.; Wade, C. G. *Macromolecules* **1996**, *29*, 8740.

(44) Jo, H.; Blum, F. D. *Langmuir* **1999**, *15*, 2444.

(45) Porter, C. E.; Blum, F. D. *Macromolecules* **2000**, *33*, 7016.

(46) Blum, F. D.; Metin, B. *Polym. Prepr.* **2008**, *49*, 667.

(47) Sargsyan, A.; Tonoyan, A.; Davtyan, S.; Schick, C. *Eur. Polym. J.* **2007**, *43*, 3113.

(48) Maddumaarachchi, M.; Blum, F. D. *J. Polym. Sci., Part B: Polym. Phys.* **2014**, *52*, 727.

(49) Reddy, S.; Kuppa, V. K. *Synth. Met.* **2012**, *162*, 2117.

(50) Harmer, M. A.; Farneth, W. E.; Sun, Q. *J. Am. Chem. Soc.* **1996**, *118*, 7708.

(51) Khatiwada, B. K.; Hetayothin, B.; Blum, F. D. *Macromol. Symp.* **2013**, *327*, 20.

(52) Metin, B.; Blum, F. D. *J. Chem. Phys.* **2006**, *125*, 054707.

(53) Nambiar, R. R.; Blum, F. D. *Macromolecules* **2008**, *41*, 9837.

(54) Rissanou, A. N.; Harmandaris, V. *Soft Matter* **2014**, *10*, 2876.

(55) Rissanou, A. N.; Harmandaris, V. *Macromolecules* **2015**, *48*, 2761.

(56) Zhang, J.; Lou, J.; Ilias, S.; Krishnamachari, P.; Yan, J. *Polymer* **2008**, *49*, 2381.

(57) Menczel, J. D.; Prime, R. B. *Thermal analysis of polymers: fundamentals and applications*; John Wiley & Sons, 2014.

(58) Sandler, S. R.; Karo, W.; Bonesteel, J.; Pearce, E. M. *Polymer synthesis and characterization: a laboratory manual*; Academic Press: Brooklyn, New York, **1998**.

(59) Danley, R. L. *Thermochim. Acta* **2002**, *395*, 201.

(60) Brown, M. *Thermochim. Acta* **1997**, *1*, 117.

(61) Zhang, F.-A.; Lee, D.-K.; Pinnavaia, T. J. *Polymer* **2009**, *50*, 4768.

(62) Wielage, B.; Lampke, T.; Marx, G.; Nestler, K.; Starke, D. *Thermochim. Acta* **1999**, *337*, 169.

(63) Hutchinson, J. M. *J. Therm. Anal. Calorim.* **2003**, *72*, 619.

(64) Jin, Y.; Bonilla, J.; Lin, Y.-G.; Morgan, J.; McCracken, L.; Carnahan, J. *J. Therm. Anal.* **1996**, *46*, 1047.

(65) Cao, J. *Thermochim. Acta* **1999**, *325*, 101.

(66) Verdonck, E.; Schaap, K.; Thomas, L. C. *Int. J. Pharm.* **1999**, *192*, 3.

(67) Zhang, T.; Xu, G.; Puckette, J.; Blum, F. D. *J. Phys. Chem. C* **2012**, *116*, 11626.

(68) Zhang, B.; Blum, F. D. *Macromolecules* **2003**, *36*, 8522.

(69) Reading, M.; Luget, A.; Wilson, R. *Thermochim. Acta* **1994**, *238*, 295.

(70) Moynihan, C. T.; Easteal, A. J.; Wilder, J.; Tucker, J. *J. Phys. Chem.* **1974**, *78*, 2673.

(71) Debenedetti, P. G.; Stillinger, F. H. *Nature* **2001**, *410*, 259.

(72) Godovsky, Y. K. *Thermophysical properties of polymers*; Springer Berlin, **1992**.

(73) Gibbs, J. H.; DiMarzio, E. A. *J. Chem. Phys.* **1958**, *28*, 373.

(74) DiMarzio, E.; Dowell, F. *J. Appl. Phys.* **1979**, *50*, 6061.

(75) Roe, R.-J.; Tonelli, A. E. *Macromolecules* **1978**, *11*, 114.

(76) Painter, P. C.; Graf, J. F.; Coleman, M. M. *Macromolecules* **1991**, *24*, 5630.

(77) Eyring, H. *J. Chem. Phys.* **1936**, *4*, 283.

(78) Fox Jr, T. G.; Flory, P. J. *J. Appl. Phys.* **1950**, *21*, 581.

(79) Fox, T. G.; Flory, P. J. *J. Polym. Sci.* **1954**, *14*, 315.

(80) Simha, R.; Boyer, R. *J. Chem. Phys.* **1962**, *37*, 1003.

(81) Blanchard, L.-P.; Hesse, J.; Malhotra, S. L. *Can. J. Chem.* **1974**, *52*, 3170.

(82) Buera, M. d. P.; Levi, G.; Karel, M. *Biotechnol. Progr.* **1992**, *8*, 144.

(83) Tager, A. *Physical chemistry of polymers*; Mir Publishers: Moscow, Russia, 1972.

(84) Krumova, M.; Lopez, D.; Benavente, R.; Mijangos, C.; Perena, J. *Polymer* **2000**, *41*, 9265.

(85) Van Krevelen, D. W.; Te Nijenhuis, K. *Properties of polymers: their correlation with chemical structure; their numerical estimation and prediction from additive group contributions*; Elsevier: Amsterdam, Netherlands, 2009.

(86) Richard, A. *Faraday Discuss.* **1994**, *98*, 219.

(87) Mayes, A. M. *Macromolecules* **1994**, *27*, 3114.

(88) Forrest, J. A.; Dalnoki-Veress, K. *Adv. Colloid Interface Sci.* **2001**, *94*, 167.

(89) Shen, M. C.; Eisenberg, A. *Prog. Solid State Chem.* **1967**, *3*, 407.

(90) Hudzinskyy, D.; Lyulin, A. V.; Baljon, A. R.; Balabaev, N. K.; Michels, M. A. *Macromolecules* **2011**, *44*, 2299.

(91) Jenckel, E.; Uberreiter, K. *Zeitschr. Phys. Chem. A* **1938**, *182*, 361.

(92) Shetter, J. A. *J. Polym. Sci., Part B: Polym. Phys.* **1963**, *1*, 209.

(93) Ute, K.; Miyatake, N.; Hatada, K. *Polymer* **1995**, *36*, 1415.

(94) Karasz, F.; MacKnight, W. *Macromolecules* **1968**, *1*, 537.

(95) Kwei, T. *J. Polym. Sci. Polym. Lett.* **1984**, *22*, 307.

(96) Sing, K. S. *Pure Appl. Chem.* **1985**, *57*, 603.

(97) Gregg, S. J.; Sing, K. S. W.; Salzberg, H. *J. Electrochem. Soc.* **1967**, *114*, 279.

(98) Kinloch, A. *Adhesion and adhesives: science and technology*; Springer Science & Business Media, 2012.

(99) Lowell, S.; Shields, J. E.; Thomas, M. A.; Thommes, M. *Characterization of porous solids and powders: surface area, pore size and density*; Springer Science & Business Media, **2012**.

(100) Brackbill, J.; Kothe, D. B.; Zemach, C. *J. Comput. Phys.* **1992**, *100*, 335.

(101) Butt, H.-J.; Graf, K.; Kappl, M. *Physics and chemistry of interfaces*; John Wiley & Sons: Berlin, Germany, 2006.

(102) Ghosh, P. *Colloid and interface science*; Rajkamal Electric Press: New Delhi, India, **2009**.

(103) Lowell, S.; Shields, J. E. *Powder surface area and porosity*; Springer Science & Business Media: New York, **2013**.

(104) Cohan, L. H. *J. Am. Chem. Soc.* **1938**, *60*, 433.

(105) Lastoskie, C.; Gubbins, K. E.; Quirke, N. *J. Phys. Chem.* **1993**, *97*, 4786.

(106) Nguyen, C.; Do, D. *Langmuir* **1999**, *15*, 3608.

(107) Donohue, M.; Aranovich, G. *Adv. Colloid Interface Sci.* **1998**, *76*, 137.

(108) Aranovich, G.; Donohue, M. *J. Colloid Interface Sci* **1998**, *200*, 273.

(109) Balbuena, P. B.; Gubbins, K. E. *Langmuir* **1993**, *9*, 1801.

(110) Sangwichien, C.; Aranovich, G.; Donohue, M. *Colloids Surf., A* **2002**, *206*, 313.

(111) Hill, T. L. *J. Phys. Chem.* **1955**, *59*, 1065.

(112) Zdravkov, B. D.; Čermák, J. J.; Šefara, M.; Janků, J. *Cent. Eur. J. Chem.* **2007**, *5*, 385.

(113) Corma, A. *Chem. Rev.* **1997**, *97*, 2373.

(114) Brunauer, S.; Emmett, P. H.; Teller, E. *J. Am. Chem. Soc.* **1938**, *60*, 309.

(115) Barrett, E. P.; Joyner, L. G.; Halenda, P. P. *J. Am. Chem. Soc.* **1951**, *73*, 373.

(116) Evans, R.; Marconi, U. M. B.; Tarazona, P. *J. Chem. Soc., Faraday Trans. 2* **1986**, *82*, 1763.

(117) Ravikovitch, P.; Wei, D.; Chueh, W.; Haller, G.; Neimark, A. *J. Phys. Chem. B* **1997**, *101*, 3671.

(118) Ravikovitch, P. I.; Haller, G. L.; Neimark, A. V. *Adv. Colloid Interface Sci.* **1998**, *76*, 203.

(119) Fraissard, J. P. *Physical Adsorption: Experiment, Theory, and Applications*; Springer Science & Business Media, **1997**.

(120) Gelb, L. D.; Gubbins, K.; Radhakrishnan, R.; Sliwinska-Bartkowiak, M. *Rep. Prog. Phys.* **1999**, *62*, 1573.

(121) Seaton, N.; Walton, J. *Carbon* **1989**, *27*, 853.

(122) Neimark, A. V.; Ravikovitch, P. I.; Grün, M.; Schüth, F.; Unger, K. K. *J. Colloid Interface Sci* **1998**, *207*, 159.

(123) Rahman, R.; Foster, J.; Haque, A. *J. Phys. Chem. A* **2013**, *117*, 5344.

(124) Karakasidis, T.; Charitidis, C. *Mater. Sci. Eng., C* **2007**, *27*, 1082.

(125) Schlick, T. *Molecular Modeling and Simulation: An Interdisciplinary Guide: An Interdisciplinary Guide*; Springer: New York, NY, **2010**.

(126) London, F. *Phys. Chem.* **1930**, *11*, 222.

(127) Jensen, J. H.; CRC Press: Boca Raton, FL, **2011**.

(128) Zhang, X.; Shi, F.; Niu, J.; Jiang, Y.; Wang, Z. *J. Mater. Chem.* **2008**, *18*, 621.

(129) Marmur, A. *Langmuir* **2004**, *20*, 3517.

(130) Ma, M.; Hill, R. M. *Curr. Opin. Colloid Interface Sci.* **2006**, *11*, 193.

(131) Lau, K. K.; Bico, J.; Teo, K. B.; Chhowalla, M.; Amaratunga, G. A.; Milne, W. I.; McKinley, G. H.; Gleason, K. K. *Nano Lett.* **2003**, *3*, 1701.

(132) Miwa, M.; Nakajima, A.; Fujishima, A.; Hashimoto, K.; Watanabe, T. *Langmuir* **2000**, *16*, 5754.

(133) Gao, L.; McCarthy, T. J. *Langmuir* **2006**, *22*, 2966.

(134) Young, T. *Philos. Trans. R. Soc. London* **1805**, 65.

(135) Mack, G. L. *J. Phys. Chem.* **1936**, *40*, 159.

(136) Chen, Y.; Helm, C.; Israelachvili, J. *J. Phys. Chem.* **1991**, *95*, 10736.

(137) Wenzel, R. N. *Ind. Eng. Chem.* **1936**, *28*, 988.

(138) Cassie, A.; Baxter, S. *Trans. Faraday Soc.* **1944**, *40*, 546.

(139) Rafiee, J.; Rafiee, M. A.; Yu, Z. Z.; Koratkar, N. *Adv. Mater.* **2010**, *22*, 2151.

(140) Méndez-Vilas, A.; Jódar-Reyes, A. B.; González-Martín, M. L. *Small* **2009**, *5*, 1366.

(141) Lin, Y.; Ehlert, G. J.; Bukowsky, C.; Sodano, H. A. *ACS Appl. Mater. Interfaces* **2011**, *3*, 2200.

(142) Bu, I. Y.; Oei, S. P. *Appl. Surf. Sci.* **2010**, *256*, 6699.

(143) Akram Raza, M.; Kooij, E. S.; van Silfhout, A.; Poelsema, B. *Langmuir* **2010**, *26*, 12962.

(144) Shirtcliffe, N. J.; McHale, G.; Newton, M. I.; Chabrol, G.; Perry, C. C. *Adv. Mater.* **2004**, *16*, 1929.

(145) Bok, H.-M.; Shin, T.-Y.; Park, S. *Chem. Mater.* **2008**, *20*, 2247.

(146) Qu, M.; Zhao, G.; Wang, Q.; Cao, X.; Zhang, J. *Nanotechnology* **2008**, *19*, 055707.

(147) Hosono, E.; Fujihara, S.; Honma, I.; Zhou, H. *J. Am. Chem. Soc.* **2005**, *127*, 13458.

(148) Sarkar, D.; Farzaneh, M. *J. Adhes. Sci. Technol.* **2009**, *23*, 1215.

(149) Chen, Z.; Guo, Y.; Fang, S. *Surf. Interface Anal.* **2010**, *42*, 1.

(150) Rao, A. V.; Latthe, S. S.; Dhere, S. L.; Pawar, S. S.; Imai, H.; Ganesan, V.; Gupta, S. C.; Wagh, P. B. *Appl. Surf. Sci.* **2010**, *256*, 2115.

(151) Sakai, M.; Kono, H.; Nakajima, A.; Zhang, X.; Sakai, H.; Abe, M.; Fujishima, A. *Langmuir* **2009**, *25*, 14182.

(152) Bhushan, B.; Jung, Y. C. *Ultramicroscopy* **2007**, *107*, 1033.

(153) Artus, G. R.; Jung, S.; Zimmermann, J.; Gautschi, H. P.; Marquardt, K.; Seeger, S. *Adv. Mater.* **2006**, *18*, 2758.

(154) Zheng, L.; Li, Z.; Bourdo, S.; Khedir, K. R.; Asar, M. P.; Ryerson, C. C.; Biris, A. S. *Langmuir* **2011**, *27*, 9936.

(155) Cao, L.; Jones, A. K.; Sikka, V. K.; Wu, J.; Gao, D. *Langmuir* **2009**, *25*, 12444.

(156) Mishchenko, L.; Hatton, B.; Bahadur, V.; Taylor, J. A.; Krupenkin, T.; Aizenberg, J. *ACS Nano* **2010**, *4*, 7699.

(157) Yang, S.; Xia, Q.; Zhu, L.; Xue, J.; Wang, Q.; Chen, Q. *Appl. Surf. Sci.* **2011**, *257*, 4956.

(158) Gao, L.; McCarthy, T. J. *Langmuir* **2007**, *23*, 3762.

(159) Stalder, A.; Kulik, G.; Sage, D.; Barbieri, L.; Hoffmann, P. *Colloids Surf., A* **2006**, *286*, 92.

(160) Williams, D. L.; Kuhn, A. T.; Amann, M. A.; Hausinger, M. B.; Konarik, M. M.; Nesselrode, E. I. *Galvanotechnik* **2010**, *101*, 2502.

(161) Werder, T.; Walther, J. H.; Jaffe, R.; Halicioglu, T.; Koumoutsakos, P. *J. Phys. Chem. B* **2003**, *107*, 1345.

(162) Novoselov, K. S.; Geim, A. K.; Morozov, S.; Jiang, D.; Zhang, Y.; Dubonos, S.; Grigorieva, I.; Firsov, A. *Science* **2004**, *306*, 666.

(163) Katsnelson, M. I. *Mater. Today* **2007**, *10*, 20.

(164) Si, Y.; Samulski, E. T. *Nano Lett.* **2008**, *8*, 1679.

(165) Geim, A. K. *Science* **2009**, *324*, 1530.

(166) Zhang, Y.; Tan, Y.-W.; Stormer, H. L.; Kim, P. *Nature* **2005**, *438*, 201.

(167) Novoselov, K.; Geim, A. K.; Morozov, S.; Jiang, D.; Katsnelson, M.; Grigorieva, I.; Dubonos, S.; Firsov, A. *Nature* **2005**, *438*, 197.

(168) Geim, A. K.; Novoselov, K. S. *Nat. Mater.* **2007**, *6*, 183.

(169) Schedin, F.; Geim, A.; Morozov, S.; Hill, E.; Blake, P.; Katsnelson, M.; Novoselov, K. *Nat. Mater.* **2007**, *6*, 652.

(170) Elias, D.; Nair, R.; Mohiuddin, T.; Morozov, S.; Blake, P.; Halsall, M.; Ferrari, A.; Boukhvalov, D.; Katsnelson, M.; Geim, A. *Science* **2009**, *323*, 610.

(171) Zhou, S.; Gweon, G.-H.; Fedorov, A.; First, P.; De Heer, W.; Lee, D.-H.; Guinea, F.; Neto, A. C.; Lanzara, A. *Nat. Mater.* **2007**, *6*, 770.

(172) Lee, C.; Wei, X.; Kysar, J. W.; Hone, J. *Science* **2008**, *321*, 385.

(173) Schniepp, H. C.; Li, J.-L.; McAllister, M. J.; Sai, H.; Herrera-Alonso, M.; Adamson, D. H.; Prud'homme, R. K.; Car, R.; Saville, D. A.; Aksay, I. A. *J. Phys. Chem. B* **2006**, *110*, 8535.

(174) Balandin, A. A.; Ghosh, S.; Bao, W.; Calizo, I.; Teweldebrhan, D.; Miao, F.; Lau, C. N. *Nano Lett.* **2008**, *8*, 902.

(175) Stoller, M. D.; Park, S.; Zhu, Y.; An, J.; Ruoff, R. S. *Nano Lett.* **2008**, *8*, 3498.

(176) Hernandez, Y.; Nicolosi, V.; Lotya, M.; Blighe, F. M.; Sun, Z.; De, S.; McGovern, I.; Holland, B.; Byrne, M.; Gun'Ko, Y. K. *Nat. Nanotechnol.* **2008**, *3*, 563.

(177) Park, S.; Ruoff, R. S. *Nat. Nanotechnol.* **2009**, *4*, 217.

(178) Obraztsov, A. N. *Nat. Nanotechnol.* **2009**, *4*, 212.

(179) Wang, S.; Zhang, Y.; Abidi, N.; Cabrales, L. *Langmuir* **2009**, *25*, 11078.

(180) Shin, Y. J.; Wang, Y.; Huang, H.; Kalon, G.; Wee, A. T. S.; Shen, Z.; Bhatia, C. S.; Yang, H. *Langmuir* **2010**, *26*, 3798.

(181) Taherian, F.; Marcon, V.; van der Vegt, N. F.; Leroy, F. *Langmuir* **2013**, *29*, 1457.

(182) Rafiee, J.; Mi, X.; Gullapalli, H.; Thomas, A. V.; Yavari, F.; Shi, Y.; Ajayan, P. M.; Koratkar, N. A. *Nat. Mater.* **2012**, *11*, 217.

(183) Shih, C.-J.; Wang, Q. H.; Lin, S.; Park, K.-C.; Jin, Z.; Strano, M. S.; Blankschtein, D. *Phys. Rev. Lett.* **2012**, *109*, 176101.

(184) Zhang, L.; Yu, J.; Yang, M.; Xie, Q.; Peng, H.; Liu, Z. *Nat. Commun.* **2013**, *4*, 1443.

(185) Worsley, M. A.; Pauzauskie, P. J.; Olson, T. Y.; Biener, J.; Satcher Jr, J. H.; Baumann, T. F. *J. Am. Chem. Soc.* **2010**, *132,* 14067.

CHAPTER II

STRUCTURE OF THE INTERFACIAL REGION IN ADSORBED POLY(VINYL ACETATE) ON SILICA

Note: This chapter was published on *Macromolecules*, **2016**, 49 (1), pp 298–307. DOI: 10.1021/acs.macromol.5b02214, and reprinted with permission from Macromolecules.

2.1. ABSTRACT

We performed a combined calorimetric and molecular modeling investigation of poly(vinyl acetate) (PVAc) on silica to characterize the intermolecular interactions and the behavior of the adsorbed polymer. From temperature-modulated differential scanning calorimetry experiments, different regions of thermal activity suggested a gradient of mobility in the adsorbed polymer. Polymer segments in more direct contact with silica (tightly-bound) showed a significantly elevated and broadened glass transition relative to the bulk polymer, while polymer further away (loosely-bound) showed only a slightly elevated transition relative to the bulk polymer. A thermal transition for PVAc at the air interface (more-mobile) was also observed and was at lower temperatures than the bulk polymer. Density profiles from molecular dynamics studies suggested a structure of the

adsorbed polymer similar to that experimentally observed. These studies were consistent with the presence of a motional gradient in the polymer segments, and concomitant glass transition changes from the silica to the air interfaces. These results also demonstrate that hydrogen-bonding interactions, at the PVAc/silica interface, are critical to the high-temperature shifts in the glass transition.

2.2. INTRODUCTION

Adsorbed polymer-substrate interactions usually lead to differences in properties of bulk and adsorbed polymers.[1-10] Interactions between adsorbed polymers and solid surfaces have been shown to provide advantageous physical, mechanical, and thermal properties, making these materials suitable as lubricants, adhesives, coatings, and corrosion resistant agents.[11-17] These properties are closely related to those that determine the glass transition, which for small amounts of adsorbed polymers depend on: film thickness, polymer molecular mass, intermolecular interactions, and the mobility of macromolecular chains.[18-20] For example, the T_g will be elevated if the interactions between the polymers and the substrate are attractive and strong.[21] Strong attractive interactions, covalent or hydrogen-bonding, between polymer segments and the substrate can potentially reduce the mobility of the adsorbed polymer segments. This reduction in mobility due to restrictions from attachment points has been proposed as the main reason for T_g elevation.[22-24]

Differential scanning calorimetry (DSC) is the most common technique used to investigate thermal characteristics of bulk polymers and composites.[25-27] Temperature-modulated DSC (TMDSC) is a variant of DSC that, in addition to providing the same information as conventional DSC, provides additional insight into the thermal behavior of materials by separating the heat flow data into reversing and non-reversing events.[28,29]

TMDSC and its derivatives have been used to resolve both weak and multicomponent transitions that would be difficult to distinguish in a conventional DSC scan.[30-34]

Molecular dynamics (MD) simulations have also been used to investigate the dynamics and thermodynamics of thin-film polymer coatings.[35-51] Simulation studies have focused on: adhesion in polyethylene, poly(lactic acid), and poly(methyl methacrylate) (PMMA) chains on silica substrates,[36,52,53] polymer flexibility on flat surfaces,[54] polymer density variation as a function of surface adhesion,[55] and the effects due to changes in the substrate chemistry and thickness,[56] as well as the structure of the polymer type.[46] Molecular simulations have the potential to uncover the fine details of the atomistic-level interactions and structure of polymeric materials at interfaces, fine details that are difficult to measure from experimental approaches.

We are interested in characterizing the effects due to specific intermolecular interactions between PVAc and silica at the polymer-substrate interface. Strong intermolecular interactions between adsorbed polymer segments and a surface can result in distinct thermal activities within the adsorbed polymer. For example, a broadened, two component transition has been reported for very small amounts of PMMA adsorbed on silica.[21,23,57] This transition shows a higher-than-bulk temperature glass transition for "*tightly-bound*" polymer with reduced mobility at the silica/polymer interface, and a bulk-like transition resulted from a "*loosely-bound*" component located further away from the polymer/substrate interface. The relative intensities of these tightly- and loosely-bound component transitions correspondingly depends on the amount of adsorbed polymer.[23,57] Along a similar lines, adsorbed PVAc-d_3 has shown the presence of both tightly- and loosely-bound polymer using deuterium NMR.[58] In addition, the deuterium

NMR powder patterns showed that there was also a third component with a lower glass transition, a "*more-mobile*" component believed to be due to the polymer at the air interface. These studies form the bases for the calorimetric studies of PVAc.

In this study, we observe phenomena consistent with tightly- and loosely-bound polymer in PVAc on silica both in TMDSC experiments and in analogous computer simulations. With calorimetry, we also observed the presence of the more-mobile component for the first time, which correlated to the region of low density at the air interface in the simulations. These findings highlight how combined experimental and theoretical investigations of a specific system can provide additional insight into the forces controlling the behavior of supported polymer films.

2.3. METHODS

2.3.1. Experimental studies

PVAc with an M_w of 260 kDa was purchased and used as received (Scientific Polymer Products, Inc. Ontario, NY, USA). The polydispersity index was determined to be 2.7 using gel permeation chromatography in tetrahydrofuran with an Optilab refractive index detector (Wyatt Technology, CA, USA). The calibration with polystyrene was used corrected with the Mark-Houwink coefficients to obtain PVAc molecular masses.[59] Cab-O-Sil M-5P fumed silica, provided by Cabot Corporation (Tuscola, IL, USA), was used as the substrate. This high specific surface area silica was used in order to increase the amount of adsorbed polymer in the samples. Cab-O-Sil consists of solid spherical particles aggregated into larger structures. The specific surface area of the fumed silica particles was determined to be 190 m^2/g using the Brunauer–Emmett–Teller (BET)

method[60] on a NOVA 2200 (Quantachrome, FL, USA). The solvent, toluene, was purchased from Pharmco-aaper (Brookfield, CT, USA) and used as received.

Adsorbed polymer samples were prepared by dispersing Cab-O-Sil fumed silica (~0.3 g) in different concentrations of polymer solutions in toluene. The tubes were placed in a mechanical shaker for 48 h, followed by centrifugation at 6000 rpm for 15 min. After removal of the supernatant liquid, the portions of the samples containing the adsorbed polymer on silica were dried using air at a slow flow rate through a Pasteur pipet until the gel turned to a dry powder. The samples were further dried in a vacuum oven at 60 °C for 72 h. The resulting samples were free flowing powders indicating that the PVAc molecules did not bridge the particles, i.e., no tie chains.

Adsorbed amounts of polymer on the surface of silica were determined using a Model 2950 thermogravimetric analysis instrument (TGA) (TA Instruments, New Castle, DE, USA). Samples were heated from room temperature to 700 °C at a heating rate of 20 °C/min in a flowing air atmosphere (40 mL/min). The adsorbed amounts of polymer on silica were calculated based on the mass loss of PVAc and the mass of residual material, which contained only silica after heating, and the specific surface area of silica.

The thermal behavior of composites in the glass transition region was investigated using a Model Q2000 DSC (TA Instruments, New Castle, DE, USA). The sample pans were referenced against empty pans and the cells were purged with a 50 mL/min nitrogen stream. The samples were held at -50 °C for 1 min and heated to 150 °C at a rate of 3 °C/min with a modulation amplitude of ±1.0 °C and a modulation period of 60 s. They were then held at 150 °C for 2 min and cooled to -50 °C at 3 °C/min with the same modulation. The samples were then held at -50 °C for 2 min in order to minimize the

effects of previous thermal history. After these heating cycles, a second heating scan was done with the same conditions as the first heating scan. Both cooling and second heating scans were analyzed and no significant difference was observed between these two measurements. The difference between the center of the glass transition (identified as the peak in the derivative curve), T_g, from the heating and the T_g from the cooling scans were about ±1.5 °C. The second heating scan results were used to determine the glass transition behavior and the amount of tightly-bound polymer in the samples. The thermograms were reported as differential reversing heat flow rates (dQ_{rev}/dT) as a function of temperature, after applying a 10 °C smoothing to reduce the high-frequency noise.

TA Universal Analysis (TA Instruments) software was used for thermal data analysis of the TMDSC scans. The perpendicular drop method was applied to split the transitions into two components. A simple two-component model, detailed below, was used to analyze the data from the areas in the thermal transition curves.

2.3.2. Computational studies

Modeling the fundamental interactions that govern polymer adhesion to silica surfaces requires detailed atomistic-level simulations. The number of atoms involved and simulation lengths needed for equilibrated sampling make long polymer chain system studies computationally prohibitive. To address these issues, a systematic series of simulations involving low molecular mass chains were performed to investigate behavior and property convergence as a function of increasing chain length and adsorbed amount of polymer. PVAc chains of 1, 2, 4, 8, 10, 12, 20 and 30-mer length were constructed with UCSF Chimera[61] for this chain length series, and adsorbed polymer simulations

were composed of systems of uniform chain length polymer on an α-quartz surface. Following literature conventions, we refer to all the systems from monomer to 30-mer of VAc as PVAc despite their potential classification as oligomeric (lower molecular mass) material.[46,55,62] The adsorbed amount of polymer in the simulated samples was varied from 0.13 to 3.10 mg PVAc/m^2 silica. For the 1 to 12-mer simulations, the (001) surface of a slab of α-quartz, with area of 3.40 × 3.93 nm^2 and thickness of 1.45 nm, was evenly functionalized with a 4.5 groups/nm^2 surface density of silanol groups to agree with silanol densities typically used in experiments.[63] A surface approximately six times larger (8.50 × 9.82 nm^2) with the same surface density of silanol groups was used for the 20 and 30-mer simulations. A *z*-axis box dimension of 50 nm was used to form an air layer and prevent the possible simultaneous interactions of the polymer chains with both the top and bottom of the silica slab.

MD simulations were carried out in the canonical (NVT) ensemble using GROMACS 4.5.5,[64] and used the optimized potentials for liquid simulations all-atom force-field (OPLS-AA) with silica parameters described by Wensink et al.[65,66] Periodic boundary conditions were employed, Lennard-Jones interactions were switched off between 1.0 and 1.2 nm, standard energy and pressure dispersion corrections were applied,[67] and the smooth particle-mesh Ewald summation was used to account for the long-range contributions to the Coulomb interactions.[68] Simulations used a time-step of 2 fs and bonds to hydrogen atoms were constrained using the P-LINCS algorithm.[69] Ten independent 20 ns simulations were performed for each adsorbed polymer system, all at a temperature of 75 °C (348.15 K), held constant with a Nose-Hoover thermostat with a 1 ps time constant.[70,71] These simulations used different initial configurations, pulled

from fluid polymer simulations at higher temperatures: 350 K for monomer and dimer, 500 K for tetramer to dodecamer, and 550 K for 20 and 30-mer polymers. The systems were then cooled to the target temperature and equilibrated for 5 ns before data collection over the 20 ns trajectories. Combined, these simulations resulted in 200 ns of sampling for each polymer composition. Additional details of the force-field parameters and simulations are described in the **Supporting Information**.

2.4. RESULTS

2.4.1. Thermal analysis shows multicomponent behavior for adsorbed polymers

Thermogravimetric analysis (TGA) was used to study the thermal decomposition of the adsorbed PVAc samples and estimate the adsorbed amounts of polymer. The decomposition curves for bulk and adsorbed PVAc on Cab-O-Sil M5P fumed silica are shown in Figure 2.1. The flat portions of the curves in Figure 2.1A, above 600 °C for the adsorbed samples, represented the relative amounts of silica in the samples. The adsorbed amounts were calculated using the amount of polymer divided by the surface area of the corresponding amount remaining in each sample. Thermal degradation temperatures (T_d) for the major decomposition peak of the adsorbed polymers were higher than that of bulk PVAc, as observed in Figure 2.1B (derivative mode). The bulk polymer showed a high temperature degradation not observed in the adsorbed samples.

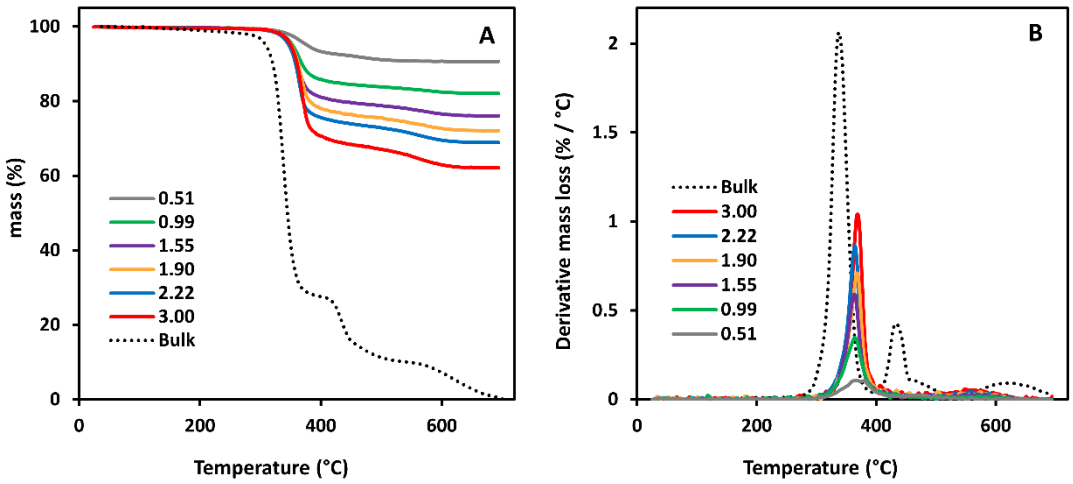

Figure 2.1. TGA thermograms of bulk and adsorbed PVAc on silica as a function of adsorbed amount of polymer in A) normal mode and B) derivative mode. The adsorbed amounts are shown as in mg polymer/m^2 silica and the order of the curves is the same as in the legend. The degradation of the main transition for the adsorbed polymer was higher than that for the bulk polymer.

The TMDSC thermograms for bulk and adsorbed PVAc on silica are shown in Figure 2.2. These thermograms are shown in derivative mode to highlight the different regions of thermal activity. The heat flow curves are shown in Figure A2 of the **Supporting Information**. The thermograms are scaled based on the mass of polymer only. The T_g for the bulk PVAc was measured to be 42.7 ± 0.2 °C. The uncertainty is based on the precision as determined by the range of three separate measurements. Three different regions of thermal activity were observed for the adsorbed PVAc samples. The smallest adsorbed-amount sample (0.55 mg/m^2) showed little thermal activity, indicating only a small tightly-bound component which was likely very broad and very weak in intensity. At small adsorbed amounts (< 1 mg/m^2), the 0.78 and 0.99 mg/m^2 samples, showed distinct thermal activity only occurred in the temperature range of 60 to 85 °C

with the center of the broad peak at 67.1 ± 1.3 °C. This activity was well above the T_g of the bulk polymer. With more adsorbed polymer (> 1 mg/m^2), a second thermal activity peak, slightly above the T_g of bulk polymer (44.2 ± 0.3 °C), was observed and corresponded to loosely-bound polymer. As the adsorbed amount increased further, the area under the loosely-bound transition increased, whereas the area of the tightly-bound transition remained constant. This tightly-bound peak was broad at small adsorbed amounts, and this peak shifted to lower temperature with increasing adsorbed amount. A third region was observed at temperatures lower than the T_g of bulk polymer. This transition corresponds to a mobile component present at the PVAc/air interface.

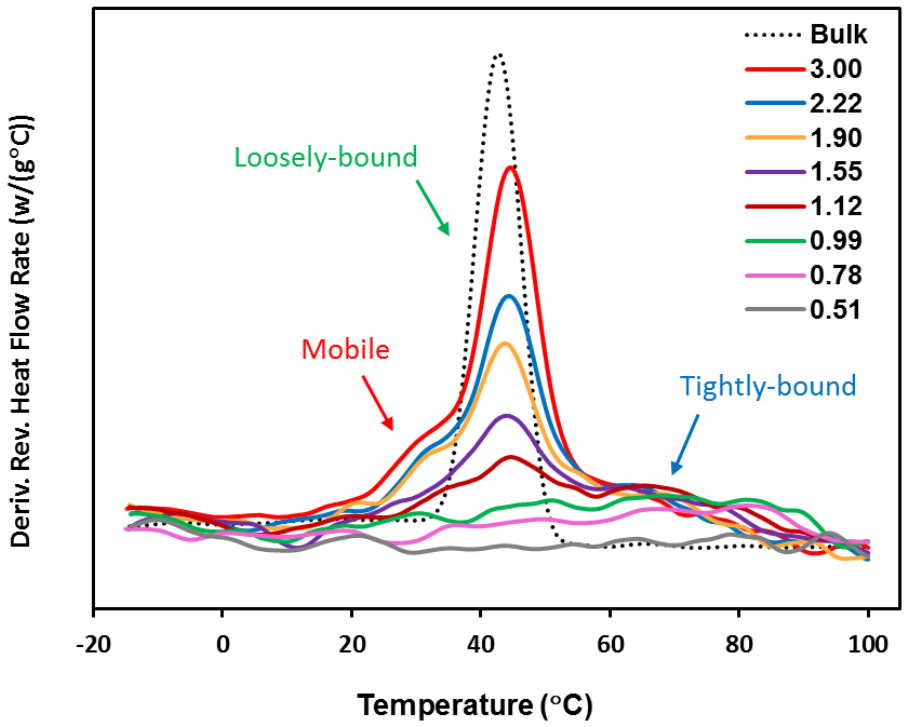

Figure 2.2. TMDSC thermograms for bulk PVAc and adsorbed PVAc on silica. The thermograms are labeled with the adsorbed amounts that are shown in mg polymer/m^2 silica. The thermograms of the main peaks for adsorbed samples are in the same order as in the legend. The area under the tightly-bound transition remained relatively constant

and the intensity of the loosely-bound polymer increased with increasing adsorbed amounts of polymer.

2.4.2. Simulated polymer density profiles show regions with varied density

The atomistic mass density profile of a polymer film is an indication of the packing of the adsorbed polymer as a function of distance from the substrate. Using MD simulations, we measured the average density $\rho(z)$ of the PVAc atoms as a function of distance from the silica surface in the z-direction. The simulation boxes were divided into 2.0 Å bins along the axis normal to the interface (z-axis). Within each bin, the total mass of atoms were determined by averaging over the configurations accumulated over the course of the MD simulations. The total mass of atoms in each bin was divided by the bin-volume to calculate the density. A snapshot side view of the simulation box and the average mass density profile of dodecamer PVAc adsorbed onto the silica are shown in Figure 2.3. The dodecamer results are well-representative of all other chain lengths studied. Based on this density profile, the interfacial area was divided into three distinct regions. The average density profile showed a peak of high density followed by a flat region. The relatively flat plateau in the curve had a density consistent with that of bulk dodecamer, suggesting that the density of loosely-bound material remained constant and bulk-like. Further from the surface, at the polymer/air interface, the density dropped off to zero over a roughly 1 nm range. The characteristics of the density profiles for samples with different thicknesses were similar, except that the absolute position of the decay in the profile was dependent on the adsorbed amounts, as expected. Additionally, no bulk-like region was observed for samples with adsorbed amounts of polymer below 1 mg/m^2 (see **Supporting Information**).

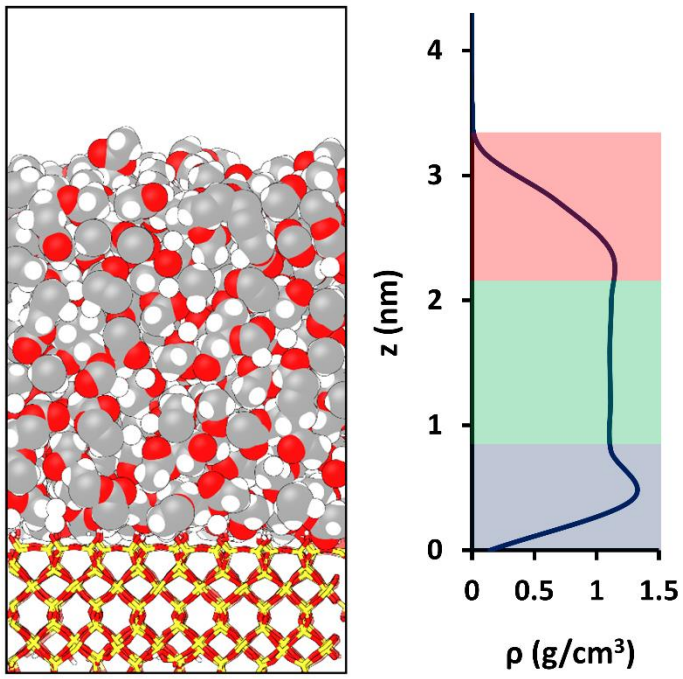

Figure 2.3. Snapshot side view of adsorbed PVAc on silica (left) and the density profile of the polymer as a function of the distance from the surface (right). Blue (upper), green (middle) and red (lower) areas in the density profile highlight the tightly-bound, loosely-bound and mobile regions of PVAc, respectively.

2.4.3. Polymer-surface intermolecular interactions are strong near the surface

To determine the presence of and estimate the strength of interactions such as hydrogen-bonding, the distance distribution function between the surface silanol groups and the carbonyl oxygen atoms of the PVAc was measured. The *z*-direction distribution function was measured over the course of the simulation every 20 ps to identify how side chain groups of polymer interact with the surface. To investigate hydrogen-bonding at the polymer/silica interface, we measured the *xy* cross-section averaged density $g(z)$ of carbonyl oxygen atoms for partition bins of 0.2 Å in the *z*-direction. The probability of

finding any specified atom at a distance *z* from the surface in the structural configuration, relative to the probability calculated for the bulk material, defines the total pair correlation function. Figure 2.4 shows the distribution profile for carbonyl oxygen atoms of tetramer PVAc as a function of distance from the oxygen atoms of silanol groups on the surface. While adsorbed tetramer PVAc is shown here, these results are consistent with other polymer lengths (see **Supporting Information**). An intense peak, observed at 2.2 Å, was a clear indicator of strong interactions between polymer and silanol groups at the interface. We also measured the radial distribution function for the polymer oxygen atoms and the hydrogen atoms of the silanol groups for calculation of the number of hydrogen-bonds present in any given configuration.

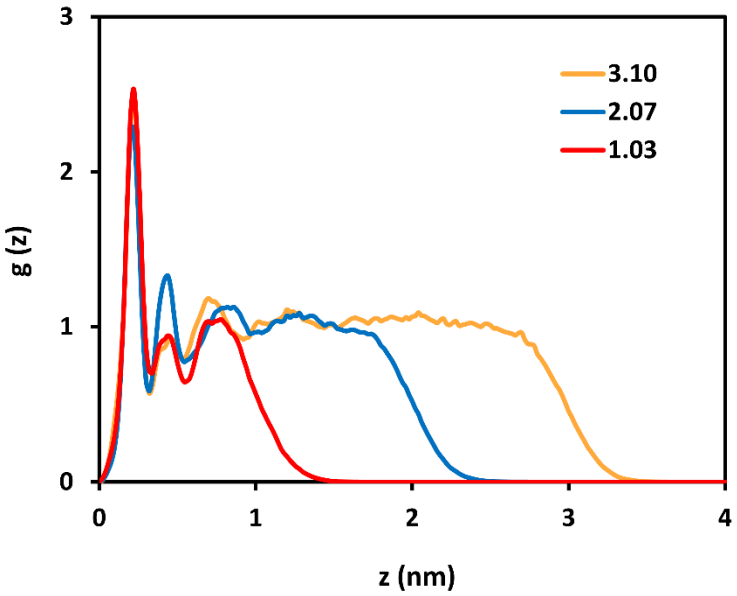

Figure 2.4. *Z*-direction distribution functions for carbonyl oxygen atoms as a function of the *z*-coordinate, the distance from silanol oxygen atoms, for tetramer PVAc. The adsorbed amounts shown in the legend are the adsorbed amounts in mg polymer/m^2

silica. The intense peak at 2.2 Å indicates the presence of strong interactions at the interface.

We further characterized the intermolecular interaction strength between polymer side chains and silanol groups (silicon, oxygen and hydrogen atoms) of silica surface. We calculated the interaction energy (kcal/mol) between these differing groups and determined the number of interactions as a function of their energy of interaction. The counts of these interactions were then binned into an energy pair distribution function.[72,73] Figure 2.5 shows the energy pair distribution functions for different adsorbed amounts of polymer. The energy pair distribution consisted of a large peak with the center at around 0 kcal/mol representing weak interactions of silanol groups with distant side-chains and a shoulder at low energy for neighboring silanol and polymer side-chains. An attractive PVAc-silica pair distribution peak was observed at -11.7 ± 0.1 kcal/mol for small adsorbed amounts of polymer. We refer to this peak, which represents the strong interactions between polymer side chains and silica silanol groups, as the "tightly-bound peak". At higher adsorbed amounts (around 0.65 mg/m^2), this energy shifted to -11.1 ± 0.1 kcal/mol. This shift to weaker surface interaction energy at larger adsorbed amounts was consistent with the slight decrease in the T_g for tightly-bound PVAC observed in the TMDSC thermograms (Figure 2.2) at larger adsorbed amounts. The energy pair distribution function as a function of chain length is shown in the **Supporting Information**.

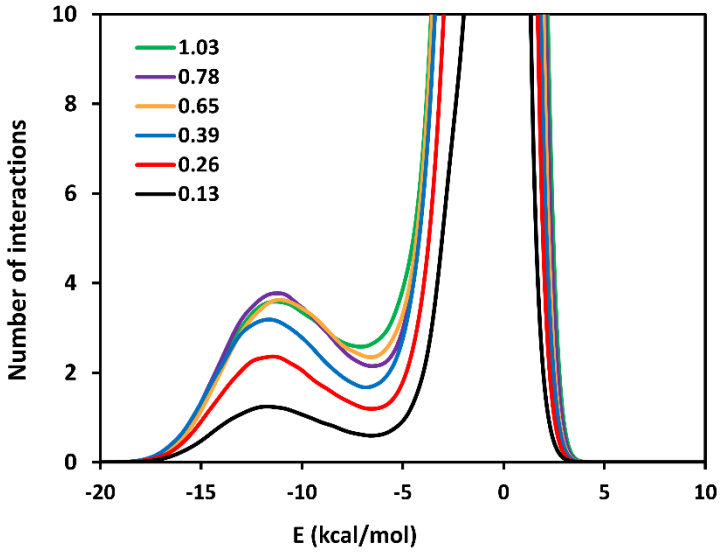

Figure 2.5. Energy pair distribution function between tetramer PVAc side-chains and silica silanol groups as a function of adsorbed amount of polymer. The adsorbed amounts are shown in the legend in mg polymer/m^2 silica. With increasing adsorbed amount, the number of interactions converges on a constant limiting value, while the average interaction energy weakens by 0.6 ± 0.1 kcal/mol.

2.5. DISCUSSION

The TGA thermograms for bulk PVAc showed three weight loss steps. The degradation process of PVAc was complicated due to a series of simultaneous reactions.[74] The main decomposition occurred in the range of 275 to 390 °C, which is attributed to the elimination of acetic acid from the polymer side-chain.[75,76] The second step occurred in the range of 405 to 520 °C, followed by a third step up to 690 °C, both corresponding to the disintegration of the polymer backbone.[74,76] The relative mass loss for bulk PVAc was 72, 18, and 10% of total mass in the first, second, and third steps, respectively. In contrast, adsorbed PVAc on silica showed a two-step decomposition. The major decomposition step occurred between 300 and 400 °C and was at a slightly higher

temperature than that for bulk PVAc. This step was followed by a smaller weight loss centered near 550 °C. The differences in decomposition between the bulk and adsorbed polymer were due to the interactions between PVAc and the silica surface.

2.5.1. TMDSC shows that adsorbed PVAc exhibits regions with varied behavior

Polymer-substrate interactions have been identified as the main factor in differences in adsorbed polymer behavior relative to their bulk counterparts.[4,21,77,78] For example, the T_g of a polymer in a nanocomposite system typically increases (or decreases) with the presence of attractive (or repulsive) interactions with the surface. It should be noted, however, that observed decreases in T_g are not necessarily solely the result of repulsive surface interactions. It has previously been shown that loosely-bound segments of poly(ethylene-stat-vinyl acetate) on silica have lower T_g values relative to the bulk polymer.[79] This effect was attributed to heterogeneity induced by surface interactions, namely, the dilution of the loosely-bound segments by ethylene segments because the vinyl acetate units were preferentially adsorbed on silica.[79]

For adsorbed homo-PVAc, we observed a shoulder in the thermogram for the loosely-bound transition on the lower temperature side. We believe that this transition is indicative of a *more-mobile* fraction of polymer located at the polymer/air interface. This *more-mobile* component has not been observed previously using calorimetry. The presence of a more-mobile component was in good agreement with previous studies on the dynamics of adsorbed PVAc[58] and poly(methyl acrylate) (PMA)[80,81] on silica in deuterium NMR studies, which showed a motional gradient in the adsorbed polymers.

The aforementioned studies also indicate that PVAc on silica has polymer segments near the silica surface, which have mobility that was significantly less than that at the

polymer/air interface. This is the tightly-bound polymer. This lowered mobility was due to hydrogen-bonding between the carbonyl groups of PVAc and the hydroxyl groups of silica particles, and resulting in the T_g shift to higher temperatures. The presence of hydrogen-bonds between the silanol groups on the silica particles and carbonyl groups of polymers such as PVAc,[79,82,83] PMMA,[84,85] and other methacrylate polymers[24] has been reported using FTIR.

At small adsorbed amounts, polymer chains strongly interact with silica to make a polymer region tightly bound to the surface. In the TMDSC curves, these segments are responsible for a broad transition, roughly 25 K higher than that of the bulk polymer. We use the term "*tightly-bound*" to describe this reduced mobility region of interfacial polymer consistent with the historical literature describing polymer attached to particles in filled elastomers.[86] One could also consider the possibility of a "*rigid amorphous fraction*", introduced by Wunderlich and used by Sargsyan et al. to describe immobilized fractions in the interfacial regions of semi-crystalline polymers[87,88] and PMMA in silica nanocomposites.[27] In the latter case, the rigid amorphous fraction was deemed to degrade before exhibiting a glass transition. In our system, even at small adsorbed amounts (less than 1 mg/m^2), the adsorbed polymer showed clear evidence of a broad, higher-temperature glass transition. Consequently, there does not appear to be any significant amount of rigid amorphous material.

With increasing adsorbed amounts, we observed increased intensity in the tightly-bound peak until the whole surface was covered with tightly-bound polymer. Samples with more adsorbed polymer showed the formation of loosely-bound polymer in addition to the tightly-bound polymer. It should be noted that while tightly- and loosely-bound

polymer may be distinguishable in terms of NMR or calorimetry, they may still be parts the same polymer, as the adsorbed amounts are in the range of the size of the polymer coil. In other words, they do not represent distinct, separable layers. As the adsorbed amount increased, the intensity of the loosely-bound peak increased and the intensity of the tightly-bound peak changed little. The T_g of the loosely-bound component was slightly higher than that of bulk polymer. This indicated that the reduced mobility of the tightly-bound polymer layer has a secondary effect that appears to extend into the loosely-bound region. On the other hand, the mobile component, which is located at the air interface, had a lower T_g than the bulk polymer. It is clear that the entire glass transition region for the adsorbed polymer is much broader than the bulk transition region, and much more complicated because of the interfaces. This broad T_g is an important indicator of a heterogeneous polymeric system.

A model for the analysis of the tightly- and loosely-bound polymer was developed for adsorbed PMMA.[23] The major premise of this model was that, with increasing adsorbed amounts of polymer, tightly-bound polymer was added until the surface was covered with an adsorbed amount, m_B, after which loosely bound polymer emerges. This tightly-bound amount of polymer can be estimated from r in equation (2.1), which is the ratio of the heat flow changes for the loosely (A) and tightly-bound (B) components, as previously shown for PMMA[23,45] or

$$r = A_A/A_B = (m'_p - m'_{pB})\,\Delta C_{pA}/(m'_{pB}\,\Delta C_{pB})$$

$$r = [\Delta C_{pA}/(m'_{pB}\,\Delta C_{pB})]m'_p - \Delta C_{pA}/\Delta C_{pB}, \qquad (2.1)$$

where the ΔC_ps represent the specific heat capacity changes in the glass transition region, and m'_p represents the normalized total polymer mass, determined from the TGA

thermograms via dividing the mass loss (total mass of adsorbed polymer) by the remaining mass (mass of silica), and the *A*'s variables are the areas under the derivative heat flow rate curves. The total polymer mass is the sum of the loosely and tightly bound components, or

$$m'_{p} = m'_{pA} + m'_{pB}. \quad (2.2)$$

Here, m'_{pA} and m'_{pB} represent the normalized masses of loosely-bound and tightly-bound polymer, respectively.

A linear relationship between the ratios of the heat flow changes for the A and B transitions and the total relative masses of polymer (m'_{p}) as described in Equation 2.1, was obtained and is shown in Figure 2.6. As evident in Equation 2.1, the amount of tightly-bound polymer can be obtained by dividing the intercept (ratio of the heat capacity increments, $\Delta C_{pA}/\Delta C_{pB}$) by the slope ($\Delta C_{pA}/(m'_{pB}\,\Delta C_{pB})$) of the line. It was more useful to convert the amounts of polymer to adsorbed amounts (mg polymer/m^2 silica) since the specific surface area of the silica is known. The *r* values for the samples with adsorbed amounts less than m'_{pB} were 0 because there were no peaks for the loosely-bound polymers. From the fit to the line, the heat capacity ratio of loosely-bound to tightly-bound PVAc was around 2.0. This indicates that the changes in mobility of the tightly-bound component around the glass transition was smaller than that of the loosely-bound component. This effect was due to the interactions of the tightly-bound polymer with the surface.

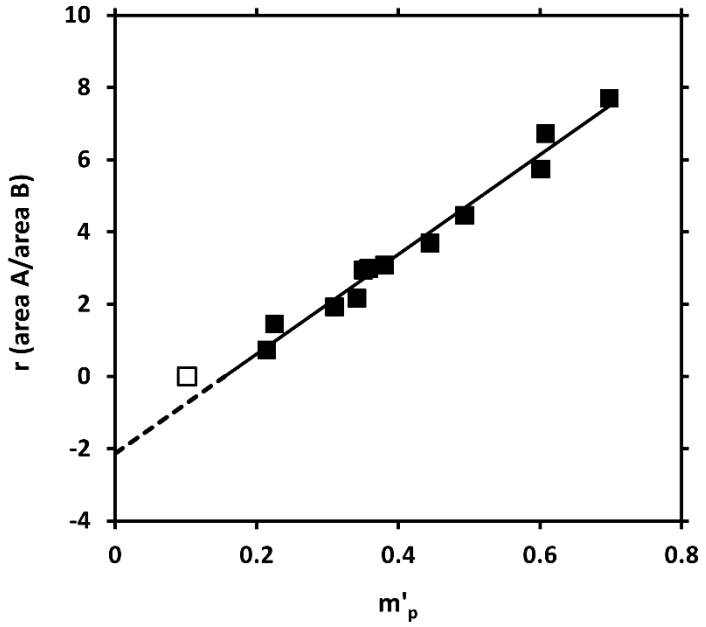

Figure 2.6. The ratio (r) of the areas under the transitions A (loosely-bound) and B (tightly-bound) as a function of the relative amounts of adsorbed polymer (m'_p).

The amount of the tightly-bound polymer for adsorbed PVAc was determined to be 0.78 ± 0.03 mg/m^2. This value is significantly less than the value reported for the adsorbed PMMA/silica system (1.21 mg/m^2).[23,57] This difference is consistent with the ΔT_g results (the difference between the T_g of tightly-bound and bulk-like polymer), which are larger for adsorbed PMMA than PVAc. This is suggestive of a stronger interaction of PMMA with silica or some inherent chain differences between the two polymers.

The bound fraction, f_B, is the ratio of the mass of tightly-bound polymer at the polymer-surface interface to the total amount of polymer. An estimate of f_B can be obtained using the ratio of the heat flow changes of loosely and tightly-bound components, or

$$f_B = m'_{pB}/m'_p = 1/(1+ r\Delta C_{pB}/\Delta C_{pA}). \quad (2.3)$$

where m_{pB} is the full tightly-bound adsorbed amount. Since no loosely-bound peak was observed for adsorbed amounts less than tightly-bound amount, all of the segments for

the samples at adsorbed amounts less than m_{pB} were considered tightly-bound. The calculation of f_B from Equation 2.3, based on $m'_{pB} = 0.78$ mg/m^2 is shown as the smooth curve shown in Figure 2.7. As expected, this shows a systematically decreasing tightly-bound fraction with increasing adsorbed amounts of PVAc. In Figure 2.7, the data points are calculated from the experimental values of r. It is obvious that the model with a fixed amount of tightly bound polymer fits the thermal data quite nicely.

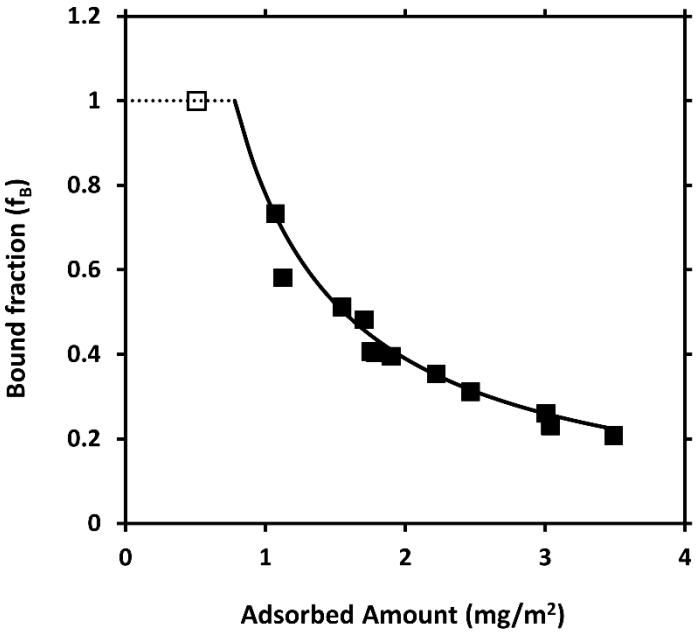

Figure 2.7. The tightly-bound fraction of PVAc on silica as a function of the adsorbed amount of polymer. The smooth curve is based on Equation 2.3 using a fixed amount of tightly-bound polymer of (0.78 mg/m^2).

2.5.2. Simulation density profiles show domains that correspond with TMDSC results

Extensive investigations previously have been done by both Fleer et al.[89,90] and Theodorou[91,92] on polymer density profiles at the polymer/solid interfaces using statistical models for polymer adsorption. These works have shown that at polymer/substrate

interface, the polymer density was enhanced in the presence of attractive interactions between polymer segments and substrate.[93] The segment density profiles of the polymer chains in this region appeared to decrease continuously as a function of distance from the solid surface.[89] In the outer regions of the adsorbed polymer (polymer/air interface), the density profile behavior was primarily influenced by long dangling segments from the ends of the adsorbed polymer chains.[90] Polymer chains in this region had more free volume and thus more rotational freedom than those in bulk and at the substrate interface.[94]

In the characterization of the polymer density profiles, we observed that the polymer segments had different packing densities based on their position relative to the silica surface (Figure 2.3). The density of polymer chains very near the polymer/silica interface was larger than that in bulk. Similar behavior has been observed for graphene oxide/PMMA and silica/polystyrene nanocomposites.[62,95] We found that the density of polymer close to the silica surface, up to around 0.8 nm, was large due to attractive intermolecular interactions, possibly due to hydrogen-bonding between the polymer and silica. Similar effects have been observed by others and attributed to surface hydrogen-bonding.[53] Further than 0.8 nm from the surface, this density effect was no longer apparent. For the regions between the two interfaces, all systems with adsorbed amounts greater than 1 mg/m^2 reached a density that was similar to the simulation density results for the corresponding bulk polymer. Finally, at the polymer/air interface, the density of the polymer decreased from the bulk value to zero, adopting sigmoidal profiles over a distance of about 1 nm, in agreement with observations seen in other work focused on

polymer/air interfaces.[96,97] At the air interface, polymer segments are more mobile and are not as densely packed as the polymer located in the bulk-like region.

The polymer density profile, as a function of the distance from the silica surface, is in agreement with the experimentally measured thermal properties of three different regions. The region with high polymer density corresponds well with polymer tightly-bound to the surface, the polymer region with a higher T_g in TMDSC thermograms. The approximate distance of 0.8 nm is similar to the amount of tightly-bound polymer of 0.78 mg/m^2. The region with bulk-like density corresponds well to the loosely-bound polymer, that with a T_g close to bulk. Finally, the region with deceasing density at polymer/air interface corresponds well with the polymer region with a T_g lower than bulk in the TMDSC thermograms. All three components were also previously observed in solid-state NMR studies.[58]

2.5.3. Tightly-bound polymer shows hydrogen-bonding to the silica surface

To study in detail the properties and structure of tightly-bound polymer chains at the polymer/silica interface, we investigated the structural configuration of carbonyl oxygen atoms of the polymer chains. As shown in Figure 2.4, the distribution function of carbonyl oxygen atoms near the silica surface is essentially independent of the adsorbed amount of polymer. The maxima in the plots indicate the most likely distance between the oxygen atoms and the surface. The density of carbonyl groups in this regime (within 0.3 nm from the surface) was about 2.5 times larger than bulk. No significant differences were observed for systems with different chain lengths.

The intense peak in the *z*-direction distribution function near the surface is due to general packing effects modified by the presence of strong interactions between polymer

and surface.[98] This enhanced density was consistent with the increase in the T_g of polymers near the surface. The peak for carbonyl oxygen, located at ~2.2 Å from the surface, indicates that the distance between the carbonyl oxygen and the silanol hydrogen atom is in the range of hydrogen-bonding.[98-102] At adsorbed amounts greater than 1 mg/m^2, the peak magnitude for the oxygen atoms no longer changed with increasing adsorbed amount of polymer. This similarity was expected based on the experimental results for larger adsorbed amounts, greater than 1 mg/m^2, of polymer. At larger adsorbed amounts, no significant changes in the center and width of peaks in the tightly-bound region of the TMDSC transitions were observed, indicating a similar nature and strength of interaction at the polymer/silica interface.

To further probe the interactions between the polymer and the surface, we studied the energy pair distribution between the polymer side chains and the surface silanol groups. The energy pair distribution function can provide information about the strength and averaged number of silanol interactions with polymer side chains. Figure 2.5 shows the calculated energy pair distribution functions for varying amounts of adsorbed amount of polymer. The tightly-bound peak in the distribution functions stretch from -6.5 to around -18.0 kcal/mol. The peak represents the average interaction energy between a silanol group and a polymer side chain present in the tightly-bound adsorbed polymer region, mostly the result of a hydrogen-bond and general electrostatic interactions between the groups. This interaction was much stronger than side chain-side chain interactions of polymer segments (~ -1 kcal/mol). The large peak centered at around 0 kcal/mol comes from the many long-range interactions between polymer side-chains further from the surface silanol groups, primarily due to distant loosely-bound polymer and mobile

component interactions with the surface. Interestingly, with increasing adsorbed amounts of PVAc, the average interaction strength weakens from -11.7 ± 0.1 kcal/mol to -11.1 ± 0.1 kcal/mol. This is a step change that occurs when the surface is fully covered with a full complement of tightly-bound polymer (at around 0.65 mg/m^2). This result suggests that there is a balance between optimal hydrogen-bonding and optimal polymer packing in the tightly-bound region. In order to increase the number of favorable hydrogen-bonding interactions, the polymer chains compete for the limited available space at the silica interface. These space constraints result in an increase in the number of less optimal hydrogen-bonds to maximize overall energetic favorability. The weakening of surface interactions was also observed in the TMDSC thermograms (Figure 2.2) as a lowering in T_g for tightly-bound polymer with increasing adsorbed amounts of polymer. The observed shifts seen in experiment and computer simulations are not in perfect correspondence with adsorbed amount due to the fact that experimental silica samples have surface irregularities and non-even silanol coverage while molecular simulations are performed on an α-quartz plane with even coverage of silanol groups. Additionally, the standard OPLS-AA force-field, while commonly used for silica interface simulations,[65,66] may not provide an optimal representation of polymeric systems.

The total number of polymer to silica interactions was determined by summing all of the interactions in the tightly-bound region of the energy pair distribution function curves. The number of interactions per nm^2 can be calculated by dividing this total number by the surface area of the silica. Additionally, the number of hydrogen-bonding interactions per nm^2 of surface at the polymer/silica interface was calculated by integrating the first peak in radial distribution function profiles between the polymer

oxygen atoms and hydrogen atoms of silanol groups. Figure 2.8 compares the number of hydrogen-bonds and the number of polymer side chain interactions with silanol groups as a function of adsorbed amounts. Snapshots of top views for each adsorbed amount are also shown below each point. The agreement between the number of polymer/silica interactions and the number of hydrogen-bonds, suggests that the critical force between the polymer side chains and the surface is strong hydrogen-bonding.

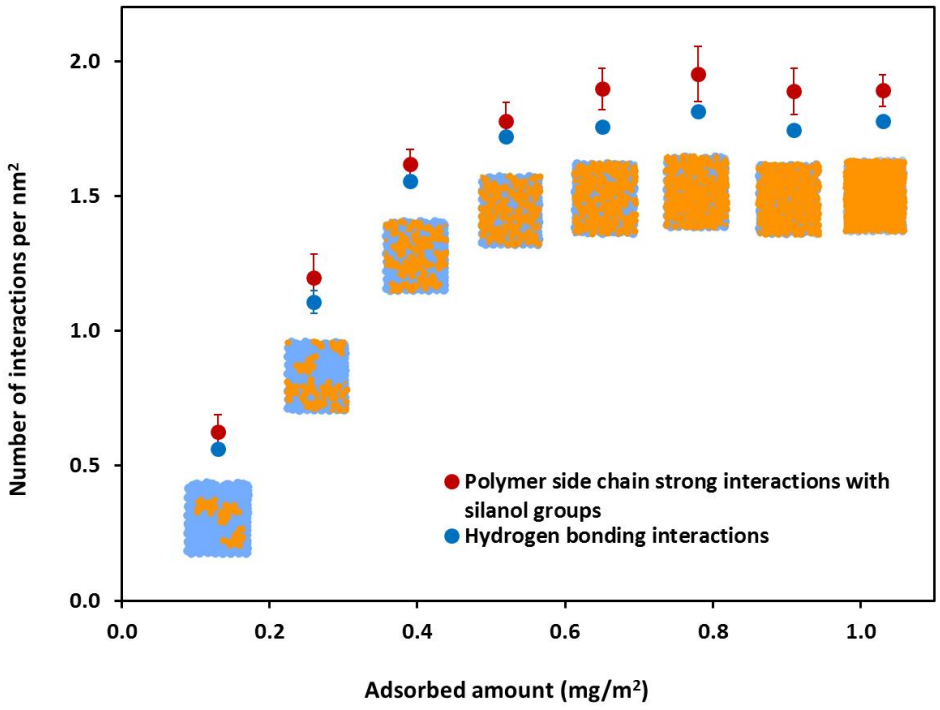

Figure 2.8. Number of polymer side chain interactions with silanol groups and hydrogen-bonds per nm2 and snapshots of top views of adsorbed tetramers on the surface as a function of adsorbed amount. In the pictures, the orange and blue represent the polymer and the silica surface, respectively. The number of interactions increased with increasing the adsorbed amount until the surface was fully covered.

For small adsorbed amounts, the areas under the energy pair distribution curves (Figure 2.5), and the number of interactions, as well as the number of hydrogen-bonds (Figure 2.8) increased with increasing adsorbed amount. This is in excellent agreement with experimental observations showing an increase in the area under the tightly-bound region with increasing adsorbed amounts of polymer. These increases continue until the surface is more or less fully covered with polymer (tightly-bound amount) in both experiments and MD simulations. With increasing adsorbed amount of polymer greater than the tightly-bound amount, the area under the curves in TMDSC thermograms, the energy pair distribution profiles, the radial distribution functions, and consequently the number of interactions per nm^2 remained constant. In other words, with increasing adsorbed amounts greater than the tightly bound amount, a bulk-like region developed. Changes in this bulk-like region did not influence the number of interactions between tightly-bound polymer segments and the silica surface.

Polymer chain length might also play a role in surface behavior. To investigate this, the fraction of strong interactions, the observed number of strong interactions determined from the tightly-bound region of energy pair distribution curve divided by the total possible strong interactions (the number of silanol groups), was calculated for polymer molecules as a function of chain length. Additionally, the H-bonding fraction, the number of silanol hydrogen atoms forming hydrogen-bonds divided by the total number of silanol groups, was computed. Both the fraction of surface silanol groups strongly interacting with polymer side chain and H-bonding fraction are shown in Table 2.1 for different chain lengths (for 1.04 ± 0.01 mg/m^2 adsorbed amount). As expected, there is direct correspondence between the strong interaction fraction and the H-bonding fraction,

indicating that each strong interaction has at least 1 hydrogen-bond. Both of these fractions decreased with increasing polymer chain length, likely due to the configurational changes of polymer very close to the surface with increasing the molecular mass. Polymer chains appear to adopt flatter structures for smaller molecular masses. The surface structure (the density and distances between silanol groups) might also affect the number of interactions with changes in the molecular mass of polymer. As the molecular mass of the polymer increased, the chains adopted more coiled conformations. The coiled conformations, as expected, will have smaller fraction of segments intimately interacting with the surface.

Table 2.1. Fraction of surface silanol groups strongly interacting with PVAc for a 1.04 ± 0.01 mg/m^2 adsorbed amount as a function of chain length.

Chain length (number of mers)	Side chain interaction[a]	H-bonding[b]
1	0.40 ± 0.01	0.369 ± 0.001
2	0.41 ± 0.02	0.377 ± 0.004
4	0.40 ± 0.03	0.379 ± 0.005
8	0.38 ± 0.02	0.37 ± 0.01
10	0.40 ± 0.07	0.367 ± 0.006
12	0.36 ± 0.03	0.346 ± 0.008
20	0.34 ± 0.05	0.33 ± 0.01
30	0.28 ± 0.04	0.272 ± 0.004

a. From the number of strong interactions with the side chains as in Figure 2.5.

b. From the PVAc oxygen atoms in closest proximity to the surface silanol groups as in Figure 2.4.

In order to compare the number of interactions formed between a polymer and silica surface in simulations with experiments, the bound fraction of carbonyl oxygen atoms, the number of carbonyl oxygen atoms participating in hydrogen-bonds divided by the total number of carbonyl oxygen atoms present, was measured. Figure 2.9 shows the results of the simulation derived tightly-bound fraction alongside measured values from FTIR experiments from PVAc.[79] While the bound fraction values from the MD simulations are larger than experimental values, there was a good agreement in the trend as a function of adsorbed amount. The systematic offset between MD and experimental results in this figure was likely due to the differing silanol group densities (MD: 4.5 OH/nm^2 versus FTIR: 3.5 OH/nm^2) used in these studies. Because of the sensitivity problems at small adsorbed amounts, the FTIR experiments have not been used to probe systems with very small adsorbed amounts of polymer. The MD results show two regions of behavior for bound fraction change with increasing adsorbed amounts of polymer: 1) a slowly changing dependence upon adsorbed amounts at small adsorbed amounts and 2) a more rapidly changing region with a fixed number of hydrogen-bonds at larger adsorbed amounts. We would expect to observe a similar behavior in more detailed experimental studies.

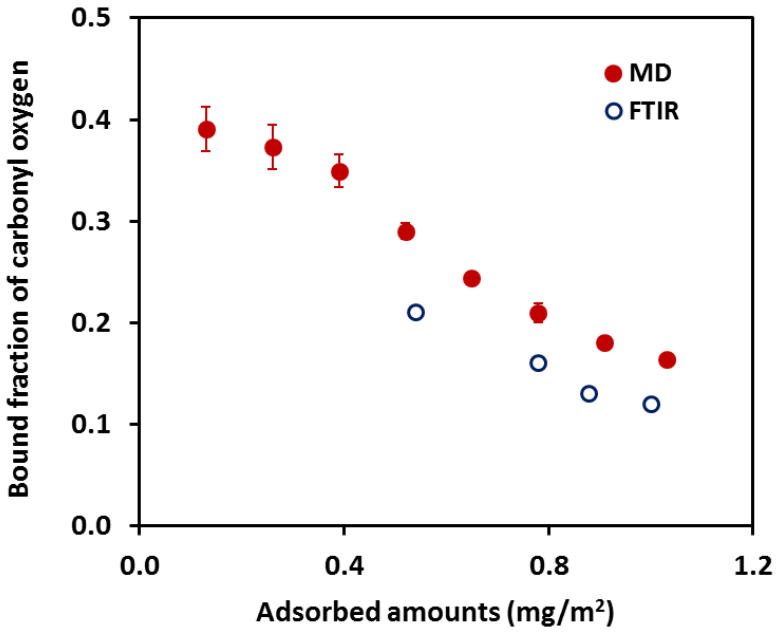

Figure 2.9. Bound fraction of PVAc carbonyl oxygen atoms interacting with silanol groups on the silica surface as a function of adsorbed amount of polymer from MD (●) and FTIR (○) studies.[79] The observed offset between MD and experiment is directly due to the fewer silanol groups present on silica surfaces in experiments.

2.6. CONCLUSIONS

In this study, we performed systematic experimental and computer simulation investigations of adsorbed PVAc on silica surfaces. The primary goal of this work was to uncover how the chemical nature at interfaces affects the thermal, structural, and dynamical properties of adsorbed polymers. Both experiments and simulations showed three distinct regions for adsorbed PVAc on silica: tightly-bound, loosely-bound, and more-mobile segments. The sensitive nature of TMDSC allowed us to identify a transition at a slightly lower temperature than the T_g of bulk-like polymer, which represents more mobile polymer segments located at the polymer/air interface. The tightly-bound region showed a significantly higher T_g than loosely-bound/bulk-like

polymer, and the tightly-bound amount was less than that observed in previous studies on PMMA, a related polymer. MD derived density profiles support the existence of these three distinct regions of adsorbed polymer. Detailed analysis of the tightly-bound region indicates that the presence of hydrogen-bonding interactions at the PVAc/silica interface are critical to the experimentally observed shifts in T_g. The agreement between the calorimetric and MD work show how combined experimental and theoretical investigations can provide additional insight into the chemistry and physics of polymer films.

2.7. ACKNOWLEDGMENTS

Authors acknowledges the financial support of the National Science Foundation (USA) under Grant No. DMR-1005606 and the startup funds provided by Oklahoma State University. The computing for this project was performed at the OSU High Performance Computing Center at Oklahoma State University supported in part through the National Science Foundation grant OCI–1126330. The authors thank Dr. Madhubhashini Maddumaarachchi for measuring the PVAc molecular mass.

2.8. REFERENCES

(1) Zou, H.; Wu, S.; Shen, J. *Chem. Rev* **2008**, *108*, 3893.

(2) Parida, S. K.; Dash, S.; Patel, S.; Mishra, B. *Adv. Colloid Interface Sci.* **2006**, *121*, 77.

(3) Shin, Y.; Lee, D.; Lee, K.; Ahn, K. H.; Kim, B. *J. Ind. Eng. Chem.* **2008**, *14*, 515.

(4) Metin, B.; Blum, F. D. *Langmuir* **2009**, *26*, 5226.

(5) Madathingal, R. R.; Wunder, S. L. *Thermochim. Acta* **2011**, *526*, 83.

(6) Lin, Y.; Liu, L.; Xu, G.; Zhang, D.; Guan, A.; Wu, G. *J. Phys. Chem. C* **2015**, *119*, 12956.

(7) Kim, S.; Mundra, M. K.; Roth, C. B.; Torkelson, J. M. *Macromolecules* **2010**, *43*, 5158.

(8) Mundra, M.; Ellison, C.; Rittigstein, P.; Torkelson, J. *Eur. Phys. J. Spec. Top.* **2007**, *141*, 143.

(9) Füllbrandt, M.; Purohit, P. J.; Schönhals, A. *Macromolecules* **2013**, *46*, 4626.

(10) Fleer, G.; Cohen Stuart, M. A.; Scheutjens, J. M. H. M.; Cosgrove, T.; Vincent, B. *Polymers at interfaces*; Springer Science & Business Media: London, UK, **1993**.

(11) Zou, D. Q.; Yoshida, H. *J. Therm. Anal. Calorim.* **2010**, *99*, 21.

(12) Lučić, S.; Kovačević, V.; Hace, D. *Int. J. Adhes. Adhes.* **1998**, *18*, 115.

(13) Soga, I. *J. Coat. Technol.* **2003**, *75*, 53.

(14) Zou, H.; Wu, S.; Shen, J. *Chem. Rev.* **2008**, *108*, 3893.

(15) Kaboorani, A.; Riedl, B. *Compos. Part A Appl. Sci. Manuf.* **2011**, *42*, 1031.

(16) Caselis, J. L. V.; Rosas, E. R.; Meneses, V. M. C. *Corros. Eng., Sci. Technol.* **2012**, *47*, 131.

(17) Ellison, C. J.; Mundra, M. K.; Torkelson, J. M. *Macromolecules* **2005**, *38*, 1767.

(18) Overney, R. M.; Buenviaje, C.; Luginbühl, R.; Dinelli, F. *J. Therm. Anal. Calorim.* **2000**, *59*, 205.

(19) Belfiore, L. A. *Physical Properties of Macromolecules*; John Wiley & Sons: Hoboken, NJ, **2010**.

(20) Yevgen, M.; Maksym, I. *Advances in Progressive Thermoplastic and Thermosetting Polymers, Perspectives and Applications*; TehnoPress editura: Iasi, Romania, **2012**.

(21) Porter, C. E.; Blum, F. D. *Macromolecules* **2000**, *33*, 7016.

(22) Tate, R. S.; Fryer, D. S.; Pasqualini, S.; Montague, M. F.; de Pablo, J. J.; Nealey, P. F. *J. Chem. Phys.* **2001**, *115*, 9982.

(23) Blum, F. D.; Young, E. N.; Smith, G.; Sitton, O. C. *Langmuir* **2006**, *22*, 4741.

(24) Krisanangkura, P.; Packard, A. M.; Burgher, J.; Blum, F. D. *J. Polym. Sci., Part B: Polym. Phys.* **2010**, *48*, 1911.

(25) Zhang, F.-A.; Lee, D.-K.; Pinnavaia, T. J. *Polymer* **2009**, *50*, 4768.

(26) Wielage, B.; Lampke, T.; Marx, G.; Nestler, K.; Starke, D. *Thermochim. Acta* **1999**, *337*, 169.

(27) Sargsyan, A.; Tonoyan, A.; Davtyan, S.; Schick, C. *Eur. Polym. J.* **2007**, *43*, 3113.

(28) Hutchinson, J. M. *J. Therm. Anal. Calorim.* **2003**, *72*, 619.

(29) Simon, S. L. *Thermochim. Acta* **2001**, *374*, 55.

(30) Jin, Y.; Bonilla, J.; Lin, Y.-G.; Morgan, J.; McCracken, L.; Carnahan, J. *J. Therm. Anal.* **1996**, *46*, 1047.

(31) Cao, J. *Thermochim. Acta* **1999**, *325*, 101.

(32) Verdonck, E.; Schaap, K.; Thomas, L. C. *Int. J. Pharm.* **1999**, *192*, 3.

(33) Zhang, T.; Xu, G.; Puckette, J.; Blum, F. D. *J. Phys. Chem. C* **2012**, *116*, 11626.

(34) Zhang, B.; Blum, F. D. *Macromolecules* **2003**, *36*, 8522.

(35) Zeng, Q.; Yu, A.; Lu, G. *Prog. Polym. Sci.* **2008**, *33*, 191.

(36) Mo, Y.-F.; Yang, C.-L.; Xing, Y.-F.; Wang, M.-S.; Ma, X.-G.; Wang, L.-Z. *Appl. Surf. Sci.* **2014**, *311*, 273.

(37) Jha, K. C.; Zhu, H.; Dhinojwala, A.; Tsige, M. *Langmuir* **2014**, *30*, 12775.

(38) Vogiatzis, G. G.; Theodorou, D. N. *Macromolecules* **2013**, *46*, 4670.

(39) Ghanbari, A.; Ndoro, T. V.; Leroy, F.; Rahimi, M.; Böhm, M. C.; Müller-Plathe, F. *Macromolecules* **2011**, *45*, 572.

(40) Singh, C.; Pickett, G. T.; Zhulina, E.; Balazs, A. C. *J. Phys. Chem. B* **1997**, *101*, 10614.

(41) Yang, M.; Koutsos, V.; Zaiser, M. *J. Phys. Chem. B* **2005**, *109*, 10009.

(42) Tallury, S. S.; Pasquinelli, M. A. *J. Phys. Chem. B* **2010**, *114*, 4122.

(43) Tallury, S. S.; Pasquinelli, M. A. *J. Phys. Chem. B* **2010**, *114*, 9349.

(44) Reddy, S.; Kuppa, V. K. *Synth. Met.* **2012**, *162*, 2117.

(45) Wang, H.; Hsieh, B.; Jiménez-Osés, G.; Liu, P.; Tassone, C. J.; Diao, Y.; Lei, T.; Houk, K. N.; Bao, Z. *Small* **2015**, *11*, 126.

(46) Rissanou, A. N.; Harmandaris, V. *Soft Matter* **2014**, *10*, 2876.

(47) Harmandaris, V. A.; Daoulas, K. C.; Mavrantzas, V. G. *Macromolecules* **2005**, *38*, 5796.

(48) Hudzinskyy, D.; Lyulin, A. V.; Baljon, A. R.; Balabaev, N. K.; Michels, M. A. *Macromolecules* **2011**, *44*, 2299.

(49) Odegard, G.; Clancy, T.; Gates, T. *Polymer* **2005**, *46*, 553.

(50) Balazs, A. C.; Lewandowski, S. *Macromolecules* **1990**, *23*, 839.

(51) Rissanou, A. N.; Harmandaris, V. *J. Nanopart. Res.* **2013**, *15*, 1.

(52) Zhang, J.; Lou, J.; Ilias, S.; Krishnamachari, P.; Yan, J. *Polymer* **2008**, *49*, 2381.

(53) Eslami, H.; Rahimi, M.; Müller-Plathe, F. *Macromolecules* **2013**, *46*, 8680.

(54) Linse, P.; Kallrot, N. *Macromolecules* **2010**, *43*, 2054.

(55) Butt, H.-J.; Duran, H.; Egger, W.; Faupel, F.; Harmandaris, V.; Harms, S.; Johnston, K.; Kremer, K.; Lin, F.-Y.; Lue, L. *Macromolecules* **2014**, *47*, 8459.

(56) Rissanou, A. N.; Harmandaris, V. *Macromolecules* **2015**, *48*, 2761.

(57) Khatiwada, B. K.; Hetayothin, B.; Blum, F. D. *Macromol. Symp.* **2013**, *327*, 20.

(58) Blum, F. D.; Xu, G.; Liang, M.; Wade, C. G. *Macromolecules* **1996**, *29*, 8740.

(59) Brandrup, J.; Immergut, E. H.; Grulke, E. A.; Abe, A.; Bloch, D. R. *Polymer handbook*; Wiley: New York, **1999**.

(60) Brunauer, S.; Emmett, P. H.; Teller, E. *J. Am. Chem. Soc.* **1938**, *60*, 309.

(61) Pettersen, E. F.; Goddard, T. D.; Huang, C. C.; Couch, G. S.; Greenblatt, D. M.; Meng, E. C.; Ferrin, T. E. *J. Comput. Chem.* **2004**, *25*, 1605.

(62) Skountzos, E. N.; Anastassiou, A.; Mavrantzas, V. G.; Theodorou, D. N. *Macromolecules* **2014**, *47*, 8072.

(63) Morrow, B.; McFarlan, A. *Langmuir* **1991**, *7*, 1695.

(64) Van Der Spoel, D.; Lindahl, E.; Hess, B.; Groenhof, G.; Mark, A. E.; Berendsen, H. J. *J. Comput. Chem.* **2005**, *26*, 1701.

(65) Wensink, E.; Hoffmann, A.; Apol, M.; Berendsen, H. *Langmuir* **2000**, *16*, 7392.

(66) van der Spoel, D.; Wensink, E. J.; Hoffmann, A. C. *Langmuir* **2006**, *22*, 5666.

(67) Allen, M. P.; Tildesley, D. J. *Computer Simulation of Liquids*; Oxford university press: New York, **1989**.

(68) Essmann, U.; Perera, L.; Berkowitz, M. L.; Darden, T.; Lee, H.; Pedersen, L. G. *J. Chem. Phys.* **1995**, *103*, 8577.

(69) Hess, B. *J. Chem. Theory Comput.* **2008**, *4*, 116.

(70) Nosé, S. *Mol. Phys.* **1984**, *52*, 255.

(71) Hoover, W. G. *Phys. Rev. A* **1985**, *31*, 1695.

(72) Jorgensen, W. L. *J. Am. Chem. Soc.* **1980**, *102*, 543.

(73) Bakó, I.; Megyes, T.; Bálint, S.; Chihaia, V.; Bellissent-Funel, M.-C.; Krienke, H.; Kopf, A.; Suh, S.-H. *J. Chem. Phys.* **2010**, *132*, 014506.

(74) Blazevska-Gilev, J.; Spaseska, D. *J. Chem. Technol. Metall.* **2005**, *40*, 287.

(75) Al-Hassany, Z.; Genovese, A.; Shanks, R. *Express Polym. Lett.* **2010**, *4*, 79.

(76) Sivalingam, G.; Madras, G. *J. Appl. Polym. Sci.* **2004**, *93*, 1378.

(77) Rittigstein, P.; Torkelson, J. M. *J. Polym. Sci., Part B: Polym. Phys.* **2006**, *44*, 2935.

(78) Porter, C. E.; Blum, F. D. *Macromolecules* **2002**, *35*, 7448.

(79) Maddumaarachchi, M.; Blum, F. D. *J. Polym. Sci., Part B: Polym. Phys.* **2014**, *52*, 727.

(80) Lin, W.-Y.; Blum, F. D. *J. Am. Chem. Soc.* **2001**, *123*, 2032.

(81) Metin, B.; Blum, F. D. *J. Chem. Phys.* **2006**, *125*, 054707.

(82) Wen, N.; Tang, Q.; Chen, M.; Wu, L. *J. Colloid Interface Sci* **2008**, *320*, 152.

(83) Beaudry, C.; Klein, L.; McCauley, R. *J. Therm. Anal. Calorim.* **1996**, *46*, 55.

(84) Frantz, P.; Granick, S. *Macromolecules* **1995**, *28*, 6915.

(85) Kulkeratiyut, S.; Kulkeratiyut, S.; Blum, F. D. *J. Polym. Sci., Part B: Polym. Phys.* **2006**, *44*, 2071.

(86) Blow, C. *Polymer* **1973**, *14*, 309.

(87) Wunderlich, B. *Prog. Polym. Sci.* **2003**, *28*, 383.

(88) Schick, C.; Wurm, A.; Mohammed, A. In *Polymer Crystallization*; Springer: Berlin Heidelberg, **2003**, p 252.

(89) Scheutjens, J.; Fleer, G. *J. Phys. Chem.* **1979**, *83*, 1619.

(90) Scheutjens, J.; Fleer, G. *J. Phys. Chem.* **1980**, *84*, 178.

(91) Theodorou, D. N. *Macromolecules* **1989**, *22*, 4589.

(92) Theodorou, D. N. *Macromolecules* **1988**, *21*, 1400.

(93) Mansfield, K. F.; Theodorou, D. N. *Macromolecules* **1989**, *22*, 3143.

(94) Mansfield, K. F.; Theodorou, D. N. *Macromolecules* **1990**, *23*, 4430.

(95) Ndoro, T. V.; Voyiatzis, E.; Ghanbari, A.; Theodorou, D. N.; Böhm, M. C.; Müller-Plathe, F. *Macromolecules* **2011**, *44*, 2316.

(96) Theodorou, D. N. *Macromolecules* **1989**, *22*, 4578.

(97) Mansfield, K. F.; Theodorou, D. N. *Macromolecules* **1991**, *24*, 6283.

(98) Barbier, D.; Brown, D.; Grillet, A.-C.; Neyertz, S. *Macromolecules* **2004**, *37*, 4695.

(99) Kumar, R.; Schmidt, J.; Skinner, J. *J. Chem. Phys.* **2007**, *126*, 204107.

(100) Wernet, P.; Nordlund, D.; Bergmann, U.; Cavalleri, M.; Odelius, M.; Ogasawara, H.; Näslund, L.; Hirsch, T.; Ojamäe, L.; Glatzel, P. *Science* **2004**, *304*, 995.

(101) Luzar, A.; Chandler, D. *Phys. Rev. Lett.* **1996**, *76*, 928.

(102) Taylor, R.; Kennard, O. *Acc. Chem. Res.* **1984**, *17*, 320.

2.9. SUPPORTING INFORMATION

S2.1. OPLS force field

The following parameters were used with the OPLS force field in Table 3-1. The assignments with the atom numbers are shown in Figure 3-1. For the surface, the OPLS parameters are given in Table 3-2 (*Langmuir* **2000**, 16, 7392, *Langmuir* **2006**, 22, 5666).

Table S2.1. OPLS-AA force-field parameters for PVAc molecules and silanol groups of the silica surface.

Atom name	Atom type	Atom charge
C1	opls_135	-0.13
C2	opls_058	0.52
C3	opls_136	0.13
C4	opls_135	-0.18
O1	opls_059	-0.44
O2	opls_062	-0.38
H	opls_140	0.06

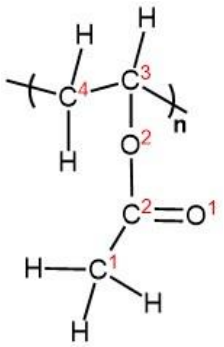

Figure S2.1. Monomer structure of PVAc molecules.

Table S2.2. OPLS-AA force-field parameters for silanol groups of the silica surface.

Atom name	Atom type	Atom charge
Si	SI	0.265
OH	opls_169	-0.700
HO	opls_170	0.435

S2.2. Reversing heat flow curves for adsorbed pvac on silica

The following Figure shows the heat flow curves as a function of temperature for bulk PVAc and adsorbed PVAc on silica.

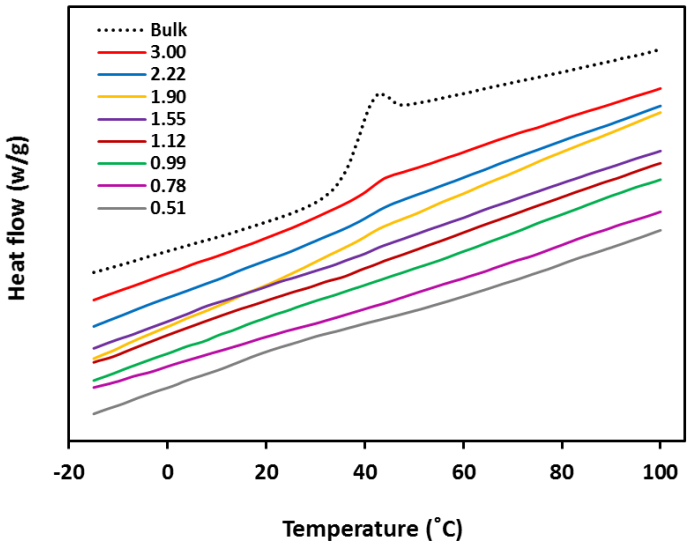

Figure S2.2. TMDSC thermograms for bulk PVAc and adsorbed PVAc on silica (reversing heat flow as a function of temperature). The thermograms are labeled with the adsorbed amounts that are shown in mg polymer/m^2 silica.

S2.3. Density profiles and atom distributions for pvac on silica

The average mass density profile of adsorbed PVAc on silica as a function of adsorbed amount is shown in Figure S2.3.

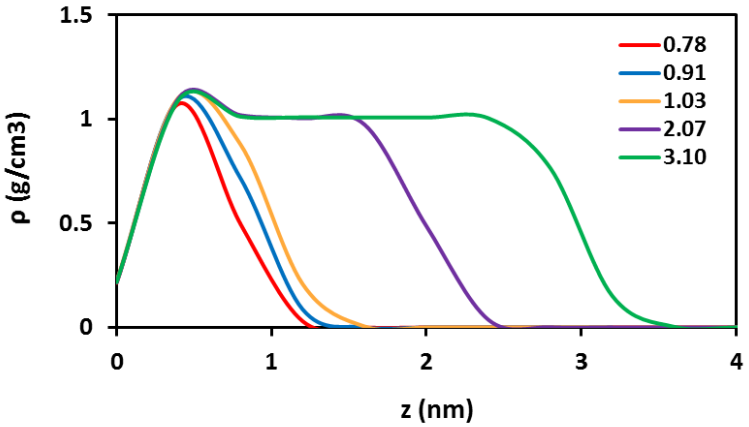

Figure S2.3. Density profile of the polymer as a function of the distance from the surface for different adsorbed amounts.

We investigated the distance distribution function between the carbonyl oxygen atoms of the PVAc and the surface silanol groups as a function of chain length to help understanding the effect of molecular mass on the interactions of polymers at the interface. Results of 1.04 ± 0.01 mg PVAc/m^2 silica samples for 1 to 8-mer chain lengths are shown in Figure S2.4 and for 10 to 30-mer chain lengths are shown in Figure S2.5.

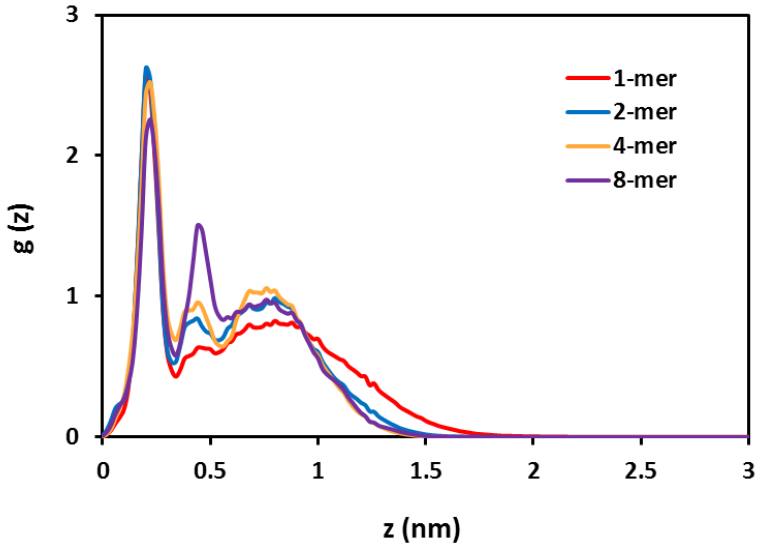

Figure S2.4. *Z*-direction distribution functions for carbonyl oxygen atoms as a function of the *z*-coordinate, the distance from silanol oxygen atoms, for monomer, dimer, tetramer, and octamer of 1.04 ± 0.01 mg PVAc/m^2 silica.

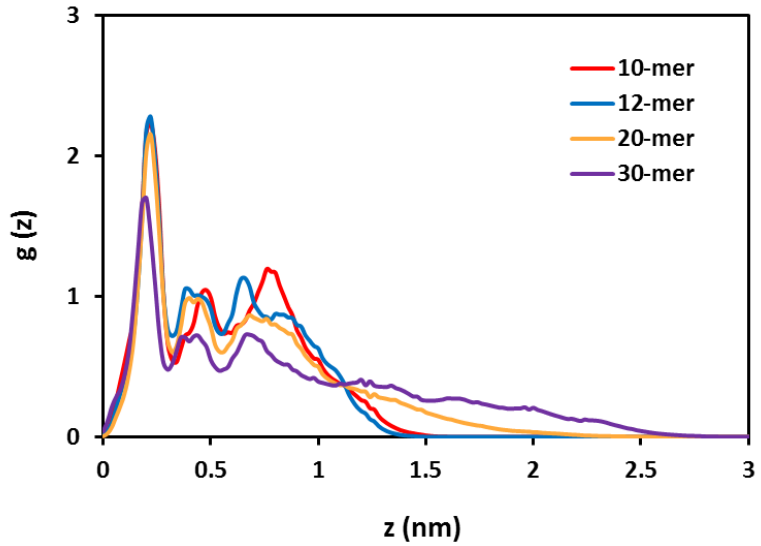

Figure S2.5. *Z*-direction distribution functions for carbonyl oxygen atoms as a function of the *z*-coordinate, the distance from silanol oxygen atoms, for decamer, dodecamer, icosamer, and triacontamer of 1.04 ± 0.01 mg PVAc/m^2 silica. The 30-mer sample showed an extended distribution in larger distance from the surface due to the large size of the

polymer and the very small number of polymer chains on the surface of 1.03 mg/m^2 coverage.

S2.4. Chain length dependence on energy pair distributions

We also investigated the effect of polymer chain length on the interaction energy between polymer side chains and silanol groups of the surface. The energy pair distribution functions for samples with 1.04 ± 0.01 mg PVAc/m^2 silica for different polymer chain lengths are shown in Figures S2.6, S2.7, and S2.8.

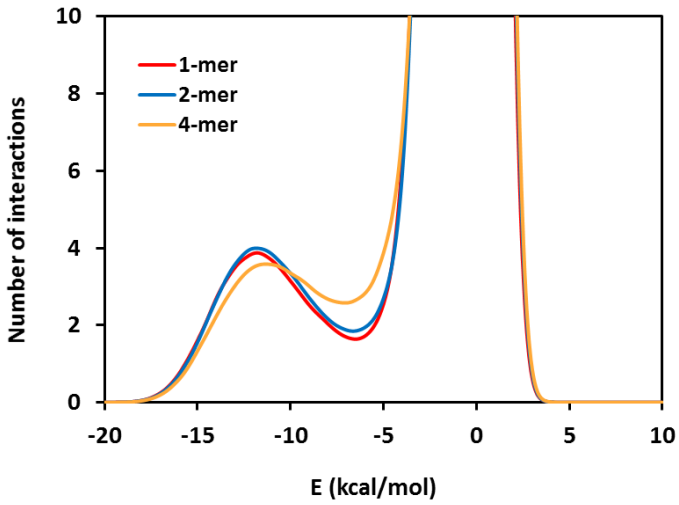

Figure S2.6. Energy pair distribution function between PVAc side-chains and silica silanol groups as a function of chain length for 1.04 ± 0.01 mg PVAc/m^2 silica.

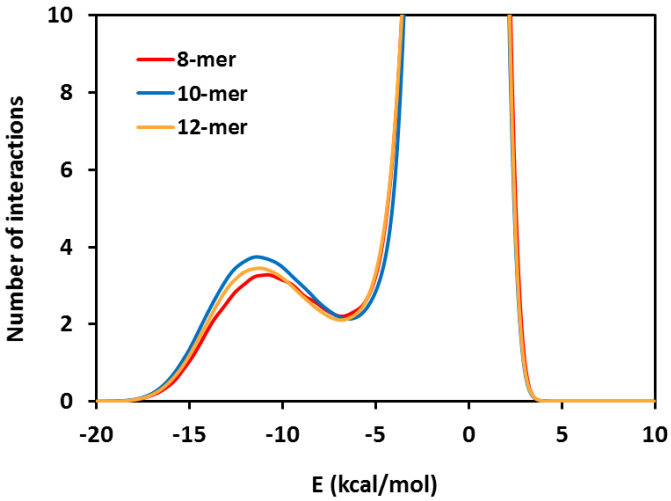

Figure S2.7. Energy pair distribution function between PVAc side-chains and silica silanol groups as a function of chain length for 1.04 ± 0.01 mg PVAc/m^2 silica.

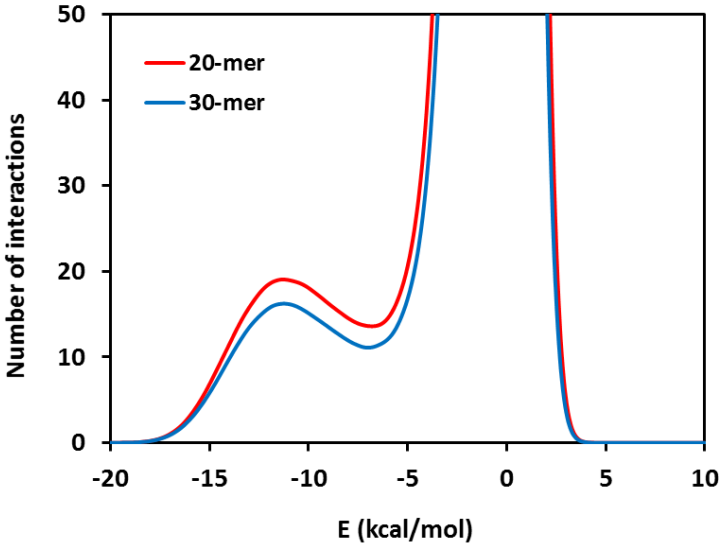

Figure S2.8. Energy pair distribution function between PVAc side-chains and silica silanol groups as a function of chain length for 1.04 ± 0.01 mg PVAc/m^2 silica. The number of interactions for these chain lengths are larger than smaller chains due to the larger silica surface used for these chain lengths.

CHAPTER III

SURFACE BONDING IS STRONGER FOR POLY(METHYL METHACRYLATE) THAN FOR POLY(VINYL ACETATE)

3.1. ABSTRACT

Polymer-substrate interactions can directly affect the thermal properties of adsorbed polymers, such as the glass transition temperature. Using temperature-modulated differential scanning calorimetry (TMDSC) and molecular modeling, we performed direct comparisons of the thermal properties and intermolecular interactions of adsorbed poly(vinyl acetate) (PVAc) and poly(methyl methacrylate) (PMMA) with similar molecular masses and adsorbed amounts on silica. Compared to their bulk counterparts, adsorbed PMMA showed a greater change in glass transition and a larger amount of tightly-bound polymer compared to adsorbed PVAc. These observations suggested that the interactions between PMMA and silica were stronger than those between PVAc and silica. Molecular modeling of these surface polymers showed that PMMA associates more strongly with silica than does PVAc through additional hydrogen-bonding interactions. Additionally, simulations show that the polymer-polymer interactions are stronger in PMMA than PVAc, helping explain why a PMMA mobile-component is not observed in TMDSC thermograms.

3.2. INTRODUCTION

The properties of polymers at interfaces are usually different from the properties of bulk polymers.[1-13] In the presence of air, small amounts of adsorbed polymers on solid substrates may be affected by both polymer/substrate and polymer/air interfaces. Previous studies of adsorbed polymers have shown a motional heterogeneity for polymers at interfaces with attractive interactions with substrates.[14-18] This heterogeneity may include *more-mobile segments* at the air interface, less mobile segments, referred to as *tightly-bound*, near the substrate, and bulk-like segments between them. As an example, it has been shown that there were three different regions of thermal activities corresponding to interfacial layers for adsorbed high molecular mass poly(vinyl acetate) (PVAc) on silica.[15,19] Hydrogen-bonding between the polymer side-chain carbonyl groups and hydroxyl groups of the silica surface has been identified as a strong contributing factor in the reduction of mobility and the elevation of glass transition temperature (T_g).[20-24]

While surface hydrogen-bonding may be a dominant factor in the changes in the properties of the adsorbed polymers, interfacial interactions can be difficult to characterize. To better assess the role that these interactions can play, we decided to investigate two chemically similar polymeric systems that have similar chemical formulae, yet different functional groups, namely PVAc and poly(methyl methacrylate) (PMMA). The differing functional groups lead to somewhat different behavior upon adsorption. Figure 3.1 shows the chemical structures for PVAc and PMMA. It is clear that both of these polymers have the ability to accept surface hydrogen-bonds, yet studies of the thermal behavior of the adsorbed polymeric systems indicate distinct and

significant differences in the changes of thermal properties upon adsorption. Previous studies of PMMA[4,22] show much larger shifts in the glass transition upon adsorption than those more recently observed in PVAc.[19] Given the similarity in chemical structures, it is unclear how, or if, hydrogen-bonding alone could be the reason for the differences in thermal behavior.

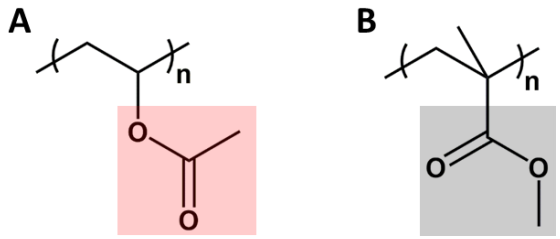

Figure 3.1. Structures of A) PVAc and B) PMMA. Both polymer units can accept hydrogen-bonds.

In order to characterize the differences in the glass transition behavior of adsorbed PVAc and PMMA, we performed temperature modulated differential scanning calorimetry (TMDSC)[25,26] experiments on polymer samples with similar molecular masses and similar adsorbed amounts. TMDSC has been used to resolve differences in adsorbed polymer regions based on thermal activity.[27] To independently investigate the fundamental intermolecular interactions between the polymer chains and surface substrate, we also performed detailed molecular dynamics (MD) experiments on similar adsorbed polymer systems. MD simulations have been shown to provide insight currently impossible to obtain from macroscopic experimental techniques.[28-35]

In this article, we report the investigation of thermal properties of bulk and adsorbed PVAc and PMMA on silica and compare the relative glass transitions of the polymers to

their bulk counterparts. The focus here is on the glass transition of the tightly-bound region of the adsorbed polymers and on direct comparisons between these adsorbed polymers under the constraints of similar molecular masses, adsorbed amounts, and environmental conditions. We also compare the interactions between the polymers and the surface in atomistic molecular simulations in order to uncover differences in the microscopic surface interactions that influence the thermal properties. The results reported indicate that while PVAc and PMMA have structural similarities and can both hydrogen-bond with the silica substrate, PMMA shows enhanced hydrogen-bonding interactions as a consequence of the orientation of its side-chain groups.

3.3. METHODS

3.3.1. Experimental studies

PVAc with molecular mass of 100 kDa was purchased and used as received (Scientific Polymer Products, Inc. Ontario, NY). PMMA with molecular mass of 90 kDa was also used as received (Aldrich Chemical Co., Milwaukee, WI). The polydispersity indices of PVAc and PMMA were determined to be 2.6 and 1.6 using gel permeation chromatography in tetrahydrofuran with an Optilab refractive index detector (Wyatt Technology, CA). Cab-O-Sil M-5P fumed silica with a specific surface area of 190 m^2/g provided by Cabot Corporation (Tuscola, IL) was used as the substrate. Toluene was purchased from Pharmco-aaper (Brookfield, CT) and used as received.

Samples were prepared using different concentrations of polymer solutions in 10 mL toluene in separate tubes. Cab-O-Sil fumed silica (~0.3 g) was added to each tube and the tubes were placed in a mechanical shaker for 48 h and then centrifuged at 6000 rpm for 15 min. After removing supernatant liquid, the samples were dried using air at a low flow

rate until the gel turned to a dry powder. The samples were then dried in a vacuum oven for 72 h to remove any residual solvent.

A model Q50 thermogravimetric analysis (TGA) instrument (TA Instruments, New Castle, DE) was used to determine the adsorbed amounts of polymer on the surface of silica based on the mass loss of polymer and the mass of residual material. Samples were heated from room temperature to 700 °C at a heating rate of 20 °C/min in flowing air atmosphere (40 ml/min).

A model Q2000 DSC (TA Instruments) was used to investigate and compare the thermal behavior of adsorbed polymers in the T_g region. The PVAc samples were run under the same conditions used in previous work.[19] The PMMA samples were held at 25 °C for 1 min, heated to 200 °C at the same heating rate used for PVAc samples (3 °C/min). The same modulation amplitude and modulation period were applied for PMMA samples (±1.0 °C each 60 s). The samples were held at 200 °C for 2 min and then cooled to 25 °C at 3 °C/min with the same modulation condition and remained at the room temperature for 2 min. The second heating scan was made with the same conditions as the first heating scan. The second heating scan results were used to determine the T_g and tightly-bound amount in the samples. After applying a 10 ºC smoothing to reduce the high-frequency noise, the thermograms were reported as differential reversing heat flow rates (dQ_{rev}/dT) as a function of temperature.

3.3.2. Computational studies

Atomistic-level simulations were used to model both PVAc and PMMA interactions with a smooth silica surface. Monomeric VAc and MMA units were constructed with UCSF Chimera,[36] and an internal program was written to build 12-mer structures and

topologies of PVAc and PMMA. Note that while these 12-mers are oligomers, we refer to these molecules as PVAc and PMMA for simplicity and to follow recent literature convention.[37,38] A silica slab, with an area of 3.93×3.40 nm^2 and thickness of 1.45 nm, was evenly functionalized with a 4.7 groups/nm^2 surface density of silanol groups, in agreement with experimental silanol densities.[39] To form a continuous silica substrate, the slab was bonded to itself at the edges of the simulation box in the form of a single molecule which spans across periodic boundaries in the *x* and *y*-dimensions to form, effectively, an infinite slab. A large *z*-axis box dimension (50 nm) was used to prevent the simultaneous interaction of adsorbed polymer chains with both the top and bottom of the silica slab.

MD simulations were carried out in the NVT ensemble using GROMACS 4.5.5.[40] The optimized potentials for liquid simulations all-atom force-field (OPLS-AA) with silica parameters described by Wensink et al.[41,42] was used for all the simulations. Periodic boundary conditions were employed and the smooth particle-mesh Ewald summation was used to account for the long-range contributions to the electrostatic interactions.[43] Bonds to hydrogen atoms were constrained using the P-LINCS algorithm.[44] Simulations used a time-step of 2 fs and 10 independent 20 ns simulations were performed for each polymer coating, all at a temperature of 75 ˚C, held constant with a Nose-Hoover thermostat with a 1 ps time constant.[45,46] The starting configurations for the 10 independent simulations were pulled from separate state-points of fluid polymer simulations at a higher temperature (225 ˚C). The independent systems were equilibrated for 5 ns after cooling to the target temperature and data was collected from subsequent 20 ns trajectories. As such,

a total of 200 ns of sampling was collected for each polymeric system. Additional details of the force-field parameters are described in the **Appendix B**.

3.4. RESULTS

3.4.1. Thermal analysis shows a larger change in glass transition for adsorbed PMMA

TMDSC thermograms (normalized by the T_g of bulk polymers) for bulk and adsorbed PVAc and PMMA are shown in Figure 3.2. While some thermograms for these polymers with different molecular masses exist in the literature,[19,22] these specific measurements compare the thermal behavior of adsorbed PMMA and PVAc with very similar molecular masses. The panels in Figure 3.2 show how the thermograms change as a function of adsorbed amounts of polymers on silica. Bulk PVAc showed a narrower glass transition width than PMMA. The intensity of the peaks at T_g for bulk and adsorbed PVAc were also larger than the intensity of peaks for bulk and adsorbed PMMA. This is because there is a larger change in the heat capacity (ΔC_p) for PVAc around the T_g.[47,48] The change in the heat capacity and thermal sensitivity of PMMA is smaller than that of PVAc.[49] The thermograms of adsorbed PVAc and PMMA showed qualitatively similar trends with increasing the adsorbed amounts. At small adsorbed amounts, we observed thermal activities only at significantly higher temperatures relative to the T_g of the bulk polymers. At larger adsorbed amounts, both PVAc and PMMA samples showed a second region of thermal activity, slightly above the T_g of bulk polymer. The temperature shifts of these peaks relative to the T_g of the bulk polymer were always greater for PMMA than PVAc. For PVAc, we observed another region of thermal activity with enhanced mobility at a lower temperature than the T_g of bulk.[19]

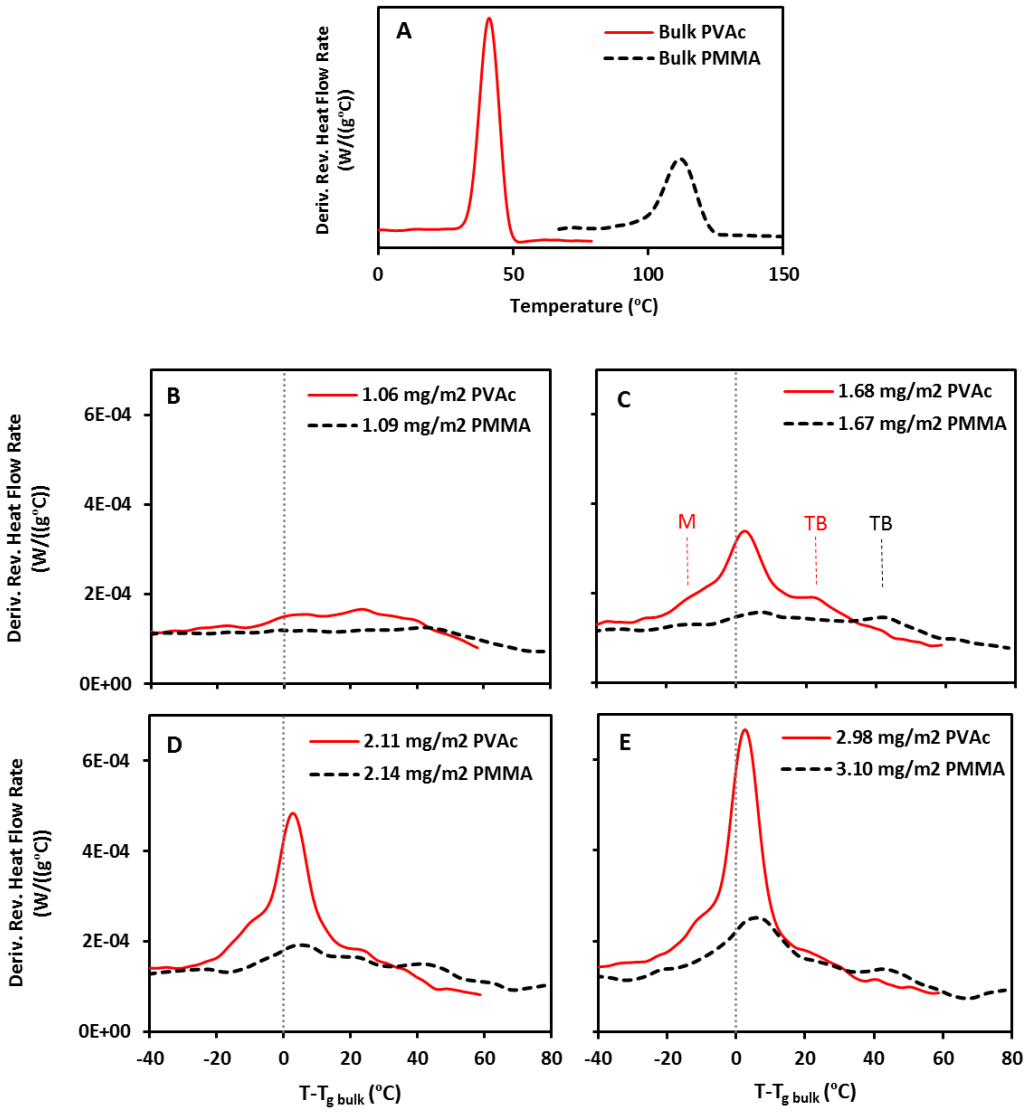

Figure 3.2. TMDSC thermograms for A) bulk, and B to E) adsorbed PVAc and PMMA on silica particles. The curves in B to E are shown relative to the bulk T_g of each polymer (dashed vertical line). The tightly-bound transition was found at a higher temperature for PMMA and the ratio of loosely to tightly-bound fraction was larger for adsorbed PVAc. A significant mobile-component was observed only for adsorbed PVAc samples. The TB and M labels indicate tightly-bound and mobile polymer thermal activities, respectively.

The presence of multiple regions of thermal activity suggests a distribution of mobility of adsorbed polymers, which is likely due to variation in intermolecular interactions at different interfaces. The regions located at the polymer/silica interface, bulk-like polymer, and polymer/air interfaces are referred to as *tightly-bound*, *loosely-bound* and more-*mobile* components, respectively.[15] The ratios of the intensity of loosely-bound to tightly-bound transitions of adsorbed PVAc were larger than those of PMMA at each adsorbed amount. The difference between the T_g values of tightly and loosely-bound polymer (ΔT_g) for PMMA was larger than that for PVAc.

3.4.2. PMMA shows stronger interactions with silica in molecular simulations

To investigate the polymers' interactions with the surface, we characterized the *z*-direction distribution function, g(*z*), of carbonyl and alkoxy oxygen atoms as a function of *z*-distance from the silanol oxygen atoms of the silica surface. The simulation boxes were divided into partition bins of 0.2 Å in the *z*-direction and the *xy* cross-section averaged density g(*z*) was measured over all configurations every 20 ps. The total pair correlation function is defined as the probability of finding any indicated atom at a distance *z* from the surface relative to the probability calculated for the bulk material.[50]

The g(*z*) plots for (A) carbonyl oxygen, (B) alkoxy oxygen, and (C) all oxygen atoms of polymers up to a 1.5 nm distance are shown in Figure 3.3. Carbonyl oxygen atoms showed roughly the same distribution profile for both PVAc and PMMA (Figure 3.3A). A strong peak located at 2.2 Å for the carbonyl oxygen atoms indicated the presence of strong interactions between the polymer and silanol groups via carbonyl oxygen atoms. In contrast, the distribution profiles for alkoxy oxygen atoms of PVAc and PMMA were rather different. The alkoxy oxygen atoms of PMMA showed a strong peak at 2.8 Å and a

secondary peak at 3.8 Å, however, the alkoxy-oxygen atoms of PVAc showed primarily a peak at 3.8 Å with only a small shoulder at 2.8 Å. Figure 3.3C indicated that the probability of finding an oxygen atom closer to the surface was larger for PMMA compared to PVAc.

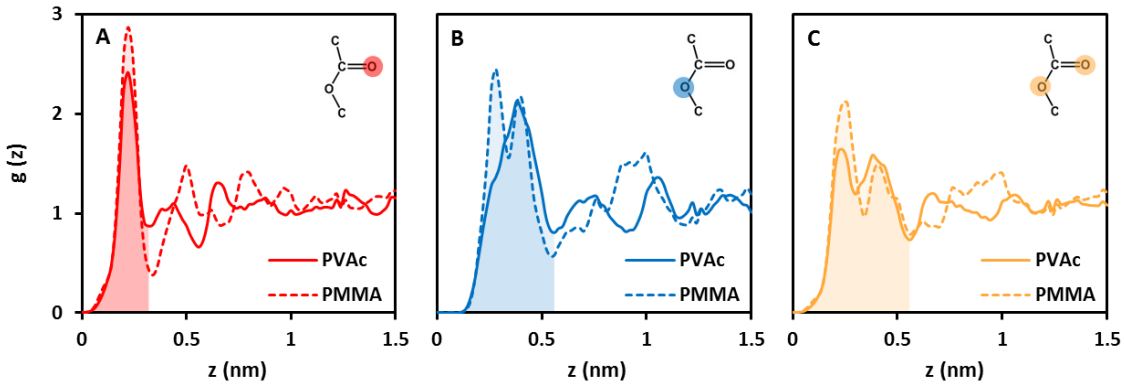

Figure 3.3. *Z*-direction distribution functions for A) carbonyl oxygen, B) alkoxy oxygen, and C) both carbonyl and alkoxy oxygen atoms of dodecamers of PVAc and PMMA. These distribution functions are constructed from the distance between the labeled polymer oxygen atoms and the silanol surface oxygen atoms. Shading of the area under the surface peaks in the hydrogen-bonding region is used to visually highlight the differences in the surface bound region of the PVAc and PMMA distributions. The carbonyl oxygens were in similar environments, however, the PVAc alkoxy oxygens were further away from the surface.

The energy pair distribution between the polymer side-chains and the silanol groups of the silica can be used to characterize and compare the average intermolecular interaction strengths.[51,52] For this distribution, the combined electrostatic and Lennard-Jones intermolecular interactions were calculated between all sets of neutral (total zero charge) groups of the silica surface and polymers, and binned accordingly. The neutral group on

silica included a surface silanol group (hydroxyl group and its connected silicon atom) and the neutral group of a given polymer included all atoms of its monomer unit, except the -CH_2 group of the backbone (Figure 3.4). It is important that the energy pair distribution calculation be performed over charge neutral groupings of atoms. If the groups are charge neutral, there will not be a slowly decaying monopolar electrostatic contribution to the pair interaction. The strongest net electrostatic interaction between distant groups will potentially be a dipole-dipole interaction, which decays two orders-of-magnitude more rapidly than monopolar pair interactions. This means that all distant interactions will have a potential energy near 0 kcal/mol, allowing us to cleanly separate strong surface interactions (which will have a negative potential energy) from weaker distant interactions. Figure 3.5 shows the measured energy pair distribution functions for adsorbed dodecamers of PVAc and PMMA on silica. These functions show small peaks at negative energies that represent strong intermolecular interactions between neighboring silanol groups and polymer side-chains. The average energy between PVAc and PMMA side-chains and silanol groups over the sets of independent MD simulations was observed at -10.6 ± 0.1 and -11.6 ± 0.2 kcal/mol, respectively.

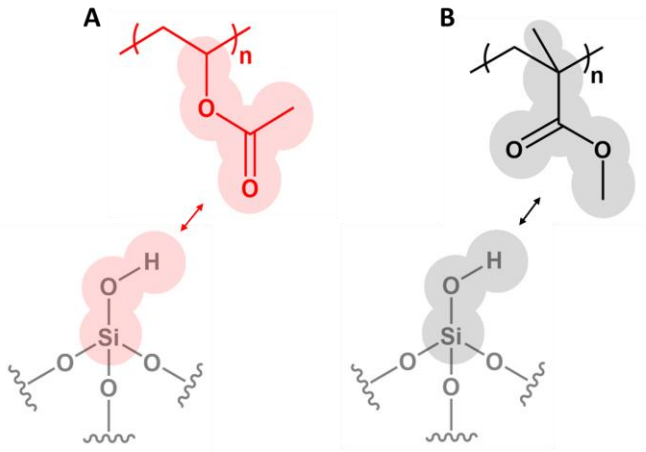

Figure 3.4. Charge neutral groups of silica and A) PVAc and B) PMMA used in computing the energy pair distribution functions. A description of the force field and relevant partial charges is available in the **Supporting Information.**

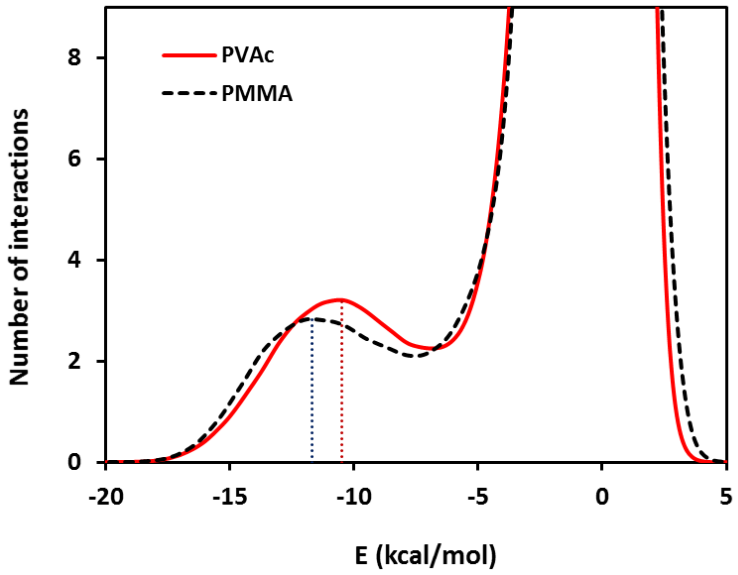

Figure 3.5. Energy pair distribution function between side-chains of dodecamers PVAc and PMMA and silica silanol groups. The average interaction energy is larger for adsorbed PMMA than adsorbed PVAc.

The energy pair distribution function was used to calculate the energy between, in this case, the side chains and the surface silanols as a function of distance between their centers of geometry. At close distances, one should expect the silanol/polymer side chain interactions to be dominated by hydrogen-bonding, while at further distances, the interactions will be mainly dipolar. To help characterize the nature of the interactions as a function of the distance between the two groups, we constructed the contour plots for adsorbed PVAc and PMMA and these are shown in Figure 3.6. The contours represent the number density of groups of a particular energy (E) and distance between the

geometric centers of group pairs (*r*) highlighted in Figure 3.4. Both PVAc and PMMA showed interactions with roughly the same energy (approximately -11 kcal/mol), at nearly the same distance to the silanol groups of the silica surface. These interaction peaks correspond to optimal hydrogen bonding to the carbonyl oxygen atoms of the polymer chains. The PMMA contour-plot showed an additional intermolecular interaction with even greater strength (approximately -13 kcal/mol) at a slightly further distance from the surface. This interaction peak is attributable to a single silanol simultaneously forming a direct strong interaction with both the carbonyl and alkoxy oxygen atoms of a polymer side chain.

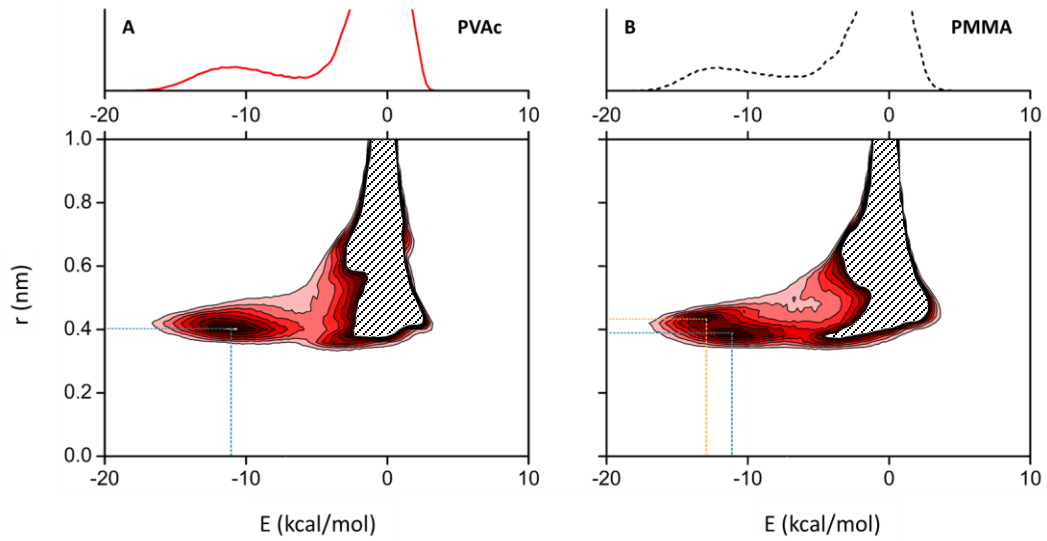

Figure 3.6. Contour-plots of the density of pair interactions as a function of energy (*E*) and the distance between the polymeric side chains of A) PVAc and B) PMMA and the surface silanol groups centers of geometry (*r*). Above each contour plot, a representative energy-pair distribution function for these systems, similar to that shown in Figure 3.5. The PMMA contour shows an additional, and stronger, intermolecular interaction at slightly further separation distances (approximately -13 kcal/mol at 0.43 nm).

Occupancy probability isosurfaces provide detailed information and a spatial view of the distribution of polymer atoms located around the surface silanol groups. Occupancy probability maps were constructed by reorienting the silanol groups relative to a reference orientation. The nearby polymer oxygen atoms were similarly reoriented and then spatially binned in cubic volumes. These bins were then used to count the numbers of the oxygen atoms at different positions relative to the silanol functional group. Atoms further than a distance of 10 Å were excluded from this binning process as interest was in the surface hydrogen bonding localization of the polymer atoms. These filled bins were then divided by the number density of the binned atoms in a bulk polymer simulation to convert the counts into an occupancy probability. Figure 3.7 shows the averaged occupancy probability isosurfaces corresponding to 30 times greater than bulk probability of finding carbonyl and alkoxy oxygen atoms of PMMA and PVAc around the silanol groups of the surface. No significant differences were observed for the isosurfaces of carbonyl groups between PMMA and PVAc. However, the alkoxy oxygen atoms of PMMA showed occupancy probability closer to the silanol oxygen groups than those observed for PVAc.

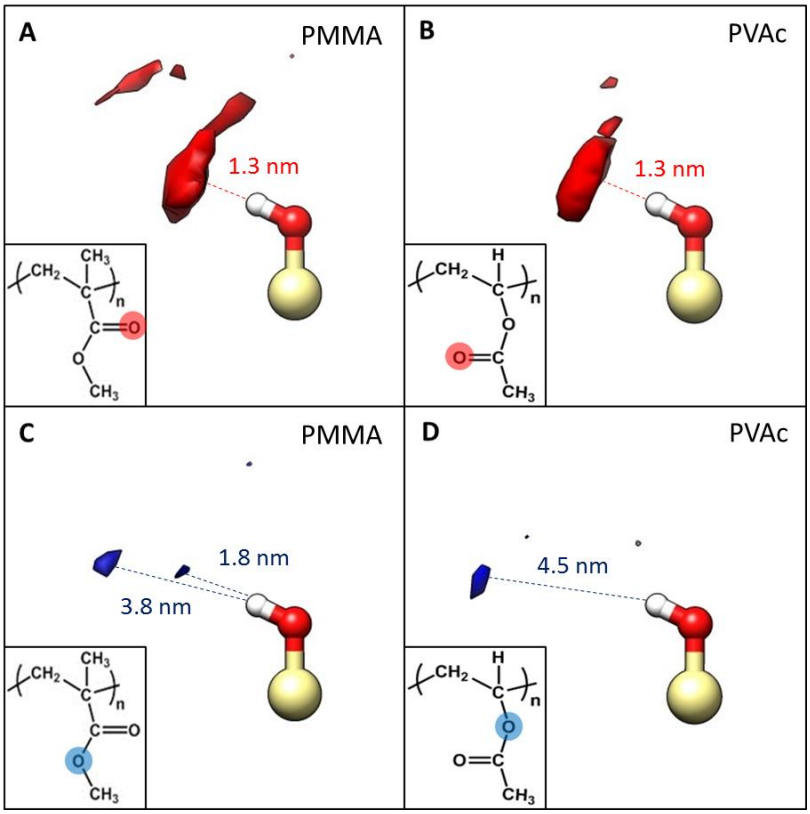

Figure 3.7. The occupancy probability isosurfaces for polymer oxygens near surface silanol atoms. The isosurfaces indicate occupancy probability 30 times larger than that of bulk polymer for the carbonyl oxygens of A) PMMA and B) PVAc; and the alkoxy oxygens of C) PMMA and D) PVAc. Similar occupancy probabilities are seen for the carbonyl oxygen atoms of both polymer types, but the PMMA alkoxy probability is seen at shorter distances than that observed for PVAc.

3.4.3. PMMA chains pack tighter than PVAC chains at the air interface

The TMDSC thermograms indicated a difference in the thermal behavior of PVAc and PMMA at the polymer/air interface. To investigate these differences in more detail, distance dependent energy pair distribution functions were calculated for the *polymer/polymer* intermolecular interactions within 1 nm of the air interface. Figure 3.8

shows the resulting two-dimensional contour-plots of the energy pair distribution (E) at a given distance (r) between the polymer side chains. While both polymers exhibited a similar close-interaction peak, PMMA (Figure 3.8B) shows an additional interaction peak at closer distances.

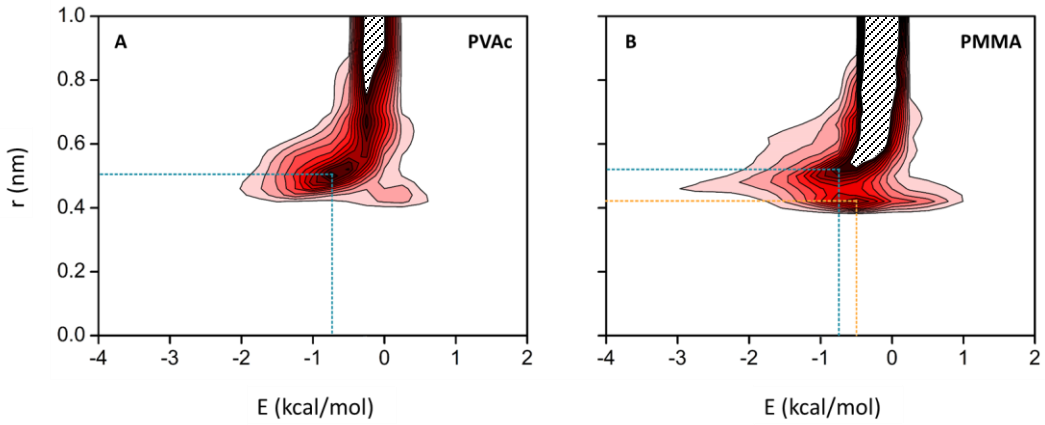

Figure 3.8. Contour-plot representation of the energy pair interaction strengths between the polymer side-chains as a function of distance between their centers of geometry for A) PVAc and B) PMMA at the polymer/air interface. PMMA shows an additional interaction peak at closer polymer side chain distances.

3.5. DISCUSSION

3.5.1. Adsorbed PMMA shows a larger tightly-bound amount and a higher glass transition

It is expected that the T_g of an adsorbed polymer will increase over that of bulk polymer if there are attractive intermolecular interactions between the polymer chains and the substrate.[19,53-56] Both PVAc and PMMA have attractive surface interactions with silica due to the hydrogen-bonding between carbonyl groups of the polymers and silanol groups of the substrate.[57-59] The strong interactions between the polymer and the surface

decrease the mobility of polymer chains and consequently increase the T_g at the polymer/silica interface (tightly-bound region).[60] The area under the tightly-bound region in the TMDSC thermograms became larger with increased adsorbed amounts of polymer until reaching the maximum number of interactions possible between the polymer and the surface. The maximum number of interactions between the polymer and silica is dependent on both the limited number of substrate silanol groups, their local distribution, and the surface packing of adsorbed polymer. After obtaining the maximum number of interactions, the intensity of the tightly-bound thermal activity region remained constant.

Although PVAc and PMMA TMDSC thermograms have similar features, they show different thermal properties at near identical adsorbed amounts. For 1.06 mg/m^2 of PVAc adsorbed on silica (Figure 3.2B), we observe transitions corresponding to tightly-bound polymer at around 24 K above the T_g of bulk polymer and loosely-bound polymer slightly above the T_g of bulk. PMMA with roughly the same adsorbed amount (1.09 mg/m^2) shows only the tightly-bound transition (~43 K above the bulk T_g). This indicates a tightly-bound amount less than 1.06 mg/m^2 for PVAc and more than 1.09 mg/m^2 for PMMA. In fact, these two tightly-bound amounts have been measured to be 0.78 and 1.21 mg/m^2 for PVAc and PMMA for polymers of very high molecular masses.[19,22] The greater ΔT_g observed for adsorbed PMMA indicates the presence of stronger interactions at the PMMA/silica interface than those at the PVAc/silica interface.

The term "*tightly-bound*" used here to refer to polymer segments at interface was first used in the literature to describe polymer segments at particles interface in filled elastomers.[61] Although the term "*rigid amorphous fraction*", has been used to describe the interfacial regions of semi-crystalline polymers that degrades before exhibiting a

glass transition,[62,63] since we observe a broad glass transition at higher-temperature even at small adsorbed amounts, we preferentially use the term, tightly-bound.

With increasing adsorbed amounts of polymer, beyond that for the tightly-bound amount, the effect of silica on the loosely-bound polymer chains resulted in greater mobility of these chains. At small adsorbed amounts, around 1.0 mg/m^2 as in Figure 3.2B, both polymers showed mainly tightly-bound polymer with transitions at temperatures significantly greater than the bulk T_g. PVAc showed a hint of a small amount of loosely–bound polymer near the T_g of the bulk polymer. At adsorbed amounts around 1.7 mg/m^2, as in Figure 3.2C, PVAc showed a considerable increase in the intensity for the loosely-bound polymer, with a thermal transition slightly higher than that of the bulk polymer. Only a small amount of loosely bound polymer was found for PMMA. The intensities of the transitions for both polymers were roughly unchanged from the 1.0 mg/m^2 samples. At this adsorbed amount, both polymers have likely saturated the surface sites with tightly-bound polymer and any additional polymer should not be tightly-bound. With additional increases in adsorbed amounts (Figures 3.2D and 2E), the intensity of the tightly-bound transitions was roughly constant and the intensity of the loosely-bound polymer peak increased as evidenced by the intensity of the loosely-bound transition. PVAc showed evidence for a mobile component, while none was found for PMMA. The mobile component was indicative of a region of higher mobility at the polymer-air interface.[64] The absence of a mobile component for adsorbed PMMA is likely due to stronger intermolecular actions among the PMMA chains.

A summary of the T_g findings for bulk, mobile-component, loosely-bound and tightly-bound polymers is presented in Table 3.1. The location of the transitions for each

polymer are nearly constant regardless the adsorbed amount. This indicates that the interactions and effects controlling the shifts in T_g are mostly constant, and the primary change (peak intensity with adsorbed amount of polymer) is a result of change in the *amounts* of adsorbed polymer. In summary, we note that the broad glass transitions observed for these adsorbed polymers were due to the motional gradient in the adsorbed polymer systems as a function of the intermolecular interactions, which are modified by the distance of a given chain segments from the surface.[15,64]

Table 3.1. Thermal properties of bulk and adsorbed PMMA and PVAc on silica.

PROPERTY	**PMMA**	**PVAC**
Bulk T_g (°C)	112.0 ± 0.3	40.9 ± 0.3
Mobile component T_g (°C)	None	31 ± 1
Loosely-bound T_g (°C)	117 ± 1	44 ± 1
Tightly-bound T_g (°C)	154 ± 3	66 ± 2
Loosely-bound ΔT_g^* (°C)	5 ± 1	3 ± 1
Tightly-bound ΔT_g^* (°C)	42 ± 3	25 ± 2
Tightly-bound amount (mg/m^2)‡	1.31 ± 0.14	0.85 ± 0.13

* $\Delta T_g = T_g - \text{Bulk } T_g$

‡ See **Appendix B**

The ratio of the area under the loosely-bound transition to the area under the tightly-bound transition for PVAc was larger than that for PMMA. This effect is a superposition of two effects, the ratio of the ΔC_p values for the loosely and tightly bound polymers and the tightly bound amount. A model based on the concept that there is a maximum amount of tightly bound polymer for a given system was used to analyze the TMDSC data,[4] and the results of this analysis are shown in the **Appendix B**. The corresponding tightly-bound amounts were 1.31 ± 0.14 for PMMA and 0.85 ± 0.13 for PVAc as shown in Table

3.1. These results are of the same order and within experimental error of previous measurements reported for each of these systems that used different polymer molecular masses.[4,19,22] The larger tightly-bound amount for PMMA is consistent with these experimental observations. We note that the tightly-bound amount represents not just contributions from those segments directly bound, but also those affected by the directly-bound segments. The larger tightly-bound amount for PMMA indicates more effective attractive interactions between the polymer chains and the silica surface. Based on the model, with a fixed tightly bound polymer amount, the calculated fraction of tightly-bound polymers, f_B, are shown in Figure 3.9 as a function of adsorbed amount. As expected from the TMDSC curves (Figure 3.2), the tightly-bound fraction of PMMA was larger than PVAc at each adsorbed amount.

The carbonyl bound fraction (the fraction of carbonyl oxygen atoms which are bound to the surface relative to the total number of carbonyl atoms) of PVAc and PMMA is a component set of the overall tightly-bound fraction, and this subset can be estimated from FTIR measurements.[3,20] Figure 3.9 includes FTIR results as determined in other work for similar systems,[3,20] and highlights the fraction of the tightly-bound carbonyls that are in direct contact with the substrate. From this, we estimate that approximately one-sixth of the tightly-bound segments were composed of polymer units directly interacting with the substrate. The remainder of the tightly-bound signal was due to indirect polymer-substrate and polymer-polymer interactions between directly adsorbed chains, both of which lead to differences in the thermal behavior of the polymer relative to the bulk polymer. These results indicate that although the carbonyl oxygens of both PVAc and PMMA have similar chance to bind to the surface, there were inherent differences in the

binding of PVAc and PMMA chains to the surface. These differences came from each polymer's unique inter- and intra-chain interactions.

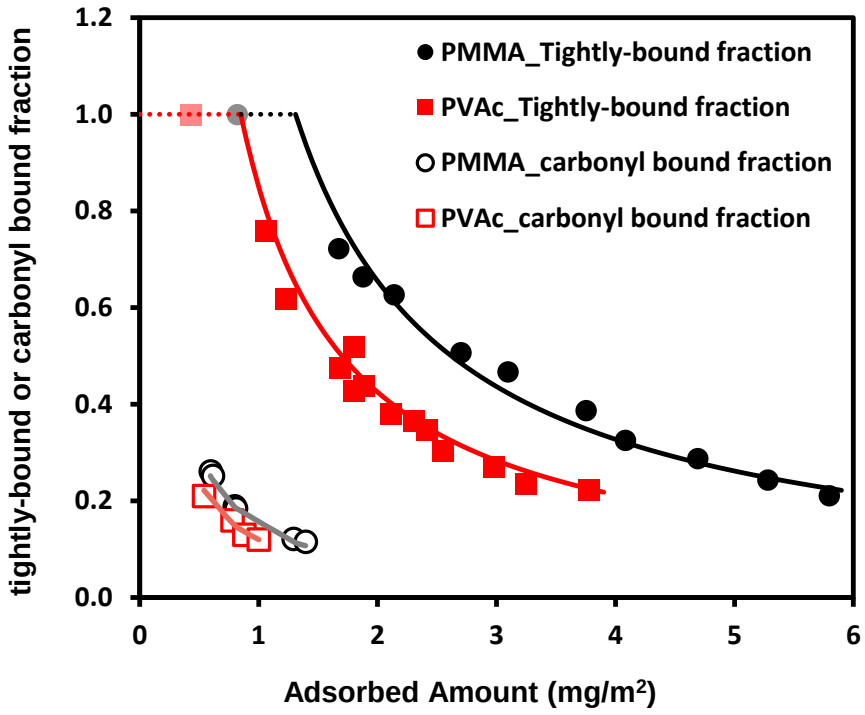

Figure 3.9. The tightly-bound and carbonyl bound fraction of PMMA and PVAc on silica as a function of adsorbed amount. The tightly-bound points are fitted by a model based on a fixed amount of tightly-bound segments (m''_B = 1.31 mg/m^2 for PMMA and 0.85 mg/m^2 for PVAc). The carbonyl bound fractions are fitted by a model based on the constant amount of bound polymer.[3,20] The pink square and gray circle points represent PVAc and PMMA samples with adsorbed amounts less than the full tightly-bound amount of their corresponding adsorbed systems, respectively. The tightly-bound fraction of PMMA is larger than PVAc for similar adsorbed amounts of polymer.

3.5.2. MD simulations show PMMA/silica interactions are stronger than PVAc/silica interactions

The character and strength of interactions between both PVAc and PMMA with the silica surface were investigated by considering the structural configurations of carbonyl and alkoxy oxygen atoms of the polymers at the polymer/silica interfaces. To explore this surface structuring, we computed *z*-direction distribution function profiles for oxygen atoms of polymers and the oxygen atoms of the surface silanol groups (Figure 3.3). The peak near the surface reflected an increase in the density of polymer oxygen atoms at the interface, and is potentially indicative of strong interactions between polymer and surface. The peak for the carbonyl oxygen was located at the same *z*-distance (2.2 Å) from the surface for both PVAc and PMMA (Figure 3.3A). The similarity between the positions of carbonyl oxygen atoms indicated that both polymers interacted with the surface in a similar way; however, the greater amplitude of the PMMA surface peak indicated a stronger overall interaction. In both polymers, alkoxy oxygen atoms were further from the surface than carbonyl oxygen atoms. The distribution function profile of alkoxy oxygen atoms showed a split peak at 2.8 and 3.8 Å for adsorbed PMMA and a singular peak at 3.8 Å for PVAc (Figure 3.3B). These peaks indicated that limited, but significant hydrogen-bonding primarily occurs between the carbonyl oxygen atoms of PVAc and PMMA and the hydroxyl groups of the surface. However, the probability of hydrogen-bonding between the alkoxy oxygen atoms and the hydroxyl groups on the surface was greater for PMMA. The larger distance between the alkoxy oxygen and the surface for PVAc was likely due to the position of alkoxy oxygen in the structure. This atom was close to the polymer backbone and more sterically hindered. This hindrance

resulted in the alkoxy oxygen of PVAc not being as accessible for direct interactions as the alkoxy oxygen of PMMA. In summary, as shown in Figure 3.3C, a broader and taller peak in the average *z*-direction distribution for all oxygen atoms of PMMA indicated a higher probability for and greater strength of potential interactions with the surface. This supported the experimentally observed larger ΔT_g values for adsorbed PMMA than adsorbed PVAc.

The differences in the energetics of PVAc and PMMA polymer/silica surface interactions were apparent in the calculated energy-pair distribution functions (Figure 3.5). We observed a shift to a stronger average interaction strength with PMMA than with PVAc (-11.6 versus -10.6 kcal/mol, respectively). The greater interaction strength for adsorbed PMMA was potentially due to a more favorable structural orientation of PMMA side-chain atoms around the silanol groups. The enhanced availability (closer proximity) of alkoxy oxygen atoms with the surface silanol groups seen in the *z*-direction distribution functions above indicated an increased likelihood of favorable side-chain interactions. This translated into the stronger interaction potential for PMMA seen here.

The energy pair distribution, as a function of separation distance between the polymer side-chains and the surface (Figure 3.6), further separated the spatial contributions to the interaction potential. As in the energy pair distribution functions in Figure 3.5, PMMA exhibited a roughly 1 kcal/mol larger average interaction energy peak than PVAc. This PMMA peak was actually composed of two signals, one peak at the same location as seen in PVAc and a second peak further from the surface and at a more negative energy. This second peak was a signal for enhanced hydrogen-bonding to the surface facilitated by alkoxy oxygen atoms of the PMMA. In PMMA the carbonyl and alkoxy oxygens can

simultaneously interact with a single silanol group, making a joint hydrogen-bond that is stronger than a hydrogen-bond between a carbonyl and silanol alone.

Analysis of the spatial occupancy probability distribution about surface silanol groups provided additional structural insight into the specific polymer/surface interactions. Figure 3.7 shows regions of enhanced occupancy relative to bulk for polymer carbonyl and alkoxy oxygen atoms near the silanol groups. The occupancy densities of carbonyl oxygen atoms for both of polymers (Figure 3.7A and 3.7B) were nearly the same. The distance between the carbonyl oxygen and the silanol hydrogen atom and the angle between that and the silanol OH bond indicated hydrogen-bonding.[65-67] PMMA alkoxy oxygen atoms (Figure 3.7C) produced a stronger probability density closer to the surface relative to PVAc alkoxy oxygen atoms (Figure 3.7D). The preferential occupancy zone for the alkoxy oxygen atoms in PVAc was further away from the silanol groups and out of the typical hydrogen bonging range.[65] The PMMA alkoxy oxygen isosurface showed occupancy closer to the silanol groups than that seen in PVAc and was split into two regions, the closer of which indicated favorable hydrogen-bonding. These results were consistent with the previous energy pair distribution analyses showing additional hydrogen-bonding interactions and stronger overall interaction energies. These findings also supported the assertion that stronger surface interactions are a likely reason for the TMDSC observed greater shift in the T_g of PMMA upon surface adsorption over that of PVAc.

3.5.3. PMMA/PMMA intermolecular interactions are stronger than PVAc/PVAc

PVAc and PMMA are different polymers and will have unique, but somewhat similar, polymer/polymer interactions that can affect the polymer/air interface thermal activity.

The energy pair interaction strength between the polymers' side chains present at the air interface as a function of pair distance was calculated to further characterize these interactions. Samples with large adsorbed amounts (~3.0 mg/m^2) were selected to minimize the effect of silica surface on the polymer chains. As shown in Figure 3.8, there is a wider distribution of interaction energies for the PMMA side-chains relative to PVAc side-chains, with both exhibiting a strong interaction peak at the same location. An additional peak at a stronger interaction energy is apparent in the PMMA distribution and is located at a closer (0.4 nm) separation distance. This indicates that the PMMA side chains pack more tightly. The difference between the packing behavior and the polymer/polymer interactions supports the observed mobile component in the TMDCS results for PVAc and not for PMMA. The PMMA chains likely have less free volume and are more restricted than the PVAc chains at the polymer/air interface.[68]

3.6. CONCLUSIONS

In this work, we investigated the thermal and structural properties of thin films of PVAc and PMMA adsorbed on silica surfaces using the TMDSC characterizations and MD simulations. These polymers exhibited different thermal behavior as a function of both the structure and the adsorbed amount. Adsorbed PMMA showed a larger amount of tightly-bound amount of polymer and also a greater shift in the adsorbed polymer T_g than PVAc. We believe that these differences in tightly-bound amounts and glass transitions of PVAc and PMMA are related to differences in the interaction strengths between the polymers and the surface. Molecular dynamics simulations allowed us to characterize these interaction strengths, and we found that the interactions between PMMA and surface is stronger than PVAc due to the enhanced probability for hydrogen-bonding

interactions by both of the oxygen atoms in the polymer side chains. Spatial density and *z*-direction distribution functions also support the presence of stronger interactions between the PMMA and the silica surface.

The combined calorimetric and computational investigation of these polymer systems has some clear benefits for insight with respect to identifying the driving forces for thermal behavior at interfaces. TMDSC provides a highly resolved picture of the changes in polymer thermal behavior upon surface adsorption. When performed on analogous systems, MD simulations provide a level of insight into microscopic interactions that is difficult to obtain from experimental techniques. We observe this microscopic view to be in general agreement with the experimental macroscopic picture of the behavior of adsorbed polymers, and this agreement highlights the importance of the fundamental chemistry and intermolecular interactions in critical changes in polymer physical properties.

3.7. ACKNOWLEDGMENTS

Authors acknowledges the financial support of the National Science Foundation (USA) under Grant No. DMR-1005606 and the research startup funds provided by Oklahoma State University. The computing for this project was performed at the OSU High Performance Computing Center at Oklahoma State University supported in part through the National Science Foundation grant OCI–1126330.

3.8. REFERENCES

(1) Parida, S. K.; Dash, S.; Patel, S.; Mishra, B. *Adv. Colloid Interface Sci.* **2006**, *121*, 77.

(2) Zou, H.; Wu, S.; Shen, J. *Chem. Rev.* **2008**, *108*, 3893.

(3) Maddumaarachchi, M.; Blum, F. D. *J. Polym. Sci., Part B: Polym. Phys.* **2014**, *52*, 727.

(4) Blum, F. D.; Young, E. N.; Smith, G.; Sitton, O. C. *Langmuir* **2006**, *22*, 4741.

(5) Metin, B.; Blum, F. D. *Langmuir* **2009**, *26*, 5226.

(6) Vogiatzis, G. G.; Theodorou, D. N. *Macromolecules* **2013**, *46*, 4670.

(7) Ndoro, T. V.; Voyiatzis, E.; Ghanbari, A.; Theodorou, D. N.; Böhm, M. C.; Müller-Plathe, F. *Macromolecules* **2011**, *44*, 2316.

(8) Lin, E. K.; Kolb, R.; Satija, S. K.; Wu, W.-l. *Macromolecules* **1999**, *32*, 3753.

(9) Madathingal, R. R.; Wunder, S. L. *Thermochim. Acta* **2011**, *526*, 83.

(10) Porter, C. E.; Blum, F. D. *Macromolecules* **2002**, *35*, 7448.

(11) DeMaggio, G.; Frieze, W.; Gidley, D.; Zhu, M.; Hristov, H.; Yee, A. *Phys. Rev. Lett.* **1997**, *78*, 1524.

(12) Rittigstein, P.; Priestley, R. D.; Broadbelt, L. J.; Torkelson, J. M. *Nat. Mater.* **2007**, *6*, 278.

(13) Ellison, C. J.; Torkelson, J. M. *Nat. Mater.* **2003**, *2*, 695.

(14) Lin, W.-Y.; Blum, F. D. *Macromolecules* **1998**, *31*, 4135.

(15) Blum, F. D.; Xu, G.; Liang, M.; Wade, C. G. *Macromolecules* **1996**, *29*, 8740.

(16) Metin, B.; Blum, F. D. *J. Chem. Phys.* **2006**, *125*, 054707.

(17) Blum, F. D. *Annual Reports on NMR Spectroscopy* **1994**, *28*.

(18) Napolitano, S.; Lupascu, V.; Wübbenhorst, M. *Macromolecules* **2008**, *41*, 1061.

(19) Mortazavian, H.; Fennell, C. J.; Blum, F. D. *Macromolecules* **2016**, *49*, 298.

(20) Krisanangkura, P.; Packard, A. M.; Burgher, J.; Blum, F. D. *J. Polym. Sci., Part B: Polym. Phys.* **2010**, *48*, 1911.

(21) Porter, C. E.; Blum, F. D. *Macromolecules* **2000**, *33*, 7016.

(22) Khatiwada, B. K.; Hetayothin, B.; Blum, F. D. *Macromol. Symp.* **2013**, *327*, 20.

(23) Forrest, J. A.; Dalnoki-Veress, K.; Dutcher, J. R. *Phys. Rev. E* **1997**, *56*, 5705.

(24) Chan, C.-K.; Chu, I.-M. *Polymer* **2001**, *42*, 6089.

(25) Simon, S. L. *Thermochim. Acta* **2001**, *374*, 55.

(26) Verdonck, E.; Schaap, K.; Thomas, L. C. *Int. J. Pharm.* **1999**, *192*, 3.

(27) Zhang, B.; Blum, F. D. *Macromolecules* **2003**, *36*, 8522.

(28) Ghanbari, A.; Ndoro, T. V.; Leroy, F. d. r.; Rahimi, M.; Böhm, M. C.; Müller-Plathe, F. *Macromolecules* **2011**, *45*, 572.

(29) Eslami, H.; Müller-Plathe, F. *J. Phys. Chem. C* **2013**, *117*, 5249.

(30) Paeng, K.; Ediger, M. *Macromolecules* **2011**, *44*, 7034.

(31) Compton, O. C.; Cranford, S. W.; Putz, K. W.; An, Z.; Brinson, L. C.; Buehler, M. J.; Nguyen, S. T. *Acs Nano* **2012**, *6*, 2008.

(32) Ediger, M.; Forrest, J. *Macromolecules* **2013**, *47*, 471.

(33) Binder, K.; Milchev, A. *J. Polym. Sci., Part B: Polym. Phys.* **2012**, *50*, 1515.

(34) Mansfield, K. F.; Theodorou, D. N. *Macromolecules* **1991**, *24*, 6283.

(35) Smith, J. S.; Bedrov, D.; Smith, G. D. *Compos. Sci. Technol.* **2003**, *63*, 1599.

(36) Pettersen, E. F.; Goddard, T. D.; Huang, C. C.; Couch, G. S.; Greenblatt, D. M.; Meng, E. C.; Ferrin, T. E. *J. Comput. Chem.* **2004**, *25*, 1605.

(37) Wei, C.; Srivastava, D.; Cho, K. *Nano Lett.* **2002**, *2*, 647.

(38) Prathab, B.; Aminabhavi, T. M.; Parthasarathi, R.; Manikandan, P.; Subramanian, V. *Polymer* **2006**, *47*, 6914.

(39) Morrow, B.; McFarlan, A. *Langmuir* **1991**, *7*, 1695.

(40) Van Der Spoel, D.; Lindahl, E.; Hess, B.; Groenhof, G.; Mark, A. E.; Berendsen, H. J. *J. Comput. Chem.* **2005**, *26*, 1701.

(41) Wensink, E.; Hoffmann, A.; Apol, M.; Berendsen, H. *Langmuir* **2000**, *16*, 7392.

(42) van der Spoel, D.; Wensink, E. J.; Hoffmann, A. C. *Langmuir* **2006**, *22*, 5666.

(43) Essmann, U.; Perera, L.; Berkowitz, M. L.; Darden, T.; Lee, H.; Pedersen, L. G. *J. Chem. Phys.* **1995**, *103*, 8577.

(44) Hess, B. *J. Chem. Theory Comput.* **2008**, *4*, 116.

(45) Nosé, S. *Mol. Phys.* **1984**, *52*, 255.

(46) Hoover, W. G. *Phys. Rev. A* **1985**, *31*, 1695.

(47) Bu, H.; Aycock, W.; Cheng, S. Z.; Wunderlich, B. *Polymer* **1988**, *29*, 1485.

(48) Gaur, U.; Wunderlich, B. B.; Wunderlich, B. *J. Phys. Chem. Ref. Data* **1983**, *12*, 29.

(49) Gaur, U.; Lau, S. f.; Wunderlich, B. B.; Wunderlich, B. *J. Phys. Chem. Ref. Data* **1982**, *11*, 1065.

(50) Allen, M. P.; Tildesley, D. J. *Computer Simulation of Liquids*; Oxford University Press: New York, **1989**.

(51) Jorgensen, W. L. *J. Am. Chem. Soc.* **1980**, *102*, 543.

(52) Bakó, I.; Megyes, T.; Bálint, S.; Chihaia, V.; Bellissent-Funel, M.-C.; Krienke, H.; Kopf, A.; Suh, S.-H. *J. Chem. Phys.* **2010**, *132*, 014506.

(53) Tsui, O.; Russell, T.; Hawker, C. *Macromolecules* **2001**, *34*, 5535.

(54) Richard, A. *Faraday Discuss.* **1994**, *98*, 219.

(55) Grohens, Y.; Brogly, M.; Labbe, C.; David, M.-O.; Schultz, J. *Langmuir* **1998**, *14*, 2929.

(56) van Zanten, J. H.; Wallace, W. E.; Wu, W.-l. *Phys. Rev. E* **1996**, *53*, R2053.

(57) Wen, N.; Tang, Q.; Chen, M.; Wu, L. *J. Colloid Interface Sci* **2008**, *320*, 152.

(58) Frantz, P.; Granick, S. *Macromolecules* **1995**, *28*, 6915.

(59) Kulkeratiyut, S.; Kulkeratiyut, S.; Blum, F. D. *J. Polym. Sci., Part B: Polym. Phys.* **2006**, *44*, 2071.

(60) Fryer, D. S.; Peters, R. D.; Kim, E. J.; Tomaszewski, J. E.; de Pablo, J. J.; Nealey, P. F.; White, C. C.; Wu, W.-l. *Macromolecules* **2001**, *34*, 5627.

(61) Blow, C. *Polymer* **1973**, *14*, 309.

(62) Sargsyan, A.; Tonoyan, A.; Davtyan, S.; Schick, C. *Eur. Polym. J.* **2007**, *43*, 3113.

(63) Wunderlich, B. *Prog. Polym. Sci.* **2003**, *28*, 383.

(64) Lin, W.-Y.; Blum, F. D. *J. Am. Chem. Soc.* **2001**, *123*, 2032.

(65) Kumar, R.; Schmidt, J.; Skinner, J. *J. Chem. Phys.* **2007**, *126*, 204107.

(66) Wernet, P.; Nordlund, D.; Bergmann, U.; Cavalleri, M.; Odelius, M.; Ogasawara, H.; Näslund, L.; Hirsch, T.; Ojamäe, L.; Glatzel, P. *Science* **2004**, *304*, 995.

(67) Luzar, A.; Chandler, D. *Phys. Rev. Lett.* **1996**, *76*, 928.

(68) Mortazavian, H.; Fennell, C. J.; Blum, F. D. *Macromolecules* (in press).

3.9. SUPORTING INFORMATION

S3.1. OPLS force field

The following OPLS force field parameters were used for silica surface (Table S3.1), PVAc (Table S3.2), and PMMA (Table S3.3). PVAc and PMMA structures with the atom numbers are shown in Figure S3.1. (Wensink, E.; Hoffmann, A.; Apol, M.; Berendsen, H. *Langmuir* **2000**, *16*, 7392, and van der Spoel, D.; Wensink, E. J.; Hoffmann, A. C. *Langmuir* **2006**, *22*, 5666).

Table S3.1. OPLS-AA force-field parameters for silanol groups of the silica surface.

Atom name	**Atom type**	**Atom charge**
Si	SI	0.265
OH	opls_169	-0.700
HO	opls_170	0.435

Table S3.2. OPLS-AA force-field parameters for PVAc molecules.

Atom name	Atom type	Atom charge
C1	opls_135	-0.13
C2	opls_058	0.52
C3	opls_136	0.13
C4	opls_135	-0.12
O1	opls_059	-0.44
O2	opls_062	-0.38
H	opls_140	0.06

Table S3.3. OPLS-AA force-field parameters for PMMA molecules.

Atom name	Atom type	Atom charge
C1	opls_135	0.07
C2	opls_058	0.52
C3	opls_137	0.05
C4	opls_135	-0.12
C5	opls_135	-0.18
O1	opls_059	-0.44
O2	opls_062	-0.38
H	opls_140	0.06

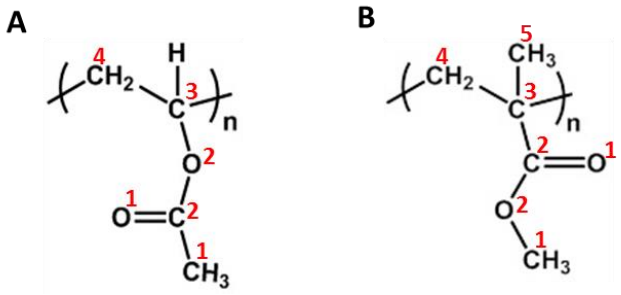

Figure S3.1. Monomer structure of A) PVAc, and B) PMMA molecules.

S3.2. Calculating the tightly-bound amount and tightly bound fraction

The tightly-bound amount was determined by a model which is based on a constant amount of polymer, m_B, in close proximity of and tightly bound to the surface. (Blum, F. D.; Young, E. N.; Smith, G.; Sitton, O. C. *Langmuir* **2006**, *22*, 4741, and Mortazavian, H.; Fennell, C. J.; Blum, F. D. *Macromolecules* **2015**, 49, 298. Equation S3.1 shows the relationship between the *r*, ratio of the heat flow changes for the loosely- (A) and tightly-bound (B) components, and ΔC_p values, the specific heat capacity changes in the glass transition region.

$$r = A_A/A_B = (m'_p - m'_{pB})\,\Delta C_{pA}/(m'_{pB}\,\Delta C_{pB})$$
$$r = [\Delta C_{pA}/(m'_{pB}\,\Delta C_{pB})]m'_p - \Delta C_{pA}/\Delta C_{pB}, \qquad \text{(S3.1)}$$

where m'_p, the normalized total polymer mass, is the summation of normalized masses of loosely-bound and tightly-bound polymer (m'_{pA} and m'_{pB} respectively). The tightly bound amounts of PVAc and PMMA were determined using the linear relationship between *r*, and m'_p, as shown in Figure S3.2. This amount was determined by dividing the intercept (ratio of the heat capacity increments) by the slope of the line. Samples with adsorbed amounts less than m'_{pB} had no loosely-bound polymers and the *r* values were 0.

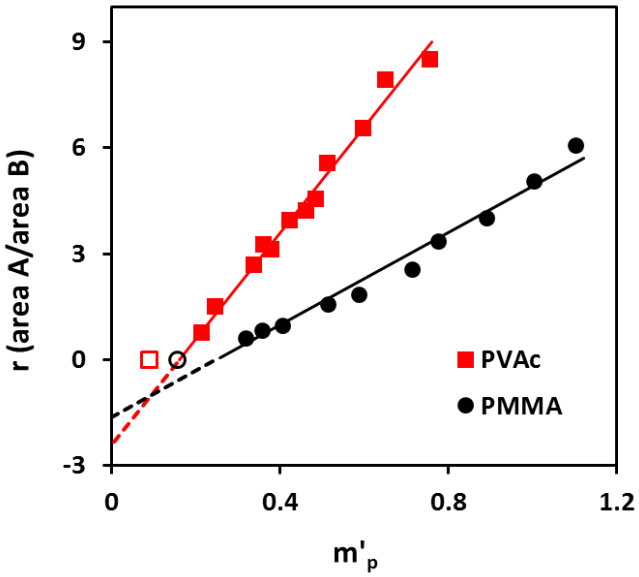

Figure S3.2. The ratio (r) of the areas under the transitions A (loosely-bound) and B (tightly-bound) as a function of the relative amounts of adsorbed polymer (m'_p) for adsorbed PVAc and PMMA. The amount of the tightly-bound polymer for adsorbed PVAc and PMMA was determined to be 0.85 ± 0.06 and 1.31 ± 0.08 mg/m^2, respectively.

An estimate of bound fraction, f_B, which is the ratio of the mass of tightly-bound polymer at the polymer-surface interface to the total amount of polymer, can be obtained using the ratio of the heat flow changes of loosely and tightly-bound components:

$$f_B = m'_{pB}/m'_p = 1/(1+ r\Delta C_{pB}/\Delta C_{pA}). \quad \text{(S3.2)}$$

The calculation of f_B from Equation S3.2 is based on the constant tightly-bound amount of adsorbed polymers on the surface.

CHAPTER IV

THERMAL ANALYSIS OF ADSORBED POLY(VINYL ACETATE) ON SILICA, THE EFFECTS OF MOLECULAR MASS AND SURFACE AREA

4.1. ABSTRACT

The thermal behavior of adsorbed poly(vinyl acetate) (PVAc) on silica was investigated using temperature-modulated differential scanning calorimetry (TMDSC). Samples were prepared using three different molecular masses of PVAc and fumed silica. A single narrow glass transition was found for the bulk PVAc samples. However, adsorbed polymers showed broader two-component transitions. Loosely and tightly-bound polymers showed slightly and significantly higher glass transition temperatures (T_g) than that of bulk polymer, respectively. We have also observed polymer at the air interface that had a T_g lower than that of bulk, which we refer to as the mobile fraction. This result was consistent with the results of the previous studies based on deuterium NMR of adsorbed PVAc. The amount of tightly-bound polymer was quantified with a two-component model using relative intensities of the transitions. It was found that after a minimum amount of adsorbed polymer, the amount of the tightly-bound component

of the tightly-bound component remained constant as additional polymer was added. The amount of tightly-bound polymer was obtained by a linear regression analysis of the ratio of the area under the two transitions. The values obtained vary from 0.52 to 0.86 mg PVAc/m^2 silica depending upon the molecular mass of PVAc and the specific surface area of fumed silica. The tightly-bound amount of PVAc adsorbed on M5P silica was found to be greater than that of PVAc adsorbed on LM130 and EH5 silica.

4.2. INTRODUCTION

Interest in adsorbed polymers on surfaces has increased, mainly due to the differences between the properties of bulk and adsorbed polymers.[1-5] Adsorbed polymer-substrate interactions usually lead to changes in properties of bulk polymers. It is known that the interactions between adsorbed polymers and surfaces may provide enhanced physical, mechanical, and thermal properties, which make these materials suitable as lubricants, adhesives, coatings, and corrosion resistant agents.[6-10]

In recent studies, glass transitions of adsorbed polymers have been probed to investigate their thermal properties, structure, and dynamics.[11] The glass transition temperature of small amounts of adsorbed polymers depends on the film thickness, molecular mass of polymer, attractive forces between molecules, and the mobility of macromolecular chains.[12-14] Hydrogen bonding and covalent interactions between the polymer segments adsorbed on the surface of silica have been proposed as the main reason for the increases in the T_g.[15,16] On the other hand, there are some studies which indicate a reduction in T_g of adsorbed polymers due to the lack of strong interactions between the polymer segments and the surface.[17]

Nuclear magnetic resonance (NMR), Fourier transform infrared spectroscopy (FTIR), and differential scanning calorimetry (DSC) techniques have been used to characterize the properties and structure of adsorbed polymers.[18-21] DSC is the most common technique to investigate the thermal transitions in bulk polymers especially at the glass transition temperature.[22,23] Characterization of the behavior of adsorbed polymers at T_g has been studied using temperature modulated DSC (TMDSC). TMDSC is a version of DSC which offers the same information as conventional DSC as well as additional information to understand many aspects of thermal behavior of materials by separating the heat flow data into reversing and non-reversing events.[24] TMDSC has been used to resolve weak transitions and those occurring at close temperatures.[25-27] TMDSC has an ability to separate overlapping transitions that are difficult to distinguish in conventional DSC. Since the TMDSC separates the total heat flow into reversing and non-reversing components, more information about the thermal properties of materials can be obtained.

Different interactions between polymers and the surface of silica can result in separate transitions in TMDSC thermograms. For example, in previous studies,[5,16] a broadened, two component transition has been reported for poly(methyl methacrylate) (PMMA) adsorbed on silica. A higher-than-bulk glass transition temperature has been reported for the "tightly-bound" adsorbed polymer in this system. A slightly evaluated glass transitions resulted from the "loosely-bound" component. The relative intensities of the two component transitions depend on the adsorbed amount of polymer on the substrate.[16]

Thermal properties of adsorbed polymers are of interest in the present paper, in which the effects of molecular mass of polymer and the surface area of silica on the TMDSC

thermograms of adsorbed polymer have also been studied. Although two higher-temperature components in the thermograms of PMMA have been observed, we observed an additional transition for adsorbed PVAc using TMDSC for the mobile part of adsorbed polymer, located at the polymer-air interface.[11] We were able to clearly differentiate between polymer-silica, polymer-polymer, and polymer-air interface with TMDSC. This finding is consistent with the results obtained in studies of adsorbed PVAc on silica using NMR.[28]

4.3. METHODS

Three different molecular masses of PVAc (100, 170, and 260 kDa) were purchased and used as received (Scientific Polymer Products, Inc. Ontario). Three different Cab-O-Sil fumed silica grades (LM130, M5P, and EH5) were used as provided by Cabot Corporation (Tuscola, IL). The specific surface areas of the fumed silica particles were determined to be 130, 190, and 315 m^2/g for LM130, M5P, and EH5, respectively, using the BET method on a NOVA 2200 instrument (Quantachrome, FL). The toluene was purchased from Pharmco-aaper (Brookfield, CT) and used as received.

Samples were prepared using different concentrations of PVAc solutions in toluene (10 mL). Cab-O-Sil fumed silica (300 mg) was added to each polymer solution. The tubes containing mixtures of silica and the PVAc solutions were placed in a mechanical shaker for 48 h and then centrifuged at 6000 rpm for 15 min. The supernatant liquid was then removed and the adsorbed polymers on the silica samples were dried using air at a low flow rate. To remove any residual solvent, the samples were then dried in a vacuum oven at 60 °C for 3 d.

The adsorbed amounts of polymer on the surface of silica from the difference between the mass of sample before and after heating were determined using a model Q50 Thermogravimetric Analyzer (TA Instruments, New Castle, DE). Samples were heated from room temperature to 700 °C at a heating rate of 20 K/min in flowing air atmosphere (40 ml/min). The adsorbed amounts of polymer on silica were calculated based on the mass of the residual material, which contains only silica after heating, and the specific surface area of silica.

The thermal behavior of the composites in the glass transition region was investigated using a TA Instruments Model Q2000 DSC (TA Instruments, New Castle, DE). The sample pans were referenced against empty pans and the cell purged with a 50 mL/min nitrogen stream. The samples were held at -50 °C for 1 min, heated to 150 °C at a rate of 3 °C/min with a modulation amplitude of ±1.0 °C and a modulation period of 60 s, held at 150 °C for 2 min, cooled to -50 °C at 3 °C/min with the same modulation. Samples, then were held at -50 °C for 2 min in order to minimize the effects of previous thermal history. After that, a second heating scan was done with the same conditions as the first heating scan. Both cooling and second heating scans were analyzed and no significant difference was observed between these two methods. The second heating scan results were used to determine the T_g and tightly-bound amount of samples. The thermograms were reported as differential reversing heat flow rates (dQ_{rev}/dT) as a function of temperature, after applying a 10 ºC smoothing to reduce the high-frequency noise.

4.4. RESULTS

Thermogravimetric analysis (TGA) was used to estimate the amount of PVAc in each sample and also study the thermal decomposition behavior of adsorbed polymers. The

decomposition thermograms of bulk and adsorbed PVAc (170 kDa) on M5P fumed silica are shown in Figure 4.1. Thermal degradation temperatures for the adsorbed polymers were higher than bulk PVAc. Although the bulk polymer started to decompose at a temperature of about 275 °C, the adsorbed polymers started to decompose at around 310 °C. The dominant decomposition step for adsorbed polymers happened between 300 to 400 °C followed by a smaller one centered around 550 °C. Although adsorbed polymer on silica samples showed primarily these two-step decompositions, the bulk PVAc showed three-step decomposition. Adsorbed polymer on silica samples showed primarily two-step decompositions. The same trend was observed for the other sets of samples with different molecular mass of polymer and the same specific surface area of silica. After determining the amount of PVAc using TGA, the adsorbed amounts of polymer on silica were calculated based on the specific surface areas of silica.

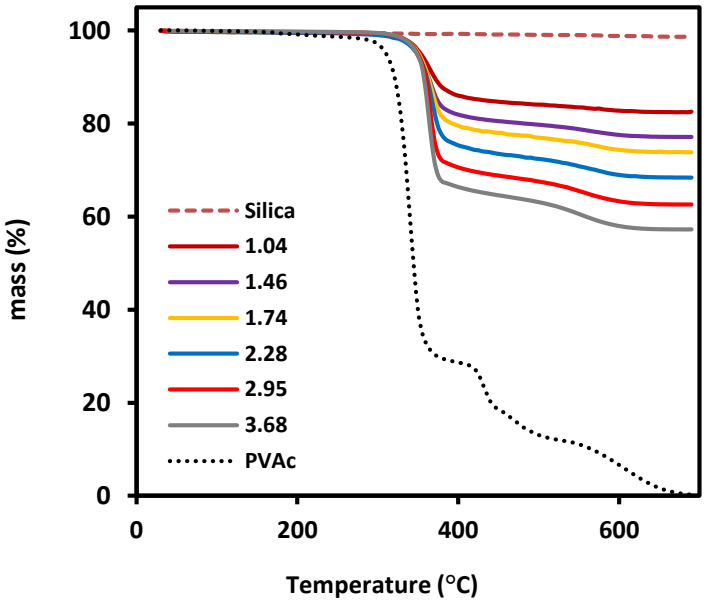

Figure 4.1. TGA thermograms of silica, PVAc adsorbed on silica, and bulk PVAc as a function of adsorbed amount of polymer. The adsorbed amounts are shown as in mg polymer/m2 silica and the order of the curves is the same as in the legend.

The thermograms for bulk and adsorbed PVAc (260 kDa) on silica are shown in Figure 4.2. A similar observation was made for the other molecular masses of adsorbed PVAc on fumed silica. The glass transition temperatures (T_g) for the bulk PVAc were found to be 40.9 ± 0.3, 40.7 ± 0.5, and 42.7 ± 0.5 °C (from the derivative heat flow of 3 ºC/min) for 100, 170, and 260 kDa, respectively. Three different regions of thermal activities were observed for the adsorbed polymers. At small adsorbed amounts, thermal activities only occurred within the temperature range of 60 to 80 ºC. At approximately 1 mg/m^2 adsorbed polymer, the intensity of this thermal activity seemed to be constant irrespective of the adsorbed amount. A second thermal activity peak appeared for samples above 1 mg/m^2 corresponding to loosely-bound polymer. In addition, a third region was found at a temperature lower than the T_g of bulk polymer. This region was small and only seen beyond almost 2 mg/m^2.

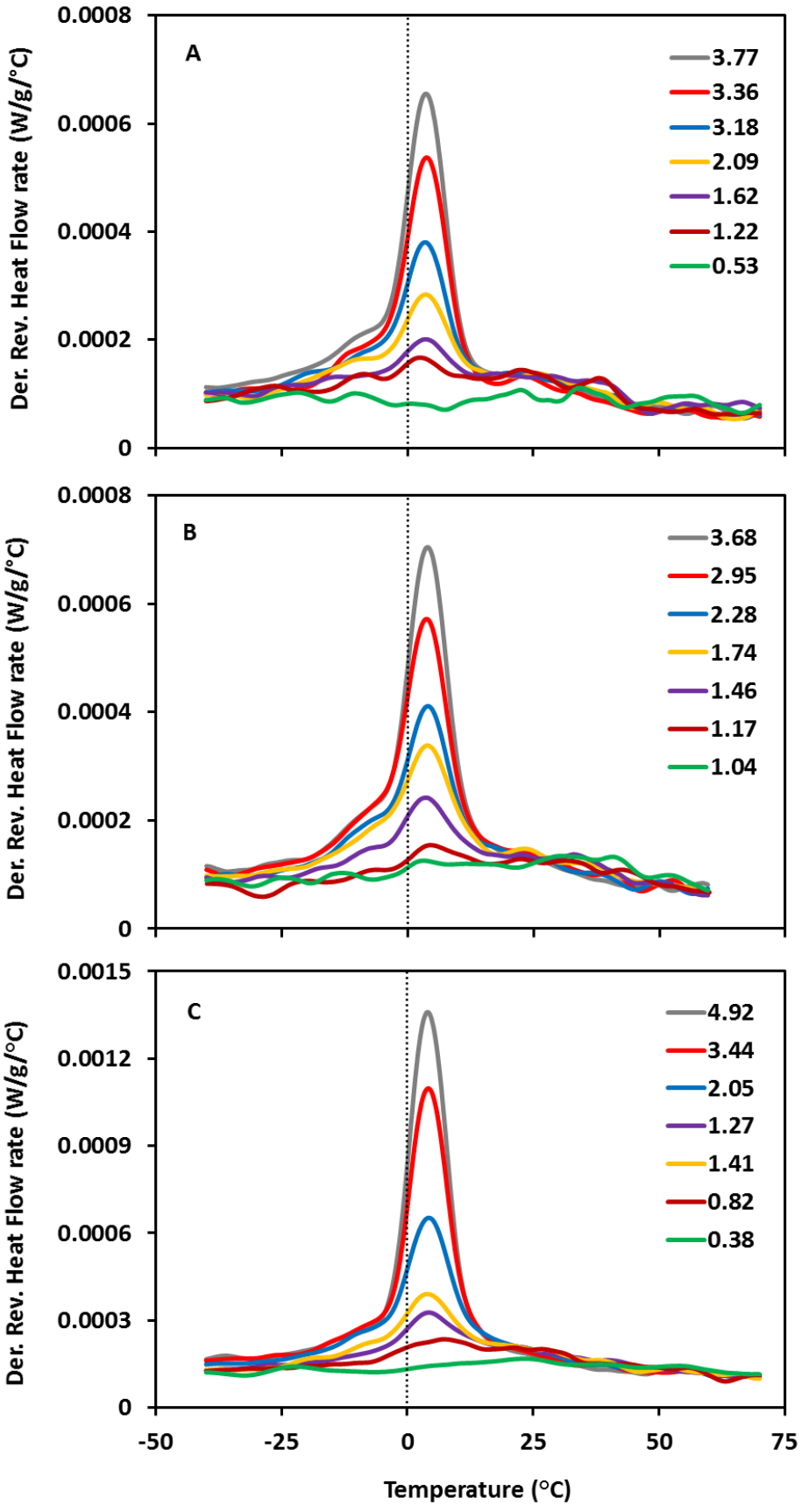
A
3.77
3.36
3.18
2.09
1.62
1.22
0.53
B
3.68
2.95
2.28
1.74
1.46
1.17
1.04
C
4.92
3.44
2.05
1.27
1.41
0.82
0.38
Der. Rev. Heat Flow rate (W/g/°C)
0.0008
0.0006
0.0004
0.0002
0
0.0015
0.0012
0.0009
0.0003
-50
-25
0
25
50
75
Temperature (°C)

Figure 4.2. TMDSC thermograms for bulk and adsorbed PVAc (170 kDa) on different fumed silica particles: A) LM130, B) M5P, and C) EH5. The intensities of the main peaks are in the same order as in the legend. The thermograms are labeled with the adsorbed amounts that are shown in mg polymer/m^2 silica and the main peaks are in the same order as in the legend. The curves are shown relative to the bulk T_g of each polymer (dashed vertical line).

The smallest adsorbed-amount samples showed only a tightly-bound component with a T_g of 66 ± 3 °C, which was ~ 25 °C higher than the transition for the bulk polymer. With a small increase in the adsorbed amount, a larger intensity of tightly-bound component was observed due to the more adsorbed polymer on the surface. After increasing the adsorbed amount beyond a certain amount, a second transition (loosely-bound component) was observed in the region of the bulk polymer transition. At larger adsorbed amounts, two distinct regions were found for the loosely-bound and the tightly-bound polymers. As the adsorbed amount increased, the area under the loosely-bound transition increased, whereas that of the tightly-bound amount remained approximately constant.

The T_g's of the samples were determined using the results of the second heating scans. The cooling scans were also analyzed to find the T_g of samples and no significant difference was observed between the glass transitions from the heating and cooling scans (± 1.5 ºC). The glass transition of the loosely-bound polymer was 3 ± 1 ºC larger than that of the bulk polymers. Since the mobile component and loosely-bound transitions were not well separated, it was difficult to estimate the glass transition temperature for the mobile components. This transition seemed to be in the range of 28 to 30 ºC. The

glass transition temperature of tightly-bound polymer was estimated by fitting of plots with a Gaussian-Lorentzian distribution function.

4.5. DISCUSSION

A number of studies have reported that adsorbed polymers behave differently than their corresponding counterparts bulk. For instance, it has been reported that silica enhances the thermal stability of PMMA.[29] As it can be seen in Figure 4.1, the thermal degradation temperature values for adsorbed polymers were higher than that for bulk PVAc, which is consistent with the presence of surface interactions that affect the degradation of samples.[16] The degradation temperature of adsorbed PVAc was around 7 to 12 ºC higher than that of the bulk polymer, and this difference depended on the molecular mass of PVAc, specific surface area of fumed silica, and also the adsorbed amount. The degradation temperature was found to be almost constant for larger adsorbed amounts and slightly higher than that for the smallest adsorbed amounts. The slight increase in T_d for adsorbed polymers indicates that the interactions between the carbonyl groups of PVAc and hydroxyl groups of silica increase with increasing amounts of polymer for small adsorbed amounts. A constant degradation temperature, after a certain adsorbed amount suggests that the tightly-bound amount does not change much with increasing amounts of polymer. In other words, higher thermal degradation temperatures of adsorbed polymers compared to bulk was likely due to the reduced molecular mobility of PVAc molecules close to the surface of silica particles.

The glass transition temperature of a polymer in nanocomposites can be either increased or decreased due to attractive or repulsive interactions, respectively, with the surface. For all sets of samples, we have been able to observe a small transition at a lower

temperature than the loosely-bound transition, which appeared as a shoulder to the peak for the loosely-bound polymer. We believe that this transition was indicative of the more mobile fraction of polymer located at the polymer-air interface. These results are in good agreement with previous studies on the dynamics of adsorbed Poly(methyl methacrylate)[30] on substrates and also adsorbed PVAc on silica based on deuterium NMR results.[28] It has been shown that there is a motional gradient in these adsorbed polymers.[28] The mobility of segments near the surface of silica was significantly less than those at the polymer-air interface. The lower mobility of the segments near the substrate was due to the interactions between the carbonyl groups of PVAc and the hydroxyl groups of silica particles which resulted in shifts to higher T_gs.

Most of the TMDSC curves showed two distinct transitions at temperatures higher than and a small transition at temperature lower than the bulk T_g's. Although previous studies[5,16] have investigated the thermal behavior of adsorbed PMMA on silica and reported two distinct transitions, the peaks were not as well separated for the adsorbed PVAc. The bulk-like transition from the loosely-bound polymer was found to be similar to, but slightly higher than that of the bulk polymer. The second transition was found at a significantly higher temperature than that for the bulk polymer. This transition was representative of the lower mobility polymer which was more closely associated with the silica surface and considered to be tightly-bound to the surface. The presence of the hydrogen bonds between the silanol groups on the silica particles and carbonyl groups of polymers such as PVAc[31,32] and PMMA[20,33] have been reported using FTIR. A broad T_g was observed for the tightly-bound which was significantly larger than that of bulk polymer. This amount has been observed to be as much as 45 ºC in case of PMMA

adsorbed on silica.[5] The broad T_g is an important indicative of a multi-component polymeric system like adsorbed polymer. On the other hand, in some cases, such as adsorbed polystyrene on silica[34], the transition broadened compared to balk, but little heterogeneity was noted, e.g., little if any tightly-bound polymer existed due to the weak interactions between polymer and substrate.

As shown in Figure 4.2, a minimum amount of adsorbed polymer needed before any loosely-bound transition was observed. For small amounts of adsorbed polymer, only tightly-bound polymer existed and with increasing adsorbed amount, a transition to loosely and mobile polymer with a similar nature to bulk polymer occurred. Different hypothetical layers of the adsorbed polymer on the silica are shown schematically in Figure 4.3. These layers are defined based on their mobility, i.e., T_g. As shown in Figure 4.3 (A and B), at small adsorbed amounts, polymer chains distribute on the surface and strongly interact with the surface to make a thin layer. This pattern continues until the whole surface is covered with a tightly attached layer of polymer to the surface. This behavior was observed in the thermogram where increments to the tightly-bound transition occurred without the addition of any transition close to that of bulk polymer (Figure 4.3 B). Ultimately, adding more polymer lead to the formation of the loosely-bound polymer on top of the tightly-bound layer (Figure 4.3 C). This layer changed the thermogram intensity at temperature close to bulk polymer without affecting the tightly-bound peak significantly. This new transition consisted of both a loosely-bound fraction and a mobile component with increased adsorbed amounts. The intensity of the loosely-bound polymer then increased with the addition of more polymer to the surface (Figure 4.3 D and E).

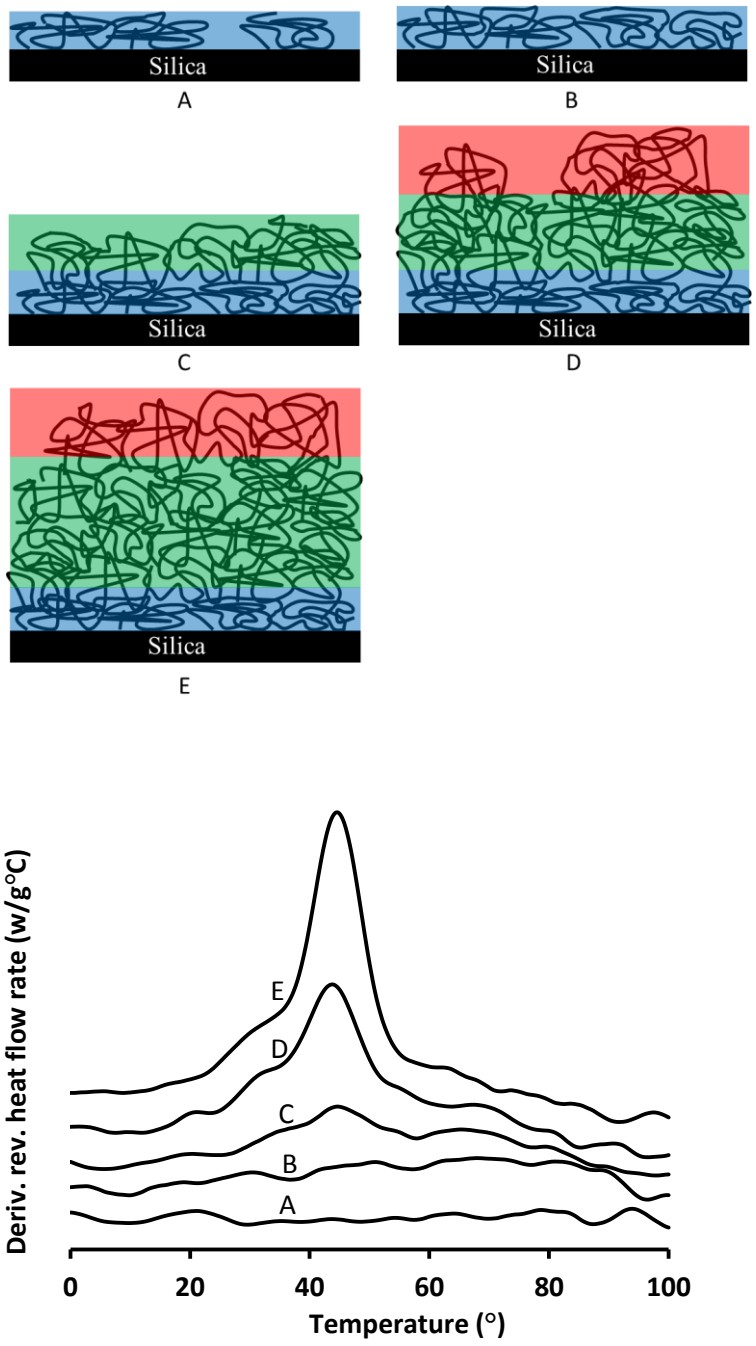

Figure 4.3. Thermograms and simplified schematic representation of five different adsorbed amounts of polymer on the surface of silica. (A) represents the smallest adsorbed amount and (E) represents the largest one. The closest layer of polymer to the silica surface with the blue background represents the tightly-bound polymer. The green and red backgrounds show the loosely-bound and the mobile component, respectively.

A two-component model, based on relative intensities of the transitions was used to interpret the thermograms of two-component transitions which were found for adsorbed polymers.[16] Component A represents the loosely-bound polymer and the mobile component which showed a slightly higher and lower T_g than that of bulk polymer respectively. Component B represents the tightly-bound polymer with significantly higher T_g than that of the bulk polymer. Figure 4.4 shows how the components A and B were separated. This model has been used to investigate the effect of molecular mass on the adsorption of PVAc on fumed silica. The amount of tightly-bound polymer (in mg polymer/m^2 silica surface) was also quantified using this model. As it has been mentioned earlier, the tightly-bound transition peak increases to a constant amount with increasing adsorbed amount. After that minimum amount, the amount of tightly-bound polymer was constant as additional polymer was added.

The amount of tightly-bound polymer can be estimated from equation (4.1), from *r*, the ratio of the heat flow changes for the loosely and tightly-bound components.[16]

$$\begin{aligned} r &= (m'_p - m'_{pB})\,\Delta C_{pA}/(m'_{pB}\,\Delta C_{pB}) \\ &= [\Delta C_{pA}/(m'_{pB}\,\Delta C_{pB})]m'_p - \Delta C_{pA}/\Delta C_{pB} \end{aligned} \qquad (4.1)$$

where the ΔC_p's represent the specific heat capacity changes in the glass transition region, m'_p represents the normalized polymer mass, which was determined using the TGA results by dividing the mass loss (total mass of adsorbed polymer) by the remaining mass (mass of silica).

$$m'_p = m'_{pA} + m'_{pB} \qquad (4.2)$$

Here the m'_{pA} and m'_{pB} represent the normalized masses of loosely-bound and tightly-bound polymers, respectively.

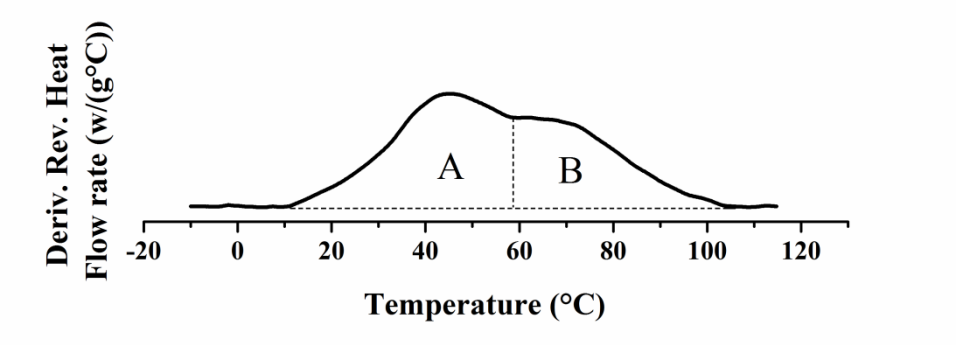

Figure 4.4. Schematic representation of the component A (loosely-bound) and B (tightly-bound) in TMDSC thermograms.

A linear relationship between the ratios for the areas under the A and B transitions and the total relative masses of polymer (m'_p) are shown in Figure 4.5. As described in equation 4.1, the amount of tightly-bound polymer can be obtained by dividing the intercept value (ratio of the heat capacity increments, $\Delta C_{pA}/\Delta C_{pB}$) by the slope ($\Delta C_{pA}/(m'_{pB}\,\Delta C_{pB})$) of the regression line. The r values for the samples with adsorbed amount below m'_{pB} were roughly equal to 0, because there was no peak for the loosely-bound polymer. The curves are extrapolated to $m'_p = 0$ to show the intercept which is needed in the calculation of the tightly-bound amount.

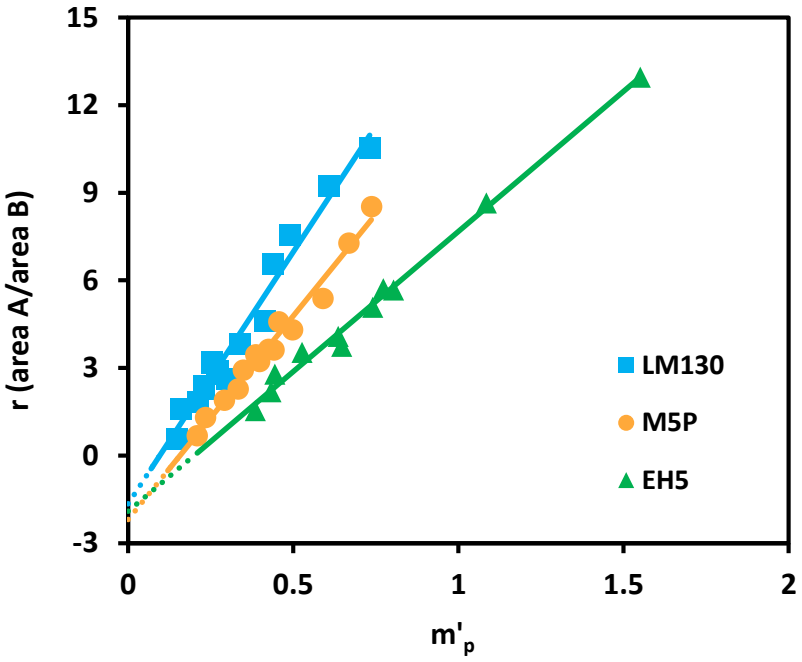

Figure 4.5. Ratio (*r*) of the areas under the transitions A (loosely-bound) and B (tightly-bound) as a function of the relative amount of adsorbed polymer (mg PVAc 170 kDa/ m^2 silica) for three different surface area of silica particles.

The tightly-bound amounts of adsorbed polymers using the analysis mentioned above are shown in Table 1. Based on this analysis, the specific surface area plays a role in determining the amount of tightly-bound polymer. Although the tightly-bound amount decreased slightly with increasing the molecular mass of PVAc for LM130 and M5P silica, this effect was smaller compared to the effect of the particle structure of silica on the tightly-bound amount. The tightly-bound amounts were found to be almost constant for different molecular masses of adsorbed PVAc on EH5 silica. The tightly-bound amount of adsorbed polymers on M5P silica was up to 35% larger than adsorbed polymers on EH5 silica.

Table 4.1. Tightly-bound amounts from the linear regression analysis of plots of relative change of areas under the transitions of two different components for each set of PVAc adsorbed on silica.

	m'_{pB} (mg/m^2)		
	LM130	M5P	EH5
PVAc 100 kDa	0.76 ± 0.09	0.86 ± 0.13	0.56 ± 0.06
PVAc 170 kDa	0.75 ± 0.08	0.83 ± 0.08	0.52 ± 0.06
PVAc 260 kDa	0.63 ± 0.08	0.78 ± 0.06	0.54 ± 0.07

As presented in Table 4.1, despite the larger specific surface area of EH5 silica, the tightly-bound amount was less than that for M5P and LM130 silica. This can be explained by defining the available surface area. Since the slits between the connected silica particles in EH5 are very narrow, the polymer chains are not able to fully cover the surface of these particles. In other words, although the surface area of EH5 fumed silica was a large value, the fraction of unavailable surface area is more than that of LM130 and M5P since the primary particles are very small. As mentioned earlier, the tightly-bound amount decreased with increased molecular mass of PVAc adsorbed on LM130 and M5P. The reason might be the presence of more strong interactions of lower molecular mass of PVAc molecules due to the smaller relative size of PVAc to silica particles and more direct contacts with the surface. Furthermore, no significant change was found for the tightly-bound amount of different molecular mass of PVAc adsorbed on the EH5.The

small size of particles and less available surface area are the dominant factor in case of EH5 silica.

The heat capacity ratio of loosely-bound to tightly-bound polymer based on analysis above was found to be in the range of 1.5 to 2.5. This suggests that the change in mobility of the tightly-bound component was smaller than that of loosely-bound component due to the strong interactions at the interface of the silica and polymer. The heat capacity ratio was found to be 3.0 in case of adsorbed PMMA on silica[5] which indicates stronger interactions of PMMA and silica at the surface. The maximum amount of the tightly-bound polymer for adsorbed PVAc was found to be 0.86 (Table 4.1) which was less than the reported tightly-bound amount for adsorbed PMMA (1.21 mg/m^2).[5] Comparing the results of ΔT_g (difference between the glass transition temperature of tightly-bound and bulk-like polymer) and the ratio of heat capacities of loosely and tightly-bound of adsorbed PMMA and PVAc on silica, it would be expected to have smaller tightly-bound amount of adsorbed PVAc on silica.

The bound fraction, f_B, is the ratio of the mass of bound polymer at the polymer-surface interface to the total amount of polymer. f_B can be also obtained using the ratio of the heat flow changes of loosely and tightly-bound components.

$$f_B = m'_{pB}/m'_p = m_{pB}/m_p = m''_{pB}/m''_p = 1/(1+ r\Delta C_{pB}/\Delta C_{pA}) \quad (4.3)$$

Since no loosely-bound peak was observed for the adsorbed amounts less than tightly-bound amount, all of the segments for the specimens at adsorbed amounts less than m''_{pB} was considered as tightly-bound. The fraction of tightly-bound polymer, f_B was calculated using equation 4.3 for the samples with adsorbed-polymer above m''_{pB}. Smooth

curves have been obtained with substituting the m''_{pB} in the equation 4.3. Figure 4.6 shows the data points and the curves for the PVAc 170 kDa on the silica surface. As shown in Figure 4.4, the tightly-bound fraction decreased with increasing adsorbed amounts.

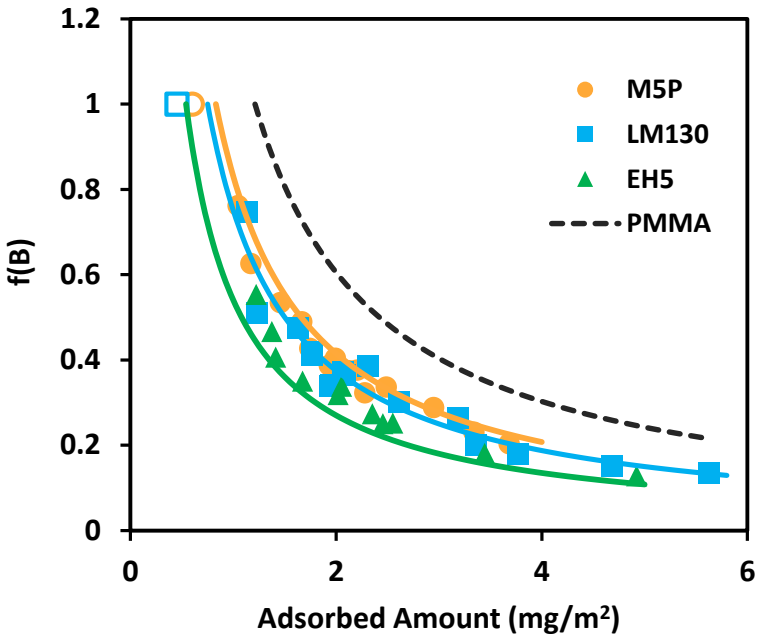

Figure 4.7. The tightly-bound fraction of PVAc 170 kDa on silica as a function of the adsorbed amount. The smooth curve is based on the model with fixed amount of tightly-bound polymer (m''_B = 0.75 mg/m^2 for LM130, m''_B = 0.83 mg/m^2 for M5P, and m''_B = 0.52 mg/m^2 for EH5). The black line represents the tightly-bound fraction of PMMA on M5P.

4.6. CONCLUSIONS

TMDSC was used to investigate the thermal characteristics of adsorbed PVAc on silica. Three distinct transitions have been observed in TMDSC results. The transitions are referred as mobile component and loosely and tightly-bound polymer on the surface

of silica. The glass transition temperature of the loosely-bound polymer was roughly 3 °C higher than that of the bulk PVAc and the transition of tightly-bound polymer was in the region of 64 to 69 °C. Another transition which was slightly lower than that of loosely-bound polymer was identified for the first time. This transition represents the mobile polymer, which is located at the polymer-air interface. This result is in agreement with the previous studies using solid NMR. The amount of tightly-bound polymer has been estimated by the relative intensities of the transitions using a simple two-component model. The amount of tightly-bound polymer was estimated to be in the range of 0.52 to 0.86 mg PVAc/m^2 silica. Although the tightly-bound amount was found to be larger for the PVAc adsorbed on M5P compared to LM130 and EH5 silica, it was less than tightly-bound amount of adsorbed PMMA on M5P. This was consistent with PVAc not being as strongly-bound to silica as PMMA.

4.7. ACKNOWLEDGEMENTS

The authors acknowledge the financial support of the National Science Foundation (USA) under Grant No. DMR-1005606 and the Oklahoma State University.

4.8. REFERENCES

(1) Parida, S. K.; Dash, S.; Patel, S.; Mishra, B. *Adv. Colloid Interface Sci.* **2006**, *121*, 77.

(2) Metin, B.; Blum, F. D. *Langmuir* **2009**, *26*, 5226.

(3) Madathingal, R. R.; Wunder, S. L. *Thermochim. Acta* **2011**, *523*, 182.

(4) Madathingal, R. R.; Wunder, S. L. *Thermochim. Acta* **2011**, *526*, 83.

(5) Khatiwada, B. K.; Hetayothin, B.; Blum, F. D. *Macromol. Symp.* **2013**, *327*, 20.

(6) Lučić, S.; Kovačević, V.; Hace, D. *Int. J. Adhes. Adhes.* **1998**, *18*, 115.

(7) Soga, I. *J. Coat. Technol.* **2003**, *75*, 53.

(8) Zou, H.; Wu, S.; Shen, J. *Chem. Rev.* **2008**, *108*, 3893.

(9) Kaboorani, A.; Riedl, B. *Compos. Part A Appl. Sci. Manuf.* **2011**, *42*, 1031.

(10) Caselis, J. L. V.; Rosas, E. R.; Meneses, V. M. C. *Corros. Eng., Sci. Technol.* **2012**, *47*, 131.

(11) Mortazavian, H.; Fennell, C. J.; Blum, F. D. *Macromolecules* **2016**, *49*, 298.

(12) Overney, R. M.; Buenviaje, C.; Luginbühl, R.; Dinelli, F. *J. Therm. Anal. Calorim.* **2000**, *59*, 205.

(13) Belfiore, L. A. *Physical Properties of Macromolecules*; John Wiley & Sons: Hoboken, NJ, **2010**.

(14) Yevgen, M.; Maksym, I. *Advances in Progressive Thermoplastic and Thermosetting Polymers, Perspectives and Applications*; TehnoPress Editura: Iasi, Romania, **2012**.

(15) Tate, R. S.; Fryer, D. S.; Pasqualini, S.; Montague, M. F.; de Pablo, J. J.; Nealey, P. F. *J. Chem. Phys.* **2001**, *115*, 9982.

(16) Blum, F. D.; Young, E. N.; Smith, G.; Sitton, O. C. *Langmuir* **2006**, *22*, 4741.

(17) Forrest, J. A.; Dalnoki-Veress, K.; Dutcher, J. R. *Phys. Rev. E* **1997**, *56*, 5705.

(18) Jo, H.; Blum, F. D. *Langmuir* **1999**, *15*, 2444.

(19) Porter, C. E.; Blum, F. D. *Macromolecules* **2000**, *33*, 7016.

(20) Kulkeratiyut, S.; Kulkeratiyut, S.; Blum, F. D. *J. Polym. Sci., Part B: Polym. Phys.* **2006**, *44*, 2071.

(21) Maddumaarachchi, M.; Blum, F. D. *J. Polym. Sci., Part B: Polym. Phys.* **2014**, *52*, 727.

(22) Biliaderis, C. G.; Page, C. M.; Maurice, T. J.; Juliano, B. O. *J. Agric. Food. Chem.* **1986**, *34*, 6.

(23) Russell, P. L.; Oliver, G. *J. Cereal Sci.* **1989**, *10*, 123.

(24) Hutchinson, J. M. *J. Therm. Anal. Calorim.* **2003**, *72*, 619.

(25) Jin, Y.; Bonilla, J.; Lin, Y.-G.; Morgan, J.; McCracken, L.; Carnahan, J. *J. Therm. Anal.* **1996**, *46*, 1047.

(26) Cao, J. *Thermochim. Acta* **1999**, *325*, 101.

(27) Verdonck, E.; Schaap, K.; Thomas, L. C. *Int. J. Pharm.* **1999**, *192*, 3.

(28) Blum, F. D.; Xu, G.; Liang, M.; Wade, C. G. *Macromolecules* **1996**, *29*, 8740.

(29) Zou, D. Q.; Yoshida, H. *J. Therm. Anal. Calorim.* **2010**, *99*, 21.

(30) Lin, W.-Y.; Blum, F. D. *J. Am. Chem. Soc.* **2001**, *123*, 2032.

(31) Wen, N.; Tang, Q.; Chen, M.; Wu, L. *J. Colloid Interface Sci* **2008**, *320*, 152.

(32) Beaudry, C.; Klein, L.; McCauley, R. *J. Therm. Anal. Calorim.* **1996**, *46*, 55.

(33) Frantz, P.; Granick, S. *Macromolecules* **1995**, *28*, 6915.

(34) Porter, C. E.; Blum, F. D. *Macromolecules* **2002**, *35*, 7448.

CHAPTER V

WETTABILITY OF FUNCTIONALIZED GRAPHENE OXIDE IS DEPENDENT ON BOTH THE SIZE AND STRUCTURE OF SURFACE MODIFYING GROUPS

5.1. ABSTRACT

The chemical nature of graphene oxide makes it a versatile material that is easy to functionalize, making it an ideal platform for studying surface properties. We performed experimental water contact angle measurements and molecular modeling investigations on functionalized graphene oxide (GO) surfaces to test how the chemical makeup and size of attached groups affect surface wettability. Experimental and molecular simulation based water contact angle measurements showed quantitative agreement for functionalizing groups with the same chain length at a variety of surface coverages. We observed a transition between hydrophobic and superhydrophobic behavior when functionalizing with alkyl-silane and fluorosilane groups, respectively, on GO surfaces with nanometer-scale roughness. We also explored the connection between hydration free energies and contact angle measurements with molecular simulations, and we used this connection in simulation predictions for the trend of water contact angles with changes in the modifying group chain length. As the alkyl or fluoroalkyl chain lengths decreased, the simulations indicated that we should expect a concurrent increase in the surface

wettability. This more hydrophilic behavior is due to both an increase in direct exposure of the GO surface to water and stronger indirect interactions between water and the GO interface via the thinner separating layers of hydrophobic functional groups.

5.2. INTRODUCTION

The wettability of a solid surface is generally controlled by both the interfacial chemical composition and surface topology, and manipulating these two features can lead to interfaces with high water repellency and self-cleaning properties.[1-6] Over the last several years, wetting properties of graphene and graphene oxide (GO) have been studied extensively both experimentally and with MD simulations.[7-12] The large number of polar sites, large specific surface area,[13] and larger surface roughness[7,14] of GO has made it a good candidate for exploring how chemical modifications can alter the interfacial hydrophobicity. GO consists of graphene sheets functionalized with hydrophilic groups, such as hydroxyl and epoxy moieties.[15] These functional groups represent the target sites for modification of the surface in order to alter the surface chemistry. For example, silane and alkylamine coupling agents have been used to enhance the water repellency of GO based composites, graphene aerogels, and GO films.[14,16-19]

Molecular dynamics (MD) simulation has been increasingly used to model the behavior of water droplets on solid surfaces,[10,20-25] with a recently growing focus on the wettability and wetting transparency of graphene.[26-28] With improvements in computational power, increasingly complex systems can be modeled, and current studies are able to explore nanometer-scale structure effects on surface wettability.[29-32] At this scale, the choice of proper intermolecular parameters for surface groups is critical if we

want to explain specific interfacial properties[27,33] and the role of surface chemical composition.[34-37]

In this study, we used experiments and molecular simulations to investigate the effect of surface modification with (heptadecafluoro-1,1,2,2-tetrahydrodecyl)trimethoxysilane and decyl(trimethoxy)silane (FDTS and DTMS respectively as pictured in Figure 5.1) and surface coverage of these functional groups on the wettability of GO. As interfacial wettability involves, a balance of surface tension and detailed chemical interactions, we also explored how changes in the hydration free energy of these fluorinated and non-fluorinated chemical groups, as well as changes in these surface modifying group chain lengths, affect the resulting contact angle measured. The goal was to provide a systematic comparison that provides a consistent picture on how chemical modification of GO can be used to alter its wettability, and to develop a model system for predicting changes in surface hydrophobicity due to chemical composition, surface coverage, and chain length of modifying groups.

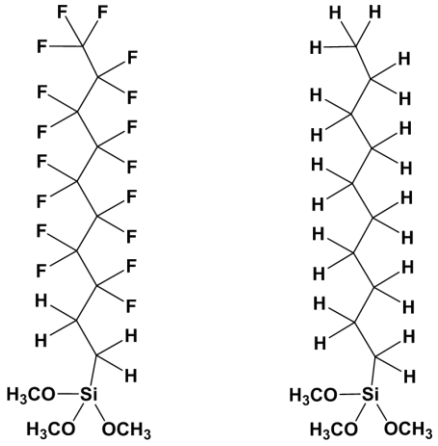

Figure 5.1. Molecular structures of A) FDTS and B) DTMS.

5.3. METHODS

5.3.1. Experimental studies

Graphene nano platelets (xGNP® grade M) were purchased from XG Sciences, Michigan. FDTS and DTMS coupling agents were purchased from Gelest Inc. USA. The improved Hummer's method was used to synthesize GO from graphene nano platelets.[38] To prepare the functionalized surfaces, GO was dispersed in toluene by ultrasonication for 72 h at room temperature, and 3 ml samples of this GO mixture (~6 mg/ml) were placed in plastic vials. Different amounts of FDTS and DTMS were added to these vials, and the reaction mixtures were heated at 350 K and shaken for 2 h in a mechanical shaker. These samples were centrifuged, the supernatant was discarded, and washed two times with ~5 ml of toluene, and were finally dispersed in 2 ml of toluene. Half of each sample was air dried for thermogravimetric analysis and another half was used to prepare coatings. In the thermogravimetric analysis (TGA), the grafted amounts of FDTS and DTMS on the GO surface were determined using a Model Q-50 TGA instrument (TA Instruments, New Castle, DE). Samples were heated from room temperature to 1225 K at a heating rate of 20 K/min in a flowing nitrogen atmosphere (40 mL/min).

To prepare the treated GO coatings, 0.2 ml droplets of the treated GO dispersion were placed on one inch square area paper strips. The coated samples were air dried and heated at 415 K for 15 min before being used for contact angle analysis. A home-built contact angle measurement instrument was used to determine the water contact angle at ambient temperature. The Low Bond Axisymmetric Drop Shape Analysis (LB-ADSA) technique[39-41] was applied to measure the contact angle of a sessile drop by fitting the best profile to an image of a 4 µl water droplet taken by a high resolution Proscope

camera. Four water droplet images were taken on different spots of the surface of each sample and the average and standard error were reported.

5.3.2. Computational surface simulations

The wettability of GO and treated GO surfaces were modeled using all-atom MD simulations. To simulate a functionalized GO surface, a single continuous sheet of graphene was assembled and extended periodically in the *x*- and *y*-dimensions. A graphene surface was used instead of GO to avoid complexities due to possible non-uniformities in distributions of functional groups on the surface. To make this surface behave like GO, the Lennard-Jones (LJ) epsilon parameter for the OPLS-AA aromatic carbon atom type in the graphene sheet was optimized to produce a contact angle of nearly 80˚, the experimental contact angle we measured for bare GO.[42] GO sheets with large surface areas, 8.5 × 8.5 to 15 × 15 nm^2 depending on the water droplet size, were used to suppress any possible interaction between water droplet periodic images. Similarly, the *z*-dimension of the simulation was fixed at 50 nm to minimize interactions between water and both faces of the GO surface. Water droplets were initially prepared as cubes of 1000 to 7000 molecules, and the SPC/E model[43,44] was used for the water force field. These cubes were positioned 2 Å above the graphene sheets to form the initial simulation configurations.

Fluorosilane and alkyl-silane treated GO surfaces were prepared by bonding the chains to the GO sheet. This was done by converting three GO aromatic carbon sites to tetrahedral carbon atom types, which would bond to the oxygen atoms of the silane group.

Systems were constructed with series of chain lengths (C_4, C_8 and C_{10}) and functional

group densities, specifically eight uniformly patterned densities spanning 0.8 to 4.8 chains per nm^2.

MD simulations were carried out in the canonical (NVT) ensemble using GROMACS 4.5.5.[45] All simulations used the optimized potentials for liquid simulations all-atom force-field (OPLS-AA).[42] The steepest descent energy minimization algorithm was used to relax the GO surface and water boxes separately. Carbon atoms were then fixed at their respective positions with harmonic restraints and simulations were performed at a temperature of 298.15 K, fixed using a Nose-Hoover thermostat.[46,47] A time step of 2 fs was used, and systems were equilibrated with 10 ns of simulation, followed by 10 ns production runs. Long-range electrostatic interactions were calculated through the smooth particle-mesh Ewald summation[48] and a cut-off distance of 12 Å was applied for other non-bonded interactions. Additional details of the force-field parameters are described in the **Supporting Information**.

5.3.3. Hydration free energy calculations

To explore the connection between hydration free energy (ΔG_{hyd}) and water droplet contact angles on functionalized surfaces, we calculated ΔG_{hyd} for small molecule constituent groups of DTMS (methane) and FDTS (tetrafluoromethane) using the OPLS-AA force field and SPC/E water. In addition to the standard OPLS-AA force field representation, we calculated ΔG_{hyd} for tetrafluoromethane using scaled LJ epsilon parameters for the fluorine atoms. The scaled parameters were chosen in order to optimize the $\Delta\Delta G_{hyd}$ between methane and tetrafluoromethane so that it matched the difference observed in experimental Henry's Law constants.[49] In other words, CF_4 is experimentally observed to be 5 kJ/mol more hydrophobic than methane, and we adjust

the Lennard-Jones parameters of the F atom to enforce this difference in the scaled force field calculations.

The ΔG_{hyd} has both a polar (ΔG_{pol}) and nonpolar (ΔG_{np}) component that can be determined independently through charging and Lennard-Jones (LJ) decoupling calculation cycles.[50] We calculated ΔG_{pol} via the difference of vacuum and solvated state charging thermodynamic integration (TI) calculations. The vacuum TI charging calculations were done over 11 λ-windows (0.0, 0.1, 0.2, 0.3, 0.4, 0.5, 0.6, 0.7, 0.8, 0.9, 1.0) while the solvated TI charging calculations were done over 6 λ-windows (0.0, 0.2, 0.4, 0.6, 0.8, 1.0). Similarly, we calculated ΔG_{np} using TI over 17 λ-window calculations (0.0, 0.05, 0.1, 0.2, 0.3 0.4, 0.5, 0.55, 0.6, 0.65, 0.7, 0.75, 0.8, 0.85, 0.9, 0.95, 1.0) over which the solute LJ function is transformed to a soft-core potential function.[51]

5.4. RESULTS

5.4.1. Grafted amounts of coupling agents were determined using TGA

Thermal decomposition thermograms for graphene, GO, and one example for fluorosilane and alkyl-silane treated GO samples are shown in Figure 5.2. Thermograms of other samples are provided in the **Supporting Information**. The thermogram of graphene showed a weight loss of 10% at 900 K and total 15% up to 1200 K. The thermogram of GO showed primarily two weight loss steps. The first step occurred below 400 K with 12% weight loss, indicating the presence of adsorbed water, followed by the second step up to 600 K with 22% weight loss. The second step was due to pyrolysis of the labile oxygen-containing functional groups.[52-56] The weight loss at temperatures above 950 K can be attributed to the combustion of the carbon skeleton.[57] Treated GO samples showed the two steps at similar temperature ranges as GO followed by a third

weight loss step in the range of 600 to 900 K with different mass loss ratios depending on both the grafted amounts and chemical makeup of the coupling agents, as well as different maximum temperatures for mass loss depending on the chemical makeup of the functional group. The mass loss ratio was greater for fluoroalkyl-silane treated surfaces due to the greater molecular mass of fluorine over hydrogen. The degradation temperature for alkyl-silane treated surfaces is greater than for fluoroalkyl-silane treated surfaces, indicating additional potential covalent contacts with the GO surface. Thermograms for treated GO showed a smaller mass loss in the first step indicating a smaller number of oxygen-containing groups on the surface compared to GO. The weight loss step after 600 K is due to the decomposition of the coupling agents. The mass ratio of FDTS and DTMS to carbon atoms of the graphene sheets was calculated using the mass loss corresponding to silane groups and the carbon skeleton.

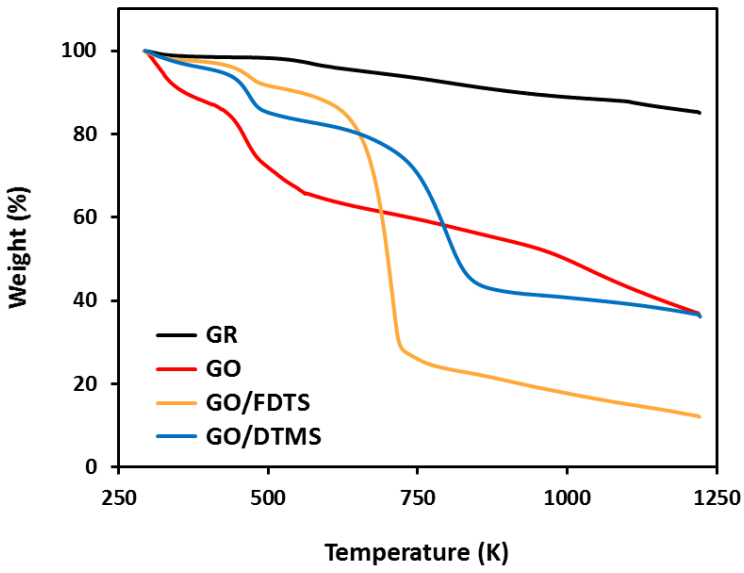

Figure 5.2. TGA thermograms of graphene, GO, fluorosilane and alkyl-silane grafted GO. GO shows two main weight loss steps and treated GO samples show three main loss steps below 900 K.

5.4.2. Contact angle measurements show surface wettability depends on functional group coverage and chemistry

The water contact angle on the GO surface can vary depending on the density of functionalized oxygen hydrophilic groups on the surface. Figure 5.3 shows how water contact angles on the surface of GO decrease with time due to wetting of these hydrophilic groups. The 80 ± 4^{o} contact angle seen after two minutes of exposure was chosen as a reference for both the functionalized samples and the MD simulations. Hence, images from all the other samples reported, were taken after two minutes from the time that droplets were placed on the surface.

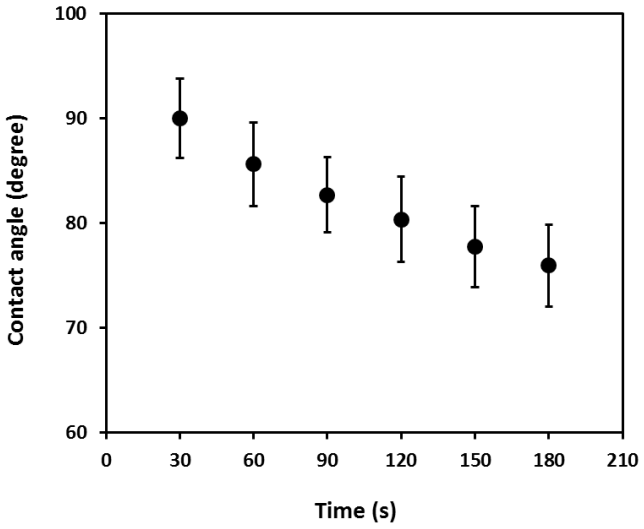

Figure 5.3. Contact angle of water droplets on GO as a function of time after being placed on the surface. The decreasing trend for the water contact angles was due to wetting of the many polar groups on the surface of GO.

Water contact angle measurements for GO and treated GO as a function of weight fraction of the coupling agents are shown in Figure 5.4. The water contact angle of treated DTMS samples increased with grafted amounts until the highest contact angle of 134 ± 2º was observed (Figure 5.4A). Samples treated with FDTS show superhydrophobic behavior (Figure 5.4B), with water contact angles exceeding 150º.

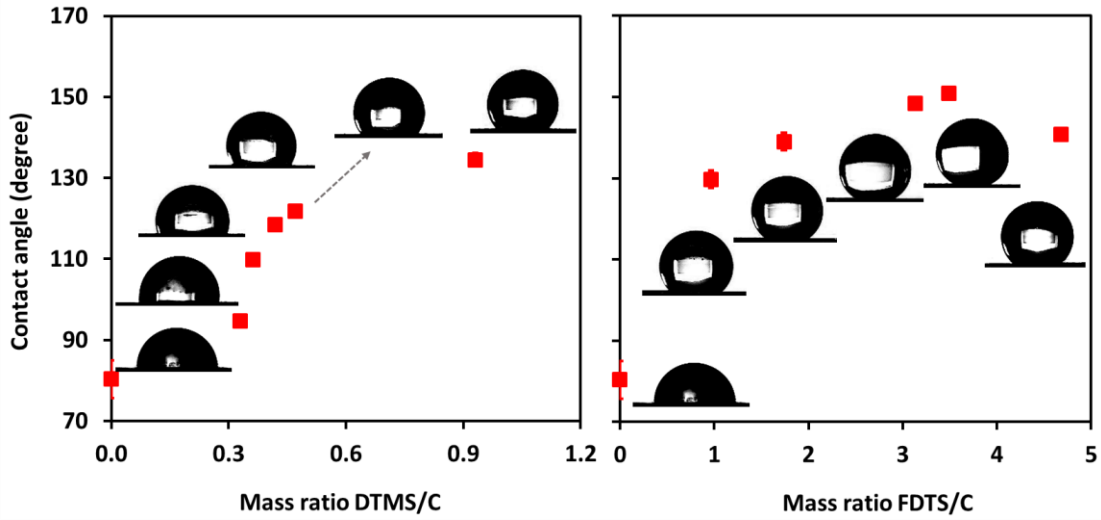

Figure 5.4. Water contact angles for treated GO samples as a function of mass ratio of coupling agents to carbon atoms of the surface for A) DTMS and B) FDTS. DTMS/GO samples only showed hydrophobic behavior and FDTS/GO samples showed superhydrophobicity.

Calculating the ratio of silane groups to the mass of skeleton carbon of the GO is not simple. The coupling agent can be chemically bonded or grafted to the surface, or

indirectly grafted to the surface via condensation to silane chains that are already present.[58] The TGA derived mass ratio of silane chains to skeleton carbons of GO depends on the number (1, 2, or 3) of grafted sites, which is actually unknown from these experiments. For all comparisons between experimental and simulation results, we assumed 2 grafting sites for each functional group as it is an average/intermediate value. The effect of variations in the number of functionalities is larger for DTMS due to smaller molecular mass of these chains compared to the molecular mass of FDTS (Figure 5.5).

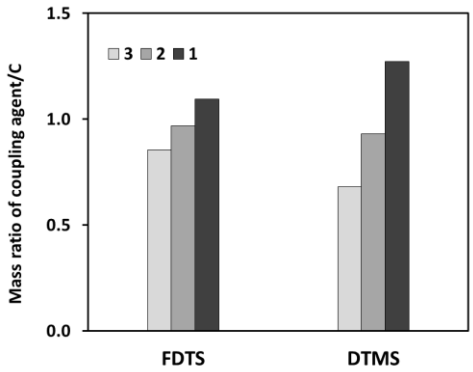

Figure 5.5. Ratio of mass of the silane chains to the mass of the carbons of GO for different numbers of linkages connecting an FDTS or DTMS molecule to the surface. The effect of variations in the number of linkages on the mass ratio for FDTS is small compared to DTMS due to fluorine having a greater molecular mass than hydrogen.

5.4.3. Interaction parameters for GO atoms were determined from MD derived contact angles

The droplet radius profile as a function of *z*, distance from the surface, was obtained by averaging 10,000 configurations of each simulation. The simulation box was divided into small bins (1 Å) along the *z*-axis and the number of water molecules in each bin was

counted. The radius of each slab then was calculated using the density of bulk water. Figure 5.6 shows an MD simulation snapshot of a droplet and the radius profile as a function of the distance from the GO surface. The contact angle was determined by the tangent of the line at the triple phase contact point on the surface of GO (z = 0.17 nm, where z = 0 is the average center of GO carbon atoms).

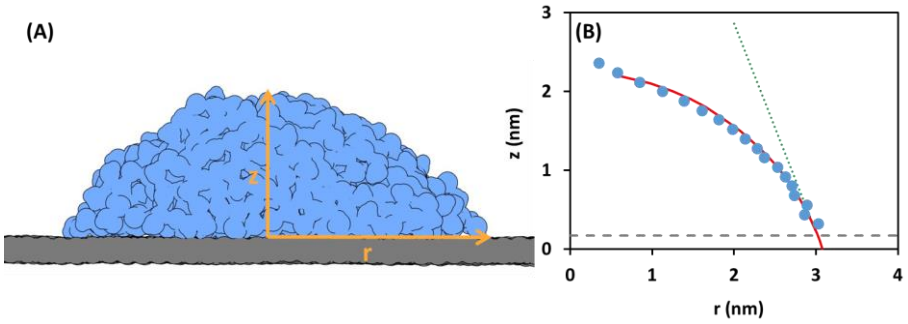

Figure 5.6. A) A representative MD simulation snapshot of a water droplet on a GO surface and B) droplet radius profile based on the distance from the GO surface. The dotted line is the tangent line at the GO surface to the best-fit curve for droplet radius as a function of distance.

The GO model in these molecular simulations used a Lennard-Jones size parameter (σ_{CC}) of 3.550 Å, following standard aromatic carbon parameters of the OPLS-AA force field. In order to optimize the GO surface model to best reproduce contact angles for experimental comparisons, a series of simulations was carried out to determine the optimal dispersion attraction parameter (ε_{CC}) for these GO carbon atoms.[59] In these simulations, ε was varied systematically between 2.2 and 4.0 kJ/mol, and the microscopic contact angle was measured. Simulations of different droplet sizes were performed for each given ε value in order to project to the macroscopic contact angle, i.e. droplets with

infinite radius. The contact angle estimated in the simulation is for a very small droplet, but can be projected to macroscopic contact angle. The macroscopic and microscopic contact angles (θ_∞ and θ respectively) are related to each other through the modified Young's equation:

$$\gamma_{SV} = \gamma_{SL} + \gamma_{LV}\cos\theta + \frac{\tau}{r_B} \tag{5.1}$$

Here, γ is the surface tension at the solid-vapor (*SV*), solid-liquid (*SL*), or liquid-vapor (*LV*) contact area radius.[59] The Young's equation for macroscopic droplet size is recovered as the contact area radius increases to infinity. The relation between microscopic and macroscopic contact angles can be written as:

$$\cos\theta = \cos\theta_\infty - \frac{\tau}{\gamma_{LV}}\frac{1}{r_B} \tag{5.2}$$

Figure 5.7 shows the projected macroscopic water contact angle on GO as a function of ε. Here, the experimentally measured contact angle for GO (~80°) corresponds to an ε_{CC} = 0.36 kJ/mol, and this value was used for all GO MD simulations.

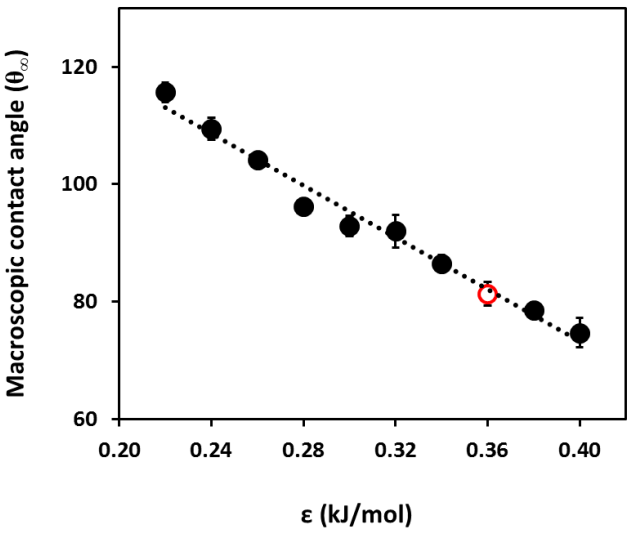

Figure 5.7. Macroscopic contact angle of SPC/E water on a model GO surface as a function of ε_{CC}. The filled red point (ε_{CC} = 0.36 kJ/mol) corresponds to the experimentally observed contact angle for water on GO, and this value was used for modeling GO in all further molecular simulations.

5.4.4. MD derived contact angles for treated GO surfaces agree well with experimental contact angles

As the surface parameter optimization process shows, the calculated contact angle from molecular simulations was highly dependent upon the parameters used for representing non-bonded interactions between water and the GO surfaces. For functionalized GO surfaces, we use the OPLS-AA force field for the initial depiction of the molecular models. However, we had concerns about the experimental utility of these parameters because of inaccuracies in their ability to reproduce the relative hydration of small molecule analogs of alkane and fluoroalkane functional groups. For example, the difference in hydration free energy ($\Delta\Delta G_{hyd}$) of methane and tetrafluoromethane is significantly less than that observed from experimentally determined Henry's Law Coefficients. A small $\Delta\Delta G_{hyd}$ between alkane and fluoroalkane solutes will likely translate to similar water droplet contact angles on both alkane and fluoroalkane functionalized surfaces. To address this potential discrepancy, we also optimize the fluorine Lennard-Jones parameters of the OPLS-AA force field to reproduce the $\Delta\Delta G_{hyd}$ between methane and tetrafluoromethane (see **Supporting Information** for finalized parameters). These optimized OPLS parameters were used in simulation predictions of water droplet contact angle as a function of fluoroalkane chain length.

Similar to the clean GO surfaces, the water contact angle of treated GO surfaces was determined from the line tangent to the triple phase point on the surface. Because of the mobility of functional group chains attached to the GO surface, identification of this triple phase point is more challenging. To determine this contact point, the average number density distribution functions in the *z*-direction were created for both water molecules and coupling agents as a function of distance from the surface carbons. The *xy* cross-section averaged number density of oxygen atoms of water and fluorine (or hydrogen) atoms of coupling agents was measured for partition bins of 0.02 Å in the *z*-direction. The crossing point of these averaged density profiles in the *z*-direction was used as the contact point of the droplet of water and the substrate. Figure 5.8 shows a simulation snapshot alongside the distribution profile (normalized number density) for fluorine atoms of the FDTS and the oxygen atoms of water molecules as a function of distance from the surface carbon atoms of GO. The crossing point of these distributions is 1.4 nm in this particular example, and it will be dependent upon the length, coverage, and chemical makeup of the functional groups attached to the GO surface.

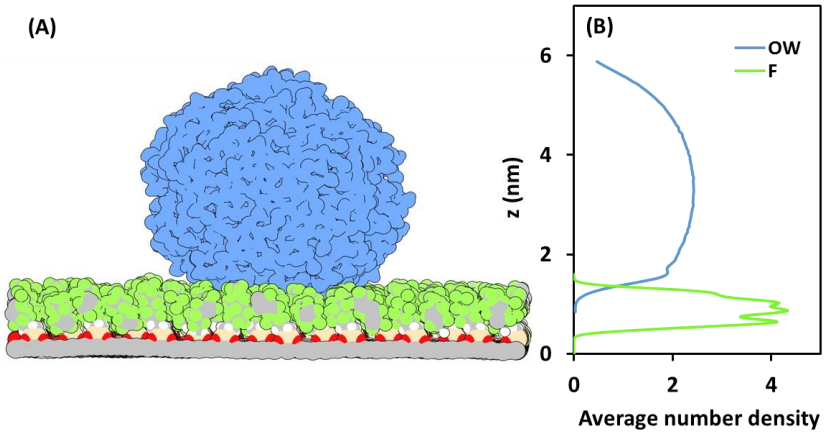

Figure 5.8. A) MD simulations snapshot of a water droplet on GO/FDTS surface and B) average number density of fluorine atoms of FDTS and oxygen atoms of water as a

function of distance from the GO surface carbon atoms. In this case, these distributions cross at 1.4 nm, and this would be taken as the triple phase point for determining the water droplet contact angle.

The method for determining macroscopic water droplet contact angles from these microscopic simulations was the same for both bare and functionalized GO. Figure 5.9 shows the macroscopic contact angles (both experimental measurements and MD simulations) as a function of the amount of coupling agents. In general, the contact angle increases with increasing the grafted amount of coupling agents. This trend was similar for both experiment and simulations, and we observed good agreement between both of these techniques. Figure 5.10 shows the results of standard OPLS and modified fluorine parameter simulations of FDTS treated GO surfaces as a function of increasing coverage of functionalizing groups. The fluorine parameter optimization worked to increase the $\Delta\Delta G_{hyd}$ between tetrafluoromethane and methane, making tetrafluoromethane more hydrophobic. This increase in hydrophobicity with these new fluorine parameters results in larger macroscopic water contact angles from the MD simulations.

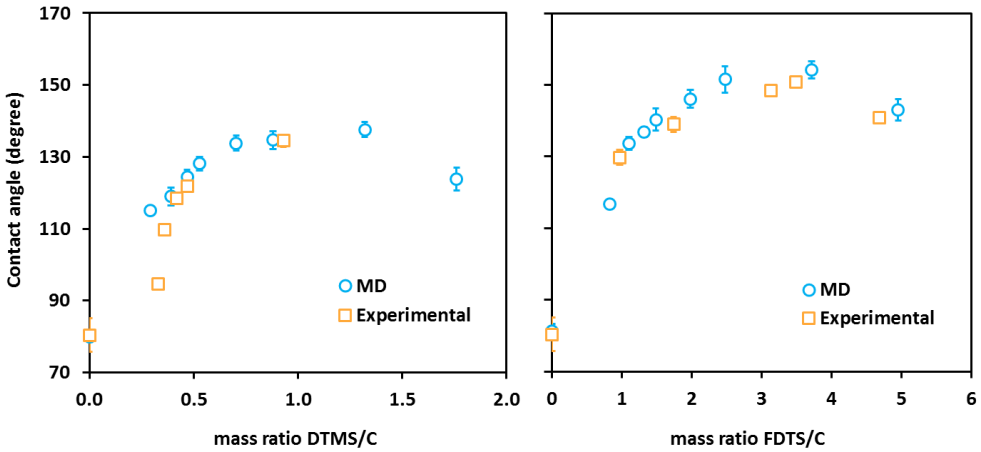

Figure 5.9: Variation of MD simulation and experimental water contact angles with increasing mass ratio of coupling agents to GO carbons for functionalized samples with (A) DTMS and (B) FDTS. The trend in macroscopic water contact angles was similar for both MD and experiment, often overlapping within error.

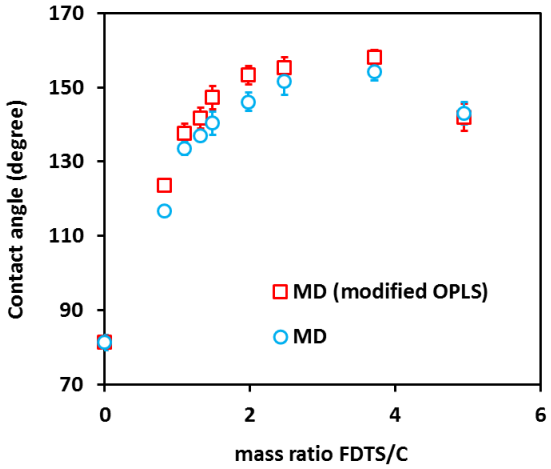

Figure 5.10: Standard OPLS and modified fluorine parameter MD simulation macroscopic contact angles with increasing mass ratio of coupling agents to GO carbons for functionalized samples FDTS. As expected, the modified fluorine parameter simulations show larger contact angles than unmodified simulations, this because the optimization worked to increase the $\Delta\Delta G_{hyd}$ between alkane and fluoroalkane functional groups.

Hydrophobicity of functionalized GO samples with different chain lengths (C_4, C_8, and C_{10}) and coverage is shown in Figure 5.11. While samples with C_8 and C_{10} functional groups showed similar trends at all chain densities, samples with C_4 showed different behavior as a function of increasing coverage. At very large functional group densities, the macroscopic contact angles of C_4 samples were only slightly smaller than

those in C_8 samples. At lower densities, the water contact angles of C_4 samples were significantly smaller than those of C_8 samples.

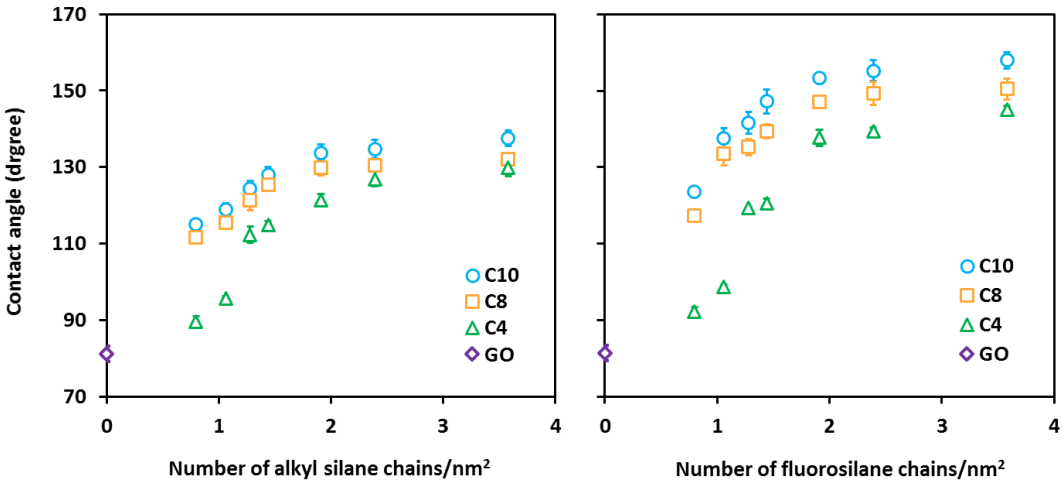

Figure 5.11: Variation of MD simulation macroscopic contact angles as a function of the amounts of coupling agents with different chain lengths for (A) fluorinated alkyl-chain and (B) alkyl-chain treated samples. For low coverage densities, the C_4 samples show contact angles only marginally greater than bare GO surfaces, indicating significant water contact with un-functionalized GO surface atoms.

5.5. DISCUSSION

5.5.1. Functionalized GO shows both hydrophobic and superhydrophobic behavior

Surface morphology, chemical composition, and surface free energy are the factors that affect surface wettability. GO is a hydrophilic surface due to the presence of many polar functional groups such as hydroxyl, carboxyl and epoxy groups. The number and density of hydrogen bonding sites, as well as density of surface defects, can affect the amount of water adhered and consequently the wettability of the surface. Measuring the water contact angle on GO is challenging because the high wettability leads to a continual

reduction of the contact angle over time (Figure 5.3). In our studies, we used the contact angle of water droplets 2 min after surface placement (~80˚). This is higher than the previously reported value of 67.4˚.[8] This difference is likely due to either a lower density of polar groups on our GO surfaces, or different measurement conditions such as smaller droplet sizes and/or faster imaging times. In order to achieve a macroscopic contact angle of 80˚ for molecular simulations of GO, the surface carbon dispersion attractiveness needed to be increased by roughly 0.07 kJ/mol over the standard OPLS aromatic carbon parameters.

Modification of GO can change the hydrophilic nature of the surface. In general, the removal of the epoxide, hydroxyl, carbonyl, and carboxylic acid functional groups from the surface increase the contact angle of GO.[60] To further enhance the hydrophobicity of the structure, low surface energy coatings can be applied. Based on the Young's equation, since the surface tension of the water droplet is constant, the only parameter which influences the wettability is the surface energy of the solid surface (γ_{SL}). Higher possible contact angles are accessible by minimizing the γ_{SL}. For example, applying silane treatments to graphene aerogels was observed by others to form superhydrophobic surfaces with contact angles as high as 160˚.[14]

The experimental mechanism for the hydrophobicity of DTMS and FDTS treated GO suggests that with applying the coupling agent solution onto the GO surface, Si-OCH_3 bonds in DTMS or FDTS react with hydroxyl groups in GO to graft the DTMS or FDTS to the surface. The alkyl or fluoroalkyl chains form a hydrophobic interface, reducing the surface energy of the hydrophilic bare GO surface.[61] Nanometer-scale roughness will also affect the hydrophobicity of functionalized GO surfaces. Studies on functionalized

carbon nanotubes (CNTs) have shown that a large amount of air trapped between the nanostructures; thus the hydrophobicity of the CNTs is dependent on both the packing of the nanostructures and the subsequent surface treatment.[61] Similar effects have been observed when depositing GO sheets on flat surfaces.[7] Many studies have investigated the wettability of graphene surfaces by focusing on the nanometer-scale and macro-scale roughness as a function of graphene and the substrate structure.[30,62-64] Recently, Bharathidasan et al. showed that the roughness due to the presence of a large density of fluorosilane chains decreases the adhesive force between water and the treated GO surface. The roughness on these surfaces might be enough to trap air inside voids on the surface, decreasing the wettability.[17]

A general enhancement in hydrophobicity of both DTMS and FDTS treated GO systems was observed in our studies as shown in Figure 5.4, and this enhancement increased with the mass fraction of coupling agents. Consistent with studies from other labs, we expect this enhancement is due to both decreasing the surface free energy and increasing the nanometer-scale roughness of the surfaces.[17] The contact angle observed for FDTS treated GO was expectedly larger than DTMS treated GO, this due to the lower surface energy of water interacting with C-F bonds relative to C-H bonds.[65] Here, the maximum water contact angles of $134 \pm 2^{\circ}$ and $151 \pm 2^{\circ}$ were measured for treated GO with DTMS and FDTS, respectively. These contact angles indicate that the decreased surface energy and the presence of nanometer-scale roughness were enough to achieve superhydrophobicity for samples treated with FDTS; however, micrometer-scale roughness would be necessary for samples treated with DTMS in order to show superhydrophobic behavior. For FDTS treated system at very high mass ratio of coupling

agent, the contact angle decreased. This is likely due to the increased density of functional groups reducing the surface roughness and porosities that trap air.[14]

This enhancement in hydrophobicity with increasing mass fraction of coupling agent behavior is supported by the analogous system molecular simulations. Figure 5.9 overlays the experimental and simulation macroscopic contact angles as a function of mass fraction of coupling agents, and the measured values often overlap within error. In the molecular simulations, we were able to observe the decrease in water contact angle near maximal packing density for FDTS as well as DTMS. While our experimental DTMS functionalized surfaces were not able to achieve the potential maximal packing densities seen in simulations and experimental FTDS systems, we would expect to observe a similar decrease in water contact angle at these very high coupling group densities. This observed decrease in water contact angle in the simulations is expectedly due to the decrease in nanoscale roughness that comes from tight packing of alkyl and fluoroalkyl chains at these high densities. Despite the generally good agreement between experiments and molecular simulations, there were some systematic differences between the trends. For example, the simulations appear to exhibit slightly more hydrophobic behavior than the experiments, with macroscopic contact angles slightly larger for similar mass ratios. This is likely due to the general uniformity of surface coverage in the simulations, essentially making them into a limiting value for potential coverage in experiments. Other factors that limited the quality of comparisons between experiment and simulations are the uncertainty in the average number of covalent contacts between coupling groups and the GO surfaces in the experiments, differences in the treatment of residual hydrophilic groups after experimental surface functionalization, and uncertainty

in the quality of the OPLS-AA force field for accurate modeling of bare and functionalized GO systems.

As a test of the force field's ability in modeling functionalized GO, we showed the results for macroscopic water contact angles on standard FDTS coated samples alongside those seen with the modified fluorine LJ parameters in Figure 5.10. In the hydration free energy optimization process, the fluorine dispersion attractiveness needed to be decreased by 0.105 kJ/mol in order to match the $\Delta\Delta G_{hyd}$ between methane and tetrafluoromethane seen in experiment. This general decrease in attractiveness shows a corresponding 5˚ increase in the water contact angle for droplets on the fluoroalkyl treated GO surfaces. This increase in contact angle is expected because the modified parameters make fluorinated solutes more hydrophobic, and this translates to a more hydrophobic surface as a whole when such solutes are grafted to a surface.

Finally, we performed predictive simulations using this modified force field in order to provide limiting value estimations for the water contact angle on coupling group grafted surfaces as a function of chain-length and coverage density. The samples with C_8 and C_{10} functional group chains show similar water contact angles, i.e. surfaces grafted with the longer C_{10} chains typically show an increase in the macroscopic contact angle of under 5˚. The differences seen between C_4 and C_8 chains were noticeably larger, particularly at lower coverage densities. This indicated that the silane chains impact the hydrophobicity of the surface by not only reducing the number of polar groups on the surface, but also by shielding local patches of the GO surface from direct interaction with water molecules. When the surface coverage is low, the longer chains are able to occlude a greater region of GO surface near the covalent attachment than the shorter chains. This effect is less

important with increasing the grafted amount because neighboring GO sites are already shielded by covalent attachment of other functional groups, explaining why we see only very minor differences in contact angle at high coverages regardless of functional group chain-length. The convergence of water contact angles regardless of chain-length in treated surfaces as a function of increasing surface coverage has been observed in other experimental studies.[66-68] For example, a sharp increase in the water contact angle of modified alumina membranes with alkyl silane chains was observed from C_2 to C_6 and then did not change much with increasing the chain length to C_8 and C_{16}.[68] In general, we would expect to see a roughly 20˚ increase in water contact angle using fluoroalkyl silane chains over similar length alkyl silane chains.

5.6. CONCLUSIONS

Graphene oxide is a hydrophilic material that provides a unique platform for evaluating the variables that affect surface interactions and wettability. Here, the water repellency of GO surfaces treated with FDTS and DTMS was evaluated using contact angle measurements in experiments and analogous molecular simulations. As the mass ratio of functional groups added increased, the GO surfaces were converted from hydrophilic to hydrophobic in nature. By using functionalizing groups with fluoroalkyl chains, the water repellency could be pushed further to achieve superhydrophobic behavior. Molecular simulations of analogous systems showed behavior consistent with experiments, and through them the extremes of surface treatment were explored. We observed that extremely high coverage leads to a decay in wettability, this through a loss in nanometer scale surface roughness. We also showed that the water repellency could be tuned by matching small molecule hydration behavior and by selecting functionalizing

group chain lengths and coverage densities. The choice of treatment group for surface functionalization indicates that one can make GO into a moderately hydrophobic surface with only small amounts of longer chain (C_8 or higher) alkyl or fluoralkyl silanes. Water repellency can be increased with increased density of silanes regardless of chain length, though only until the density is great enough that nanometer scale roughness is smoothed out.

5.7. ACKNOWLEDGEMENTS

The computing for this project was performed at the OSU High Performance Computing Center at Oklahoma State University supported in part through the National Science Foundation grant OCI–1126330.

5.8. REFERENCES

(1) Li, X.-M.; Reinhoudt, D.; Crego-Calama, M. *Chem. Soc. Rev.* **2007**, *36*, 1350.

(2) Miwa, M.; Nakajima, A.; Fujishima, A.; Hashimoto, K.; Watanabe, T. *Langmuir* **2000**, *16*, 5754.

(3) Gao, L.; McCarthy, T. J. *Langmuir* **2006**, *22*, 2966.

(4) Akram Raza, M.; Kooij, E. S.; van Silfhout, A.; Poelsema, B. *Langmuir* **2010**, *26*, 12962.

(5) Song, X.; Zhai, J.; Wang, Y.; Jiang, L. *J. Phys. Chem. B* **2005**, *109*, 4048.

(6) Oliveira, N. M.; Reis, R. L.; Mano, J. o. F. *ACS Appl. Mater. Interfaces* **2013**, *5*, 4202.

(7) Rafiee, J.; Rafiee, M. A.; Yu, Z. Z.; Koratkar, N. *Adv. Mater.* **2010**, *22*, 2151.

(8) Wang, S.; Zhang, Y.; Abidi, N.; Cabrales, L. *Langmuir* **2009**, *25*, 11078.

(9) Shin, Y. J.; Wang, Y.; Huang, H.; Kalon, G.; Wee, A. T. S.; Shen, Z.; Bhatia, C. S.; Yang, H. *Langmuir* **2010**, *26*, 3798.

(10) Taherian, F.; Marcon, V.; van der Vegt, N. F.; Leroy, F. *Langmuir* **2013**, *29*, 1457.

(11) Zhang, L.; Yu, J.; Yang, M.; Xie, Q.; Peng, H.; Liu, Z. *Nat. Commun.* **2013**, *4*, 1443.

(12) Lee, J.-S.; Yoon, J.-C.; Jang, J.-H. *J. Mater. Chem. A* **2013**, *1*, 7312.

(13) Stoller, M. D.; Park, S.; Zhu, Y.; An, J.; Ruoff, R. S. *Nano Lett.* **2008**, *8*, 3498.

(14) Lin, Y.; Ehlert, G. J.; Bukowsky, C.; Sodano, H. A. *ACS Appl. Mater. Interfaces* **2011**, *3*, 2200.

(15) Lerf, A.; He, H.; Forster, M.; Klinowski, J. *J. Phys. Chem. B* **1998**, *102*, 4477.

(16) Yang, X.; Wang, X.; Yang, J.; Li, J.; Wan, L. *Chem. Phys. Lett.* **2013**, *570*, 125.

(17) Bharathidasan, T.; Narayanan, T. N.; Sathyanaryanan, S.; Sreejakumari, S. *Carbon* **2015**, *84*, 207.

(18) Lin, Z.; Liu, Y.; Wong, C.-p. *Langmuir* **2010**, *26*, 16110.

(19) Shanmugharaj, A.; Yoon, J.; Yang, W.; Ryu, S. H. *J. Colloid Interface Sci* **2013**, *401*, 148.

(20) Lee, W.-J.; Ju, S.-P. *J. Phys. Chem. B* **2009**, *113*, 13269.

(21) Scocchi, G.; Sergi, D.; D'Angelo, C.; Ortona, A. *Phys. Rev. E* **2011**, *84*, 061602.

(22) Walther, J. H.; Werder, T.; Jaffe, R.; Gonnet, P.; Bergdorf, M.; Zimmerli, U.; Koumoutsakos, P. *Phys. Chem. Chem. Phys.* **2004**, *6*, 1988.

(23) Tummala, N. R.; Striolo, A. *J. Phys. Chem. B* **2008**, *112*, 1987.

(24) Wang, F.-C.; Zhao, Y.-P. *Colloid. Polym. Sci.* **2013**, *291*, 307.

(25) Yiapanis, G.; Maclaughlin, S.; Evans, E. J.; Yarovsky, I. *Langmuir* **2014**, *30*, 10617.

(26) Rafiee, J.; Mi, X.; Gullapalli, H.; Thomas, A. V.; Yavari, F.; Shi, Y.; Ajayan, P. M.; Koratkar, N. A. *Nat. Mater.* **2012**, *11*, 217.

(27) Shih, C.-J.; Wang, Q. H.; Lin, S.; Park, K.-C.; Jin, Z.; Strano, M. S.; Blankschtein, D. *Phys. Rev. Lett.* **2012**, *109*, 176101.

(28) Raj, R.; Maroo, S. C.; Wang, E. N. *Nano Lett.* **2013**, *13*, 1509.

(29) Ritchie, J. A.; Yazdi, J. S.; Bratko, D.; Luzar, A. *J. Phys. Chem. C* **2012**, *116*, 8634.

(30) Singh, E.; Thomas, A. V.; Mukherjee, R.; Mi, X.; Houshmand, F.; Peles, Y.; Shi, Y.; Koratkar, N. *ACS nano* **2013**, *7*, 3512.

(31) Wei, N.; Lv, C.; Xu, Z. *Langmuir* **2014**, *30*, 3572.

(32) Khan, S.; Singh, J. K. *Mol. Simul.* **2014**, *40*, 458.

(33) Giovambattista, N.; Debenedetti, P. G.; Rossky, P. J. *J. Phys. Chem. B* **2007**, *111*, 9581.

(34) Dalvi, V. H.; Rossky, P. J. *Proceedings of the National Academy of Sciences* **2010**, *107*, 13603.

(35) Layfield, J. P.; Troya, D. *J. Phys. Chem. B* **2011**, *115*, 4662.

(36) Park, S. H.; Carignano, M. A.; Nap, R. J.; Szleifer, I. *Soft Matter* **2010**, *6*, 1644.

(37) Vanzo, D.; Bratko, D.; Luzar, A. *J. Chem. Phys.* **2012**, *137*, 034707.

(38) Marcano, D. C.; Kosynkin, D. V.; Berlin, J. M.; Sinitskii, A.; Sun, Z.; Slesarev, A.; Alemany, L. B.; Lu, W.; Tour, J. M. *ACS nano* **2010**, *4*, 4806.

(39) Rotenberg, Y.; Boruvka, L.; Neumann, A. *J. Colloid Interface Sci* **1983**, *93*, 169.

(40) Williams, D. L.; Kuhn, A. T.; Amann, M. A.; Hausinger, M. B.; Konarik, M. M.; Nesselrode, E. I. *Galvanotechnik* **2010**, *101*, 2502.

(41) Stalder, A. F.; Melchior, T.; Müller, M.; Sage, D.; Blu, T.; Unser, M. *Colloids Surf., A* **2010**, *364*, 72.

(42) Jorgensen, W. L.; Tirado-Rives, J. *J. Am. Chem. Soc.* **1988**, *110*, 1657.

(43) Mark, P.; Nilsson, L. *J. Phys. Chem. A* **2001**, *105*, 9954.

(44) Berendsen, H.; Grigera, J.; Straatsma, T. *J. Phys. Chem.* **1987**, *91*, 6269.

(45) Van Der Spoel, D.; Lindahl, E.; Hess, B.; Groenhof, G.; Mark, A. E.; Berendsen, H. J. *J. Comput. Chem.* **2005**, *26*, 1701.

(46) Nosé, S. *Mol. Phys.* **1984**, *52*, 255.

(47) Hoover, W. G. *Phys. Rev. A* **1985**, *31*, 1695.

(48) Essmann, U.; Perera, L.; Berkowitz, M. L.; Darden, T.; Lee, H.; Pedersen, L. G. *J. Chem. Phys.* **1995**, *103*, 8577.

(49) Hine, J.; Mookerjee, P. K. *J. Org. Chem.* **1975**, *40*, 292.

(50) Shirts, M. R.; Pitera, J. W.; Swope, W. C.; Pande, V. S. *J. Chem. Phys.* **2003**, *119*, 5740.

(51) Steinbrecher, T.; Mobley, D. L.; Case, D. A. *J. Chem. Phys.* **2007**, *127*, 214108.

(52) Li, M.; Huang, X.; Wu, C.; Xu, H.; Jiang, P.; Tanaka, T. *J. Mater. Chem.* **2012**, *22*, 23477.

(53) Hassan, H. M.; Abdelsayed, V.; Abd El Rahman, S. K.; AbouZeid, K. M.; Terner, J.; El-Shall, M. S.; Al-Resayes, S. I.; El-Azhary, A. A. *J. Mater. Chem.* **2009**, *19*, 3832.

(54) Stankovich, S.; Dikin, D. A.; Piner, R. D.; Kohlhaas, K. A.; Kleinhammes, A.; Jia, Y.; Wu, Y.; Nguyen, S. T.; Ruoff, R. S. *Carbon* **2007**, *45*, 1558.

(55) Wang, G.; Yang, Z.; Li, X.; Li, C. *Carbon* **2005**, *43*, 2564.

(56) Liu, P.; Gong, K.; Xiao, P.; Xiao, M. *J. Mater. Chem.* **2000**, *10*, 933.

(57) Du, F.-P.; Wang, J.-J.; Tang, C.-Y.; Tsui, C.-P.; Zhou, X.-P.; Xie, X.-L.; Liao, Y.-G. *Nanotechnology* **2012**, *23*, 475704.

(58) García, N.; Benito, E.; Guzmán, J.; Tiemblo, P. *J. Am. Chem. Soc.* **2007**, *129*, 5052.

(59) Werder, T.; Walther, J. H.; Jaffe, R.; Halicioglu, T.; Koumoutsakos, P. *J. Phys. Chem. B* **2003**, *107*, 1345.

(60) Lin, Z.; Yao, Y.; Li, Z.; Liu, Y.; Li, Z.; Wong, C.-P. *J. Phys. Chem. C* **2010**, *114*, 14819.

(61) Bu, I. Y.; Oei, S. P. *Appl. Surf. Sci.* **2010**, *256*, 6699.

(62) Meyer, J. C.; Geim, A. K.; Katsnelson, M.; Novoselov, K.; Booth, T.; Roth, S. *Nature* **2007**, *446*, 60.

(63) Pourzand, H.; Pai, P.; Tabib-Azar, M. In *Sensors, 2013 IEEE*; IEEE: 2013, p 1.

(64) Li, T.; Zhang, Z. *J. Phys. D: Appl. Phys.* **2010**, *43*, 075303.

(65) Claesson, P. M.; Christenson, H. K. *J. Phys. Chem.* **1988**, *92*, 1650.

(66) Horr, T. J.; Ralston, J.; Smart, R. S. C. *Colloids Surf., A* **1995**, *97*, 183.

(67) Wasserman, S. R.; Tao, Y. T.; Whitesides, G. M. *Langmuir* **1989**, *5*, 1074.

(68) Gao, N.; Ke, W.; Fan, Y.; Xu, N. *Appl. Surf. Sci.* **2013**, *283*, 863.

5.9. SUPORTING INFORMATION

S5.1. OPLS force field

The OPLS force field parameters of the graphene oxide, fluorinated and alkyl silane chains are shown in Table S5.1. The determined parameters for aromatic carbons of graphene oxide were 3.55 Å and 0.360 kJ mol-1. These parameters for fluorine atom were determined to be 2.94 Å and 0.150 kJ mol-1.

Table S5.1. OPLS-AA force-field parameters for PVAc molecules and silanol groups of the silica surface.

Atom name	Atom type	Atom charge
CA	new_C	0.00
CT	opls_516	0.06
OS	OS	-0.40
Si	SI	0.60
CH_2	opls_516	-0.44
CH_3	opls_516	-0.66
H	opls_140	0.22
CF_2	opls_516	-0.41
CF_3	opls_516	-0.62
F	opls_164	-0.21
F (modified)	new_F	-0.21

The SPC/E model (Mark, P.; Nilsson, L. *J. Phys. Chem. A* **2001**, *105*, 9954 & Berendsen, H.; Grigera, J.; Straatsma, T. *J. Phys. Chem.* **1987**, *91*, 6269) of water-water interactions were used. This model consists of coulombic interactions between partial charges on O (-0.8476) and H (+0.4238) atoms, and an O-O Lennard Jones interaction with

$\varepsilon_{O\text{-}O}$ = 0.6502 kJ mol^{-1} and $\sigma_{O\text{-}O}$ = 3.166 Å. Harmonic bond and angle constraints are used to keep the O-H distance close to 1 Å and the H-O-H angle close to 109.47º (Rafiee, J.; Mi, X.; Gullapalli, H.; Thomas, A. V.; Yavari, F.; Shi, Y.; Ajayan, P. M.; Koratkar, N. A. *Nat. Mater.* **2012**, *11*, 217).

S5.2. Thermal characterizations

Thermal decomposition thermograms for alkyl-silane and fluorosilane treated GO samples are shown in Figure S5.1.

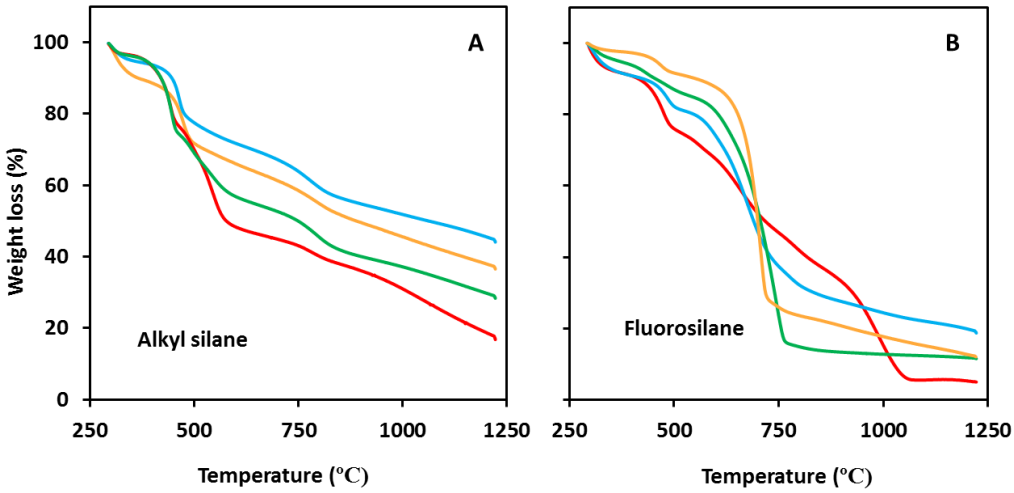

Figure S5.1. TGA thermograms of alkyl-silane and fluorosilane grafted GO.

S5.3. MD simulations, contact angle mesurements

An example of projection to macroscopic contact angle is shown is Figure S5.2. Molecular dynamics simulation snapshots of water droplets with different sizes on GO surface are shown in Figure S5.3.

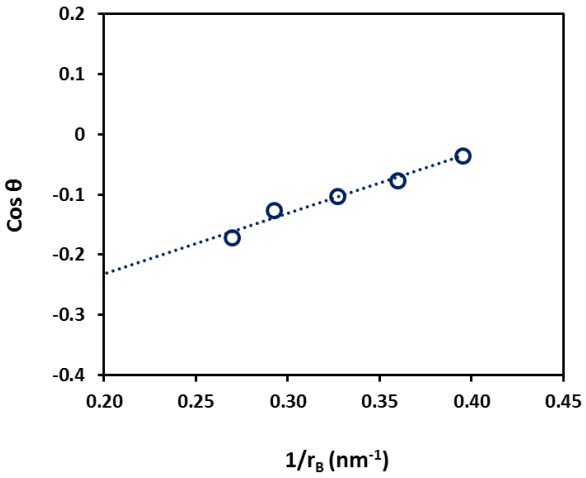

Figure S5.2. Results of cosθ as a function of the inverse of contact area radius for different sizes of water droplet with the same ε value ε_{CC} = 0.22 kJ mol^{-1}.

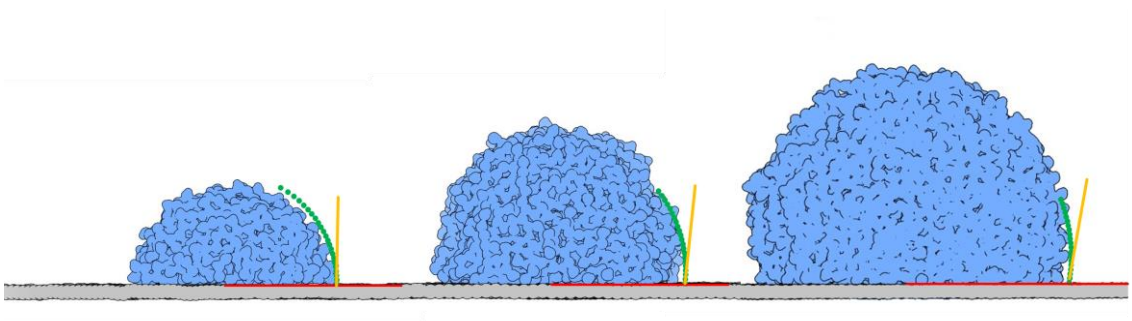

Figure S5.3. Representative MD simulation snapshots of a water droplets with different sizes on a GO surface.

CHAPTER VI

SURFACE CHARACTERIZATION OF ADSORBED POLY(METHYL METHACRYLATE) (PMMA) ON SILICA

6.1. ABSTRACT

The surface characterization of adsorbed poly(methyl methacrylate) (PMMA) on silica was studied by nitrogen adsorption desorption isotherms, pore volume, pore size distributions, and BET surface area measurements. The presence and the amount of the polymer segments strongly associated with the surface (tightly-bound) were probed using temperature-modulated differential scanning calorimetry (TMDSC). Pore size distribution and pore volume development of adsorbed PMMA samples showed different behaviors below and above the "tightly-bound amount" of polymer. Bulk silica showed a disordered mesoporous structure with a wide distribution of micro and mesopores. Adsorbing small amounts of PMMA on fumed silica covered the micropores and increased the total pore volume and the ratio of mesopores relative to those of the bulk silica. Increased mesopores and pore volume with increasing the adsorbed polymer, below the tightly bound amount, was mainly due to the non-uniform distribution of polymer chains on the silica surface. With increasing the adsorbed amount beyond the

tightly-bound amount, the total pore volume decreased due to the smoothing effect of additional polymeric layer.

6.2. INTRODUCTION

Polymer composites in which the polymer is mixed with another material, usually a fiber or filler, have widespread applications in various fields. Among the various classes of polymer composites, studying polymers adsorbed on a surface such as silica is important due to the numerous applications of those systems.[1,2] Adsorbed polymer layers show different properties and structures depending upon their interaction with and distance from the silica surface.[3-6] Poly(methyl methacrylate) (PMMA) is an important polymer which shows strong intermolecular interactions with silica surfaces.[7-9] PMMA segments very close to the silica surface (tightly-bound) are strongly attached to the surface via hydrogen-bonding and are known as tightly-bound.[10,11] Polymer chains further from surface are known as loosely-bound polymer and have less interaction with the surface. Silica surface coverage and packing of the polymer chains can be different for tightly-bound and loosely-bound components. Investigating the specific surface area and porosity of adsorbed polymers can provide information about the morphology and the packing behavior of the adsorbed polymers on the surface.

Nitrogen adsorption is an important experimental method for characterizing the specific surface area, pore volume, and pore size distribution. A variety of pore sizes from micro- to meso- and even macropores can be determined using this method. Pores are classified into different categories based on the IUPAC classifications: micropores (size < 2 nm), mesopores (2 nm < size < 50 nm), and macropores (size > 50 nm).[12-14] Various theories and methods have been developed to characterize and interpret the

micro- and mesoporous materials using sorption isotherms. Methods like Horvath-Kawazoe[15] (HK) and theory developed by Stoeckli[16,17] are often used to study the microporosity of materials. Barrett, Joyner, and Halenda have developed the BJH method which is valid for pores larger than 2 nm.[18,19] A similar model proposed by Dollimore and Heal[20] (DH) was proposed to evaluate mesopores size distributions. Developing macroscopic approaches such as density functional theory (DFT) and grand canonical Monte Carlo simulations describe adsorption and porosity in the molecular level.[21-24] The nonlocal density functional theory (NLDFT) has often been applied to characterize the micro- and mesoporous materials[25-31] accurately.[21,32]

The principal objective of this investigation is to provide insight into the morphology and packing behavior of adsorbed polymers on high surface area fumed silica using adsorption and desorption of nitrogen. We primarily studied the pore size, pore volume, and the BET surface area of adsorbed polymers as a function of polymer layer thickness on the silica surface. We applied the DFT model to characterize the pore size distribution and pore volume and BJH and DH methods to evaluate the pore volume.

6.3. EXPERIMENTAL

Cab-O-Sil fumed silica (M5P) was used as provided by Cabot Corporation (Tuscola, IL). PMMA (30 kDa) was also used as received (Aldrich Chemical Co., Milwaukee, WI). Samples were prepared using various concentrations of polymer solutions in 10 mL toluene. Cab-O-Sil fumed silica (300 mg) was added to each polymer solution. The tubes containing mixtures of silica and the PMMA solutions were placed in a mechanical shaker for 48 h and then centrifuged at 6000 rpm for 15 min. After removing supernatant

liquid, the adsorbed polymers on silica were dried using air at a low flow rate. The silica samples were then dried in a vacuum oven for 72 h to remove any residual solvent.

A model Q50 thermogravimetric analysis (TGA) instrument (TA Instruments, New Castle, DE) was used to determine the adsorbed amounts of polymer on silica from the weight loss of the samples after heating. Samples were heated from room temperature to 700 °C at a heating rate of 20 °C/min. TMDSC analysis was carried out on the adsorbed samples using a model Q2000 DSC (TA Instruments, New Castle, DE). The sample pans were referenced against empty pans and the cell was purged with a 50 mL/min nitrogen stream. The PMMA samples were held at 25 °C for 1 min, heated to 200 °C at a rate of 3 °C/min with a modulation amplitude of ±1.0 °C, and a modulation period of 60 s. The samples were then held at 200 °C for 2 min, cooled to 25 °C at 3 °C/min with the same modulation situation. A second heating scan was done with the same conditions as the first heating scan. The second heating scan results were used to determine the tightly-bound amount in the samples.

BET surface area measurements and the pore structures were carried out by nitrogen adsorption using a NOVA 2200 instrument (Quantachrome, FL). Prior to nitrogen gas adsorption, the samples were outgassed under vacuum at 100 ºC for at least 2 h. The adsorbed gas volume at 77 K was calculated by measuring the pressure change that resulted from the adsorption of nitrogen gas. Nitrogen adsorption isotherms were measured over a relative pressure range from 0.005 to 0.990 (P/P_0). The BET surface area was determined using at least five relative pressures within the range of linearity of the physical adsorption theory ($0.05 < P/P\text{o} < 0.35$) by means of the standard Brunauer–Emmett–Teller (BET) equation (using a molecular cross-sectional area of 0.162 nm^2 for

N_2).[33] Pore volume distributions were measured by the BJH (Barrett-Joyner-Halenda)[19] method from the dinitrogen desorption isotherms. The pore size distributions were determined using the density functional theory (DFT) in the relative pressure range from 10^{-7} to 1.

6.4. RESULTS

6.4.1. Thermal analysis

The adsorbed amount of polymer on silica (mg of polymer/m^2 of silica) was determined using thermogravimetric analysis (TGA). The adsorbed amount was calculated by dividing the mass loss (PMMA content) by the surface area of the remaining mass of silica. Figure 6.1 A shows the weight loss (%) of bulk PMMA and one adsorbed sample (2.70 mg of PMMA/m^2 of silica). The temperature-modulated differential scanning calorimetry thermograms (TMDSC) for these samples in the temperature range around the glass transition temperature of PMMA are shown in Figure 6.1 B. The TMDSC thermograms were used to determine the tightly-bound amount of PMMA on silica similar to previously reported.[6,7] The TMDSC graphs showed two regions of thermal activity, the tightly-bound region with T_g significantly above that of bulk and the loosely-bound region with the a slightly elevated T_g compared to the T_g of bulk PMMA.

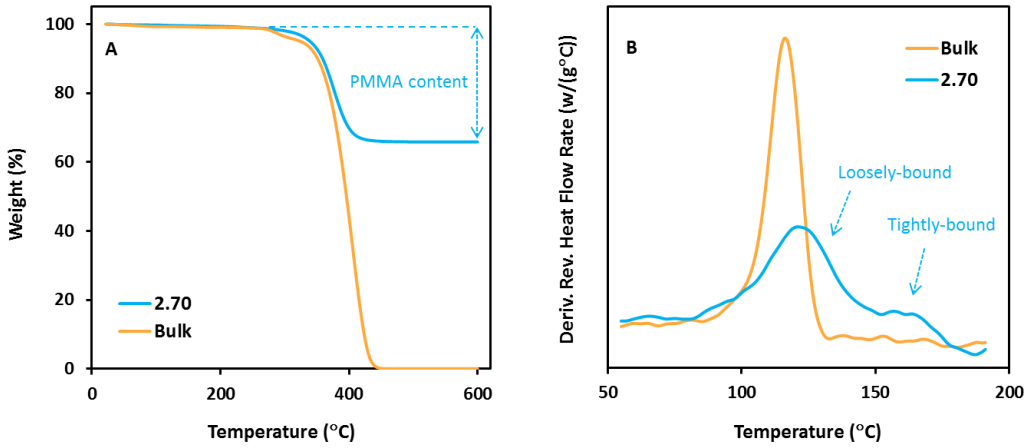

Figure 6.1. A) TGA thermograms and B) TMDSC thermograms of bulk and adsorbed PMMA (2.70 mg/m^2) on silica. TMDSC plots for adsorbed polymers showing two thermally active regions for tightly-bound and loosely-bound polymer.

6.4.2. Nitrogen adsorption/desorption isotherms, pore size distribution and pore volume characterization

Nitrogen adsorption/desorption isotherms of bulk silica and adsorbed samples of PMMA with low adsorbed amounts are shown in Figure 6.2. The isotherms for samples with other adsorbed amounts are shown in the **Supporting Information**. The amounts of nitrogen adsorbed on bulk silica and adsorbed samples were different. For small adsorbed amounts of polymer, the amount of adsorbed nitrogen increased with increased adsorbed amount of polymer. The adsorbed amount of nitrogen increased significantly close to saturation pressure due to the pore condensation into meso and macropores. All the samples showed hysteresis loops indicative of mesoporosity.

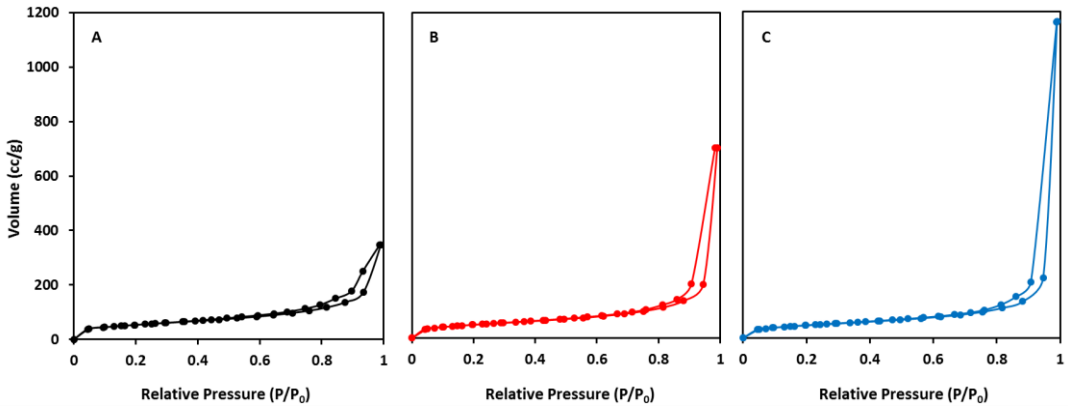

Figure 6.2. Nitrogen adsorption/desorption isotherms on A) silica, B) 0.31 mg/m^2 adsorbed PMMA on silica, and C) 0.46 mg/m^2 adsorbed PMMA on silica. The amount of adsorbed nitrogen increased with increased adsorbed amounts.

Non-local density functional theory was applied to characterize the pore size and pore volume distribution in both micro and mesopores.[34] Figure 6.3 shows the cumulative (Figure 6.3A) and incremental pore volume distributions (Figure 6.3D) of silica and adsorbed samples with small adsorbed amounts (0.31 and 0.46 mg/m^2) (Figure 6.3B and C) calculated from nitrogen adsorption isotherm applying NLDFT model. Most of the pores in silica were found in the range of micropores (Figure 6.3A and 6.3D). The sample with the smallest adsorbed amount (0.31 mg/m^2) showed a smaller population of micropores and larger population of mesoporous compared to silica. This sample showed a sharp rise in the cumulative pore volume for mesopores with a half width around 8 nm indicative of the formation of additional mesopores. Figure 6.3C and 6.3D show that the number of micropores for 0.31 mg/m^2 sample decreased to almost half of that for silica. With increasing the adsorbed amount of PMMA to 0.46 mg/m^2, no micropores were observed (Figures 6.3A and 6.3B).

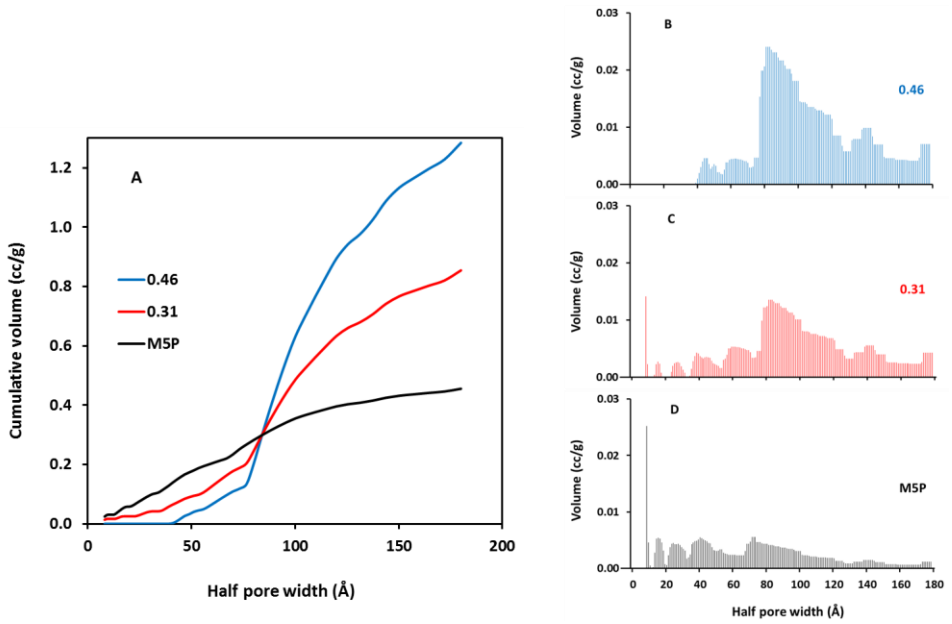

Figure 6.3. A) Cumulative pore volume distributions for bulk silica (M5P) and small adsorbed amounts of PMMA on silica calculated from nitrogen adsorption isotherms at 77 K using the NLDFT model. B and C) Incremental pore volume distribution for 0.46 and 0.31mg/m^2, respectively, and D) incremental pore volume distribution for silica. With increasing the adsorbed amounts, micropores intensity decreased and mesopores intensity increased.

Pore size distribution curves from nitrogen sorption of silica and adsorbed PMMA on silica using the NLDFT model are shown in Figure 6.4. Although the NLDFT pore size distribution showed micropores with pore width less than 2 nm and mesopores in the range of 2 to 20 nm for M5P silica, most of the adsorbed samples did not show micropores. Samples with small adsorbed amounts developed small mesopores. The intensity of the mesopores increased with increasing the adsorbed amount until the first layer of polymer covered the surface (up to 1.38 mg/m^2). With increasing adsorbed amount to 1.84 mg/m^2 (after the first layer of polymer covered the silica surface) the

intensity of small mesopores decreased dramatically and the intensity of medium mesopores increased. With increasing the adsorbed amounts (up to 2.70 mg/m^2), the number of medium mesopores decreased

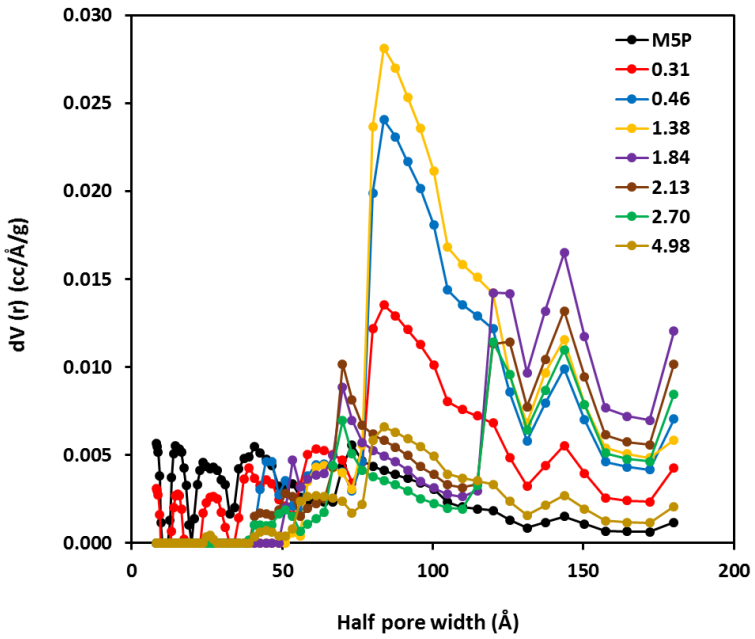

Figure 6.4. NLDFT pore size distribution curves from nitrogen sorption for silica and adsorbed PMMA on silica. The adsorbed amounts are expressed in mg PMMA/m^2 silica. With increasing the adsorbed amount, the micropores decreased and then were eliminated and then extra mesopores developed. Mesopore development showed different patterns below and above 1.38 mg/m^2.

The correlation between the adsorbed amounts of PMMA on silica and the pore volume determined using the BJH model is shown in Figure 6.5. With increasing the adsorbed amount up to 1.38 mg/m^2, the pore volume increased and then decreased.

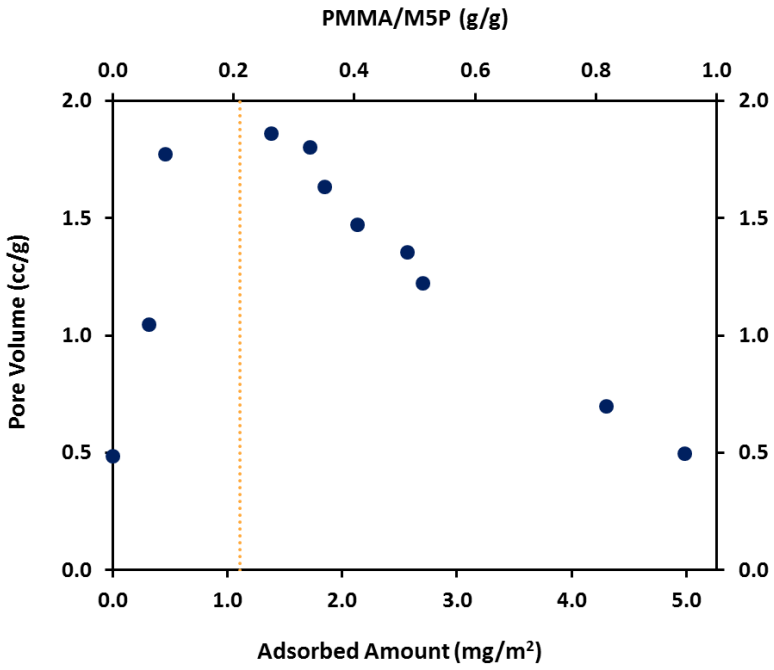

Figure 6.5. Pore volume of silica and adsorbed PMMA on silica as a function of adsorbed amount using the BJH method. The broken line represents the tightly-bound amount of PMMA on silica calculated from the TMDSC results. The total pore volume showed different behavior for adsorbed amounts below and above the tightly-bound amount.

BET surface area measurements with varied adsorbed amounts of the polymers are shown in Figure 6.6. A linear correlation between the adsorbed amounts of polymer and the BET surface areas was observed. The surface area for perfectly distributed PMMA on a spherical silica particles (the model shown with brown line) was calculated based on the surface area of the perfect sphere per total mass of silica and polymer. The curvature of the sphere model in the figure is due to the changing total mass due to the differences in densities between the silica and polymer.

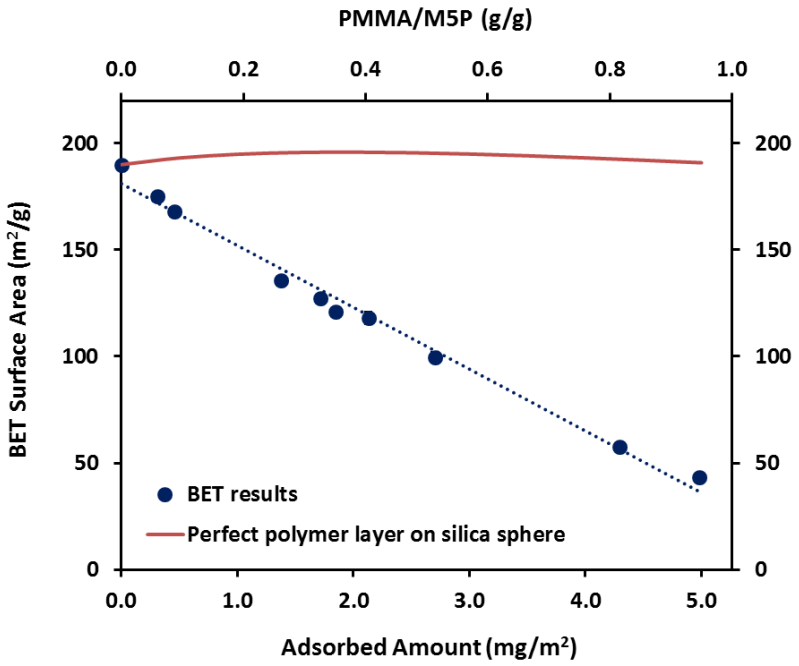

Figure 6.6. BET surface area measurements of silica and adsorbed PMMA on silica as a function of the adsorbed amount of polymer. A linear correlation between the BET surface area and the silica content is apparent. The error bars were generally smaller than the symbol sizes.

6.5. DISCUSSION

6.5.1. Thermal analysis

The TMDSC results were used to determine the nature of adsorbed PMMA on the silica surface. PMMA adsorbed on silica primarily showed two thermal activities associated with loosely- and tightly-bound regions (Figure 6.1B). The amount of PMMA which is tightly associated with the surface was found to be 1.1 ± 0.1 mg/m^2. Details on calculating the tightly-bound amount can be found elsewhere.[35] The tightly-bound amount represents the first portion of polymer bound to the surface via hydrogen bonding. At small adsorbed amounts, polymer chains were closely associated with the

surface, and with increased adsorbed amount, more of the surface became covered until tightly-bound amount was completed. After that the polymer chains for additional adsorbed polymer which were not directly bound to the surface and called loosely-bound polymer component. There was no loosely-bound component for the adsorbed samples with adsorbed amount less than tightly-bond amount, i.e., the entire polymer was tightly-bound to the surface in samples with adsorbed amounts less than the tightly-bound amount. When the amount of polymer was more than tightly-bound amount, the loosely-bound fraction of polymer increased while the amount tightly-bound component remained almost constant.

6.5.2. Adsorption/desorption isotherms and porosity analysis

Physical adsorption occurs with the contact of an adsorptive (gas) and an adsorbent (surface). The physical adsorption of many gases is caused by van-der Waals forces. The type and shape of adsorption isotherm is determined by the strength of adsorptive/adsorbent and adsorptive/adsorptive interactions and the thermodynamic stability of adsorptive held in the pores.[21] The standard adsorptive used in the determination of pore volume and pore size distribution is nitrogen at 77 K. The nitrogen adsorption-desorption isotherms (Figure 6.2) showed similar behavior for silica and adsorbed polymers. They all showed type IV isotherm according to the IUPAC classification.[36] The small sloped region in the middle of isotherms indicate the first few multilayers. The small slope indicates the presence of a wide distribution of pore sizes. The shape of this region remained unchanged up to around $P/P0 = 0.70$. The nitrogen sorption isotherms showed a sharp capillary condensation step in the relative pressure range of 0.70 to 0.99 P/P_0.

At small adsorbed amounts, smaller than tightly-bound amount, the maximum volume in nitrogen sorption isotherms increased with increased adsorbed amount. This indicated an increase in pore volume with increasing the adsorbed amount from 0 to 0.31 and 0.46 mg/m^2. After reaching a certain level of adsorbed amount (1.38 mg/m^2), the volume of adsorbed nitrogen decreased representative of a smaller total pore volume. The hysteresis loops showed almost the same width which suggested the same nature of mesopores. In other words, one might expect the same kind of porosities with different intensities for different adsorbed amounts.

Micropore filling which occurs in the pores with diameters close to the cross-section of the gas, occurred at very low relative pressures (less than 0.01 p/p_0) because of the high adsorption potential and narrow pore width. The filling of these narrow pores happens due to the adsorption forces between adsorbent and adsorptive.[18] Filling of the mesopores, pore sizes in the range of 2 to 50 nm occurs at higher relative pressure compare to the micropores. The filling of mesopores depends on both adsorbent/adsorptive and adsorptive/adsorptive attractive interactions. The sorption behavior in mesopores occurred with multilayer adsorption and pore condensation at pressure, P, less than the saturated pressure P_0 of the bulk liquid.

The ratio of the volume of pores to the volume of the solid material provides information about the porosity. Macroscopic models such as NLDFT are able to predict the porosity behavior qualitatively and quantitatively. The pore size is usually identified as the width of the internal slit-like pores or the diameter of the spherical and cylindrical pores. The change in the cumulative and incremental pore volume of silica and adsorbed polymers (0.31 and 0.46 mg/m^2) as a function of pore width determined with NLDFT

model is shown in Figure 6.3. Variation of the cumulative and incremental pore volume in terms of the adsorbed amount indicate that the addition of polymer segments to the silica surface fills or blocks the micropores present in the bulk silica surface and forms mesopores instead. Further, according to the Figure 6.3, 0.46 mg/m^2 polymer is sufficient to completely cover the micropores. The larger uptakes of nitrogen in the mesopores of this sample indicated the formation of extra mesopores with increasing adsorbed amounts from 0.31 to 0.46 mg/m^2. In other words, the packing nature of a small amount of adsorbed polymers on the silica is the way that they generate greater mesoporosity and they cover the micropores.

To have a better view of the packing of PMMA with higher adsorbed amounts, we studied the pore size distribution using the NLDFT. The pore size distribution measurements for silica and adsorbed polymers, shown in Figure 6.4, show a disordered mesoporous material with wide distribution including micro and mesopores. At very small amounts of PMMA (e.g., 0.31 mg/m^2), the amount of micropores decreased and the intensity of mesopores increased compared to those of the silica. All the micropores in the samples with larger adsorbed amount (0.46 m^2/g) were covered and the intensity of mesopores increased significantly. The increase of the very large amount of meso-porosity at low adsorbed amounts, might be due to the non-uniformity of polymer coverage at the silica surface. Absence of microporousity at higher adsorbed amount suggested that the polymer structure on the surface smoothed the surface of silica out and covered the slits and other sources of micropores. Further, according to the Figure 6.4, it seemed like the development of mesoporosity continued up to 1.38 mg/m^2 which is about the amount of the tightly bound polymer. Based on these results, it seemed as if the first

layer of polymer on the surface, developed small (below 120 Å) and medium (above 120 Å) mesopores with increasing the adsorbed amount. This indicated that polymer adsorbed on the surface in a non-uniform configuration creating new internal mesopores and also mesopores as a result of the structural shape of the polymer segment between each domain of polymer on the surface. Results showed that the addition of a second layer of polymer to the silica surface (above 1.38 mg/m^2) filled the internal pores and the small pores between the polymer domains on the surface. Hence, they provided a smoother surface with larger number of medium size pores made in between them. The decrease in the number of medium mesopores with further increased amount of the polymer (2.70 mg/m^2) on the surface indicated that additional polymer layers made the surface smoother. It seemed that a large adsorbed amount of PMMA (4.98 mg/m^2) changed the morphology of the surface similar to the bare silica except that there was no significant micropores observed. It might not be simple to differentiate between the porosity and roughness, especially for the larger adsorbed amount samples.[21] Therefore, the pore size distribution presented in Figure 6.4 might be due to wide surface irregularities representing the roughness of the surface or a deeper voids representing the porosity of the surface. A schematic of polymer packing on surface of fumed silica as a function of adsorbed amount is shown in Figure 6.7.

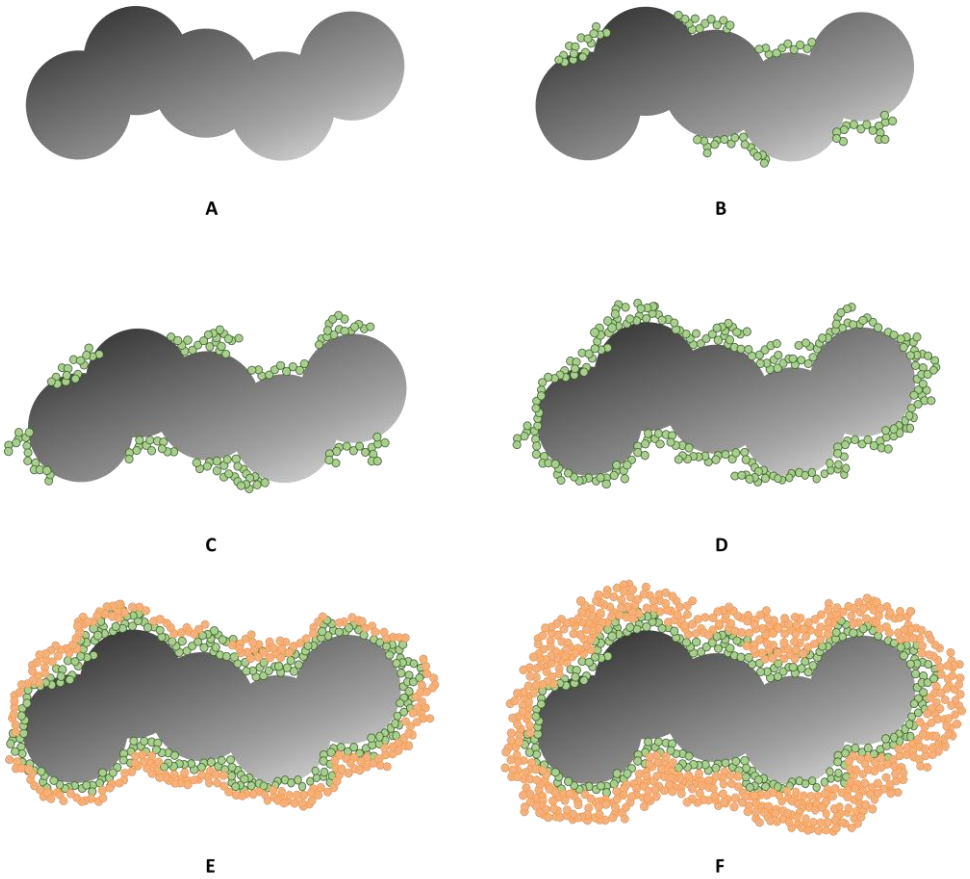

Figure 6.7. A Schematic representative of polymeric chains packing on the surface of fumed silica as a function of adsorbed amounts, A) bare silica, B) 0.31, C) 0.46, D) 1.38, E) 2.13, and F) 4.98 mg/m^2.

The pore volume analysis can be performed via methods such as BJH based on the macroscopic Kelvin equation which can describe the capillary condensation phenomena. The Kelvin equation provides a relationship between the relative pressure on nitrogen in the condensation step and the pore radius. BJH method is a widely used technique to characterize the pore volume and pore size distributions of mesoporous materials. The correlation between the pore volumes of samples and the silica contents is shown in Figure 6.5. Total pore volume results determined by BJH method was in agreement with

the pore size distribution data. As discussed earlier, samples with small adsorbed amounts generated some additional mesopores on the surface. The number of these pores increased with increased amount of polymer on the surface below the tightly-bound amount. Addition of loosely-bound polymer to the surface started to cover the pores as more polymers were added to the surface. As a result, the pore volume of the adsorbed polymers on silica increased up to a certain value and then decreased to almost the same level of bare silica at very large adsorbed amounts. In addition to the BJH method, DH and NLDFT methods were also used in the analysis of pore volumes. Table 6.1 summarizes the pore volume data obtained from different models (BJH, DH, and DFT) along with the BET surface area for the samples with the different adsorbed amounts. The pore volumes determined by all of the above models followed the same trend. They showed an increasing trend until the surface is covered by the first layer of polymer and then a decreasing trend. The DH results showed slightly smaller pore volume (up to 4 % smaller) compared to the pore volume determined by BJH method. The DFT method also showed the same trend as the other models, although the pore volume was found to be smaller than BJH and DH pore volume for all the samples.

Table 6.1. BET surface area (m^2/g) and pore volume (cc/g) obtained from BJH, DH, and DFT models and as a function of adsorbed amounts of PMMA on silica.

Adsorbed Amount (mg/m^2)	BET Surface area (m^2/g)	Pore Volume (cc/g)		
		BJH	DH	DFT
0.00	190.0 ± 1.9	0.49	0.48	0.46
0.31	175.3 ± 1.6	1.05	1.02	0.85
0.46	168.0 ± 1.4	1.77	1.72	1.28
1.38	135.9 ± 0.9	1.86	1.81	1.41

1.84	121.0 ± 0.9	1.64	1.60	1.00
2.13	118.1 ± 2.9	1.48	1.43	0.90
2.70	99.6 ± 2.7	1.22	1.19	0.71
4.98	43.2 ± 0.3	0.50	0.48	0.38

The most frequently applied technique to evaluate the specific surface area of nonporous and mesoporous materials is BET method. A linear correlation between the adsorbed amount of polymer and the BET specific surface area was observed as shown in Figure 6.6. This correlation was significantly different from the surface area of the perfect surface with a monodispersed spherical morphology. Although the pore volume and also the intensity of pore radius were larger for adsorbed samples, the specific surface area decreased with adsorbed amount. This difference is likely due to the increase in the size of the adsorbed samples with increasing the adsorbed amount, and also the fact that the silica surface is not exposed to the sorption anymore. Non-uniform dispersion of polymers on the surface of silica might also affect the specific surface area. These effects canceled each other out the way that provided a decreasing linear relationship between the specific surface area and the adsorbed amount of polymer.

6.6. CONCLUSIONS

Application of nitrogen sorption and methods based on statistical mechanics such as nonlocal density functional theory, we were able to characterize the structural morphology and packing nature of adsorbed polymers. The development of pore size distribution and pore volume of adsorbed polymers were different below and above the tightly bound-amount. At small adsorbed amounts, additional mesopores were generated suggesting the presence of a non-uniform coating of polymer on the silica. With

increasing the adsorbed amount, the pore volume increased until the first layer of polymer covered the silica surface and then decreased. The BET measurements showed a linear relationship between the specific surface area of adsorbed polymers and the adsorbed amounts.

6.7. ACKNOWLEDGEMENTS

The authors acknowledge the financial support of the National Science Foundation (USA) under Grant No. DMR-1005606 and the Oklahoma State University.

6.8. REFERENCES

(1) Metin, B.; Blum, F. D. *Langmuir* **2009**, *26*, 5226.

(2) Lin, Y.; Liu, L.; Xu, G.; Zhang, D.; Guan, A.; Wu, G. *J. Phys. Chem. C* **2015**, *119*, 12956.

(3) Krisanangkura, P.; Packard, A. M.; Burgher, J.; Blum, F. D. *J. Polym. Sci., Part B: Polym. Phys.* **2010**, *48*, 1911.

(4) Maddumaarachchi, M.; Blum, F. D. *J. Polym. Sci., Part B: Polym. Phys.* **2014**, *52*, 727.

(5) Shin, Y.; Lee, D.; Lee, K.; Ahn, K. H.; Kim, B. *J. Ind. Eng. Chem.* **2008**, *14*, 515.

(6) Mortazavian, H.; Fennell, C. J.; Blum, F. D. *Macromolecules* **2016**, *49*, 298.

(7) Blum, F. D.; Young, E. N.; Smith, G.; Sitton, O. C. *Langmuir* **2006**, *22*, 4741.

(8) Madathingal, R. R.; Wunder, S. L. *Thermochim. Acta* **2011**, *526*, 83.

(9) Zou, D. Q.; Yoshida, H. *J. Therm. Anal. Calorim.* **2010**, *99*, 21.

(10) Zhang, B.; Blum, F. D. *Macromolecules* **2003**, *36*, 8522.

(11) Kabomo, M. T.; Blum, F. D.; Kulkeratiyut, S.; Kulkeratiyut, S.; Krisanangkura, P. *J. Polym. Sci., Part B: Polym. Phys.* **2008**, *46*, 649.

(12) Kaneko, K. *J. Membr. Sci.* **1994**, *96*, 59.

(13) Lowell, S.; Shields, J. E.; Thomas, M. A.; Thommes, M. *Characterization of porous solids and powders: surface area, pore size and density*; Springer Science & Business Media, **2012**.

(14) Lastoskie, C.; Gubbins, K. E.; Quirke, N. *J. Phys. Chem.* **1993**, *97*, 4786.

(15) HORVÁTH, G.; KAWAZOE, K. *J. Chem. Eng. Jpn.* **1983**, *16*, 470.

(16) Stoeckli, H. *J. Colloid Interface Sci* **1977**, *59*, 184.

(17) Dubinin, M.; Stoeckli, H. *J. Colloid Interface Sci* **1980**, *75*, 34.

(18) Storck, S.; Bretinger, H.; Maier, W. F. *Appl. Catal., A* **1998**, *174*, 137.

(19) Barrett, E. P.; Joyner, L. G.; Halenda, P. P. *J. Am. Chem. Soc.* **1951**, *73*, 373.

(20) Dollimore, D.; Heal, G. *J. Appl. Chem.* **1964**, *14*, 109.

(21) Thommes, M. *Chem. Ing. Tech* **2010**, *82*, 1059.

(22) Evans, R.; Marconi, U. M. B.; Tarazona, P. *J. Chem. Soc., Faraday Trans. 2* **1986**, *82*, 1763.

(23) Olivier, J.; Conklin, W.; Szombathely, M. *Stud. Surf. Sci. Catal.* **1994**, *87*, 81.

(24) Neimark, A. V.; Vishnyakov, A. *Phys. Rev. E* **2000**, *62*, 4611.

(25) Seaton, N.; Walton, J. *Carbon* **1989**, *27*, 853.

(26) Ravikovitch, P. I.; Vishnyakov, A.; Russo, R.; Neimark, A. V. *Langmuir* **2000**, *16*, 2311.

(27) Neimark, A. V.; Ravikovitch, P. I.; Grün, M.; Schüth, F.; Unger, K. K. *J. Colloid Interface Sci* **1998**, *207*, 159.

(28) Ravikovitch, P.; Wei, D.; Chueh, W.; Haller, G.; Neimark, A. *J. Phys. Chem. B* **1997**, *101*, 3671.

(29) Serrano, D.; Aguado, J.; Morales, G.; Rodriguez, J.; Peral, A.; Thommes, M.; Epping, J.; Chmelka, B. *Chem. Mater.* **2009**, *21*, 641.

(30) Occelli, M.; Olivier, J.; Perdigon-Melon, J.; Auroux, A. *Langmuir* **2002**, *18*, 9816.

(31) Landers, J.; Gor, G. Y.; Neimark, A. V. *Colloids Surf., A* **2013**, *437*, 3.

(32) Ravikovitch, P. I.; Neimark, A. V. *Colloids Surf., A* **2001**, *187*, 11.

(33) Brunauer, S.; Emmett, P. H.; Teller, E. *J. Am. Chem. Soc.* **1938**, *60*, 309.

(34) Jagiello, J.; Thommes, M. *Carbon* **2004**, *42*, 1227.

(35) Khatiwada, B. K.; Hetayothin, B.; Blum, F. D. *Macromol. Symp.* **2013**, *327*, 20.

(36) Sing, K. S. *Pure Appl. Chem.* **1985**, *57*, 603.

6.9. SUPORTING INFORMATION

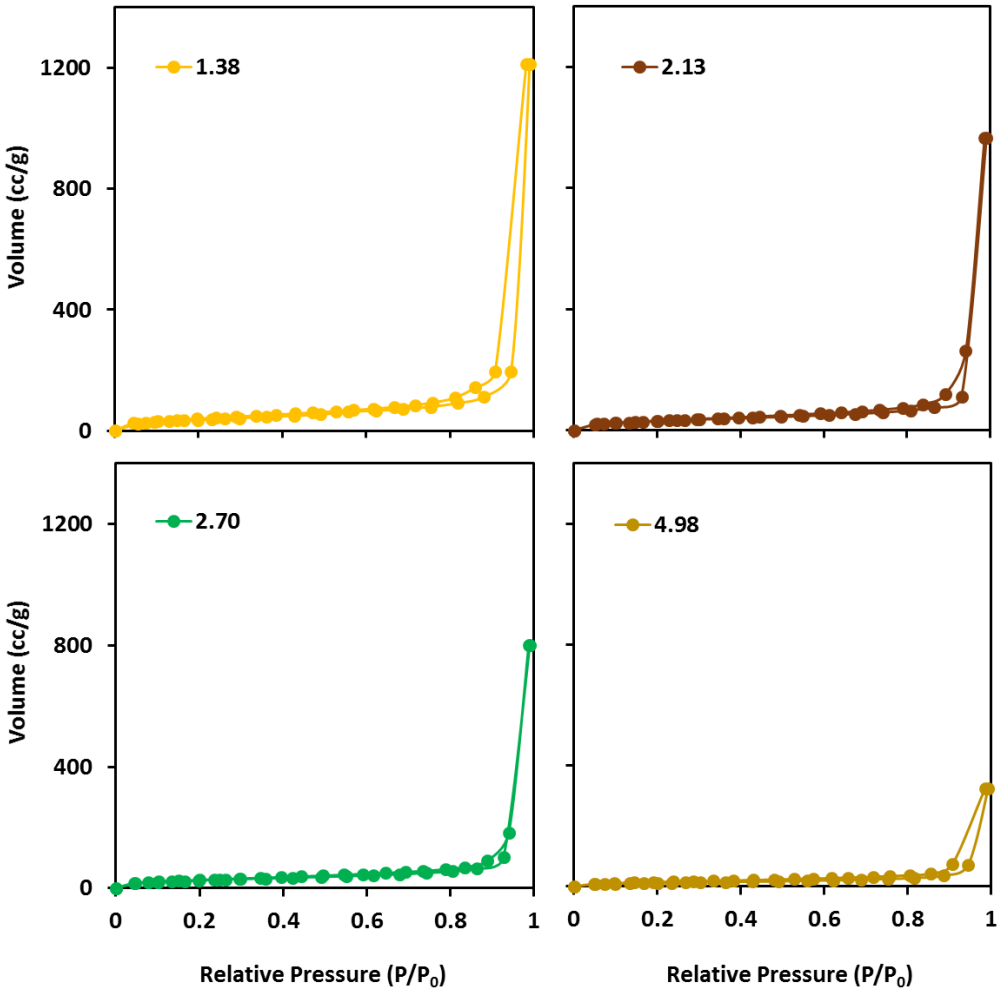

Figure S6.1. Nitrogen adsorption/desorption isotherm of adsorbed PMMA on silica with respect to adsorbed amounts.

VITA

Hamid Mortazavian

Candidate for the Degree of

Doctor of Philosophy

Thesis: POLYMER ADSORPTION ON SILICA AND WETTABILITY OF GRAPHENE OXIDE SURFACES, EXPERIMENTS AND SIMULATIONS

Major Field: Polymer Chemistry

Biographical:

Education:

Completed the requirements for the Doctor of Philosophy in Polymer Chemistry at Oklahoma State University, Stillwater, Oklahoma in May, 2016.

Completed the requirements for the Master of Science in Composite Engineering at Malekashtar University of Technology, Tehran, Iran in 2010.

Completed the requirements for the Bachelor of Science in Polymer Engineering at Amirkabir University of Technology, Tehran, Iran in 2007.

Experience:

Teaching and research assistant, Department of Chemistry, Oklahoma State University, USA, 2011-2016.

Professional Memberships:

American Chemical Society (Polymer division)
Golden Key International Honor Society
Society of Plastic Engineers
Graduate and Professional Student Government Association